THE MATERIAL PROPERTIES OF THE CHORDAE TENDINEAE OF THE MITRAL VALVE: AN *IN VITRO* INVESTIGATION

A Thesis
Presented to
The Academic Faculty

By

Jennifer Lynn Ritchie

In Partial Fulfillment
Of the Requirements for the Degree
Master of Science in Bioengineering

Georgia Institute of Technology
August, 2004

THE MATERIAL PROPERTIES OF THE CHORDAE TENDINEAE OF THE MITRAL VALVE: AN *IN VITRO* INVESTIGATION

Approved By:

Dr. Ajit P. Yoganathan, Advisor

Dr. Raymond Vito

Dr. Robert Guldberg

Dr. Michael Sacks

Date Approved: August 19, 2004

For my family and husband,
without whom I would not have survived.

ACKNOWLEDGEMENTS

First and foremost, I would like to thank my family for always being by my side. Without their continual support, I would not have survived. I would like to especially thank my husband Steve for being by my side the entire time, making all the trips to Atlanta to visit me, and not allowing me to give up. I love you more than you know.

Special thanks goes to my advisor Dr. Ajit P. Yoganathan for his support and exceptional opportunities he gave me during my time at Georgia Tech. I would also like to thank Dr. Raymond Vito, Dr. Robert Guldberg, and Dr. Michael Sacks for being part of my thesis committee.

I would like to thank all the members of the Cardiovascular Fluid Dynamics Laboratory for your support and friendship. Zhaoming and Jorge, thank you for everything you helped me to accomplish. Without you, I would not have been able to complete this work. Dennis, thank you for developing the autotracking software! James and Tracey, thanks for all your help with the histology and biochemical work. To Diane for her wonderful friendship, keep swimming. To Anna, Ashley, Helene, Yun, Suchitra, Leo, Dave, Hiroumi, Kartik, Kerem, Josie, Kelly, Lisa, and Mark, it was great working with you. I would also like to thank Dr. Guldberg's lab for the use of the uniaxial testing machine. Special thanks goes to Angela Lin for all her help in getting the machine to work.

To Jim McEntee and the Holifield Slaughter house, thank you for your contributions to my work. In addition, I would like to thank the National Heart, Lung, and Blood Institute for the support which made my work possible (grant # HL52009).

TABLE OF CONTENTS

LIST OF TABLES

LIST OF FIGURES

SUMMARY

The material properties of the mitral valve chordae tendineae are important for the understanding of leaflet coaptation configuration and chordal pathology. However, there is limited information about the mechanical properties of the chordae during physiologic loading. This research combines basic histology with standard mechanical tests to determine the functioning role of the chordae tendineae during the cardiac cycle.

Dual camera stereo photogrammetry was used to measure strains of the chordae tendineae *in vitro* under normal physiologic loading conditions. Two high speed (500 fps); high resolution (1280 X 1023) cameras were set up to capture the movement of graphite markers attached to the central section of the chordae using autotracking software developed in house. A uniaxial test simulating the same loading conditions as the left heart simulator was conducted on the same chordae using the same markers. The final strain/time and load/time curves were correlated to the pressure distribution obtained from the flow loop measurements in order to determine the behavior of the chordae tendineae during the cardiac cycle. Mitral valve chordae tendineae from fresh porcine hearts were stained for collagen and elastin using either a Verhoeff/van Gieson stain, or Verhoeff/light green stain. Cellular distribution was determined using a Hematoxylin and Eosin stain. Immunohistochemistry was used to verify the findings of vasculature. Biochemical assays were performed to quantify DNA, collagen, and elastin content of each of the six different types of chordae tendinae.

Six porcine mitral valves were used for the *in vitro* flow loop study. It was found that the maximum strain experienced during the cardiac cycle was 4.29% ± 3.43% and was experienced at 249 msec after the start of valve closure. The loading rate (valve closure)

was slightly higher at 75.3% ± 48.6% strain per second than the unloading rate (valve opening) at -54.8% ± -56.6% strain per second. The strut chordae which inserted into the anterior lateral papillary muscle had a slightly higher maximum strain (5.7% ± 3.8%) and loading rate (80.5% ± 51.9% strain per second) than the strut chordae which inserted into the posterior medial papillary muscle (5.5% ± 2.3% strain and 68.1% ± 48.3% strain per second). The strut chordae which inserted into the posterior medial papillary muscle had a higher unloading rate (-68.5% ± -59.1% strain per second) than the strut chordae which inserted into the anterior lateral papillary muscle (-44.9% ± -57.2% strain per second).

Histological examination revealed blood vessels in both the longitudinal and circumferential directions of the chordae. Each chordae contained vessels; however, it was found that the anterior strut chordae contain significantly more vessels than the other chordae. The anterior strut chordae contained 4.73±3.13 vessels, the anterior marginal chordae contained 1.50±2.07 vessels, the commissural chordae contained 1.50±1.35 vessels, the basal posterior chordae contained 1.27±1.74 vessels, the posterior intermediate chordae contained 1.43±1.13 vessels, and the posterior marginal chordae contained 1.00±1.53 vessels. Different structural levels were observed for all chordae tendineae. The inner layer was characterized by a higher concentration of collagen; whereas, the middle layer was mostly collagen with interwoven elastin fibers. The collagen microstructure was characterized by directional crimping. The Hematoxylin and Eosin stain showed fibroblasts evenly distributed throughout both the inner and outer layer of the chordae tendineae.

The anterior and posterior marginal chordae contained statistically significantly more DNA per mg of tissue than the other chordae ($p<0.01$). The anterior strut chord was

found to contain significantly less DNA per mg of tissue (0.63 ± 0.19 μg of DNA per mg of tissue dry weight) than all the other chordae ($p<0.01$). There was no significant difference between the amount of DNA per mg of tissue for the commissural, posterior intermediate, and basal posterior chordae. There was also no significant difference between the anterior (1.90 ± 1.14 μg of DNA per mg of tissue dry weight) and posterior (2.70 ± 1.24 μg of DNA per mg of tissue dry weight) marginal chordae.

The collagen assay results showed that the posterior marginal chord contained significantly more collagen per mg of tissue than the other chordae ($p<0.01$). The posterior marginal chordae contained 14.89 ± 6.83 μg of collagen per mg of tissue dry weight. There was no significant difference between the other chordae.

The Fastin Elastin assay results showed no significant difference in the amount of elastin per mg of tissue between the chordae.

This study demonstrates the first *in vitro* examination of the strain experienced by the chordae tendineae of the mitral valve. This technique allows the investigation of the behavior of biological tissues under physiologic loading conditions. It was found that the chordae experience different strain rates in the loading and unloading phases when the valve opens and closes. Three features can be observed from the uniaxial tests: a non-linear stress-strain relationship; a hysteresis loop in cyclic loading and unloading; and preconditioning in repeated cycles which all are typical responses of biological soft tissues. This suggests that the chordae exhibit similar material properties to those of tendons which are supported by their histological examination.

Histological examination indicated that previous studies had not adequately described the histological composition of the chordae tendineae. Contrary to earlier belief, vessels

were found in the chordae running from the papillary muscle to the insertion sites of the chordae on the mitral leaflets. Chordae tendineae of the mitral valve have different microstructures according to chordal type. Biochemical examination showed that the chordae contain different amounts of collagen, elastin, and DNA depending on chordal type. It was concluded that the amounts of these different components is related to the function and location of the chordae.

The findings in this study confirm that the mitral apparatus is composed of many components which work together in a complex, dynamic environment to ensure proper function. Further understanding of the mitral apparatus, including the chordae tendineae, will help better define surgical techniques aimed at repairing the mitral valve to its normal functioning state.

CHAPTER 1

INTRODUCTION

In 2001, one-third of all deaths, 16.6 million people, were related to cardiovascular diseases, according to the World Health Organization[1]. By 2020, the World Health Organization estimates that approximately 25 million people will die each year from cardiovascular diseases. The total cost spent on cardiovascular disease for the 64,400,000 people that have cardiovascular disease was estimated at $368.4 billion[2]. Since 1900, cardiovascular disease has been the number one killer in the United States. Nearly 2,600 Americans die of cardiovascular disease each day, an average of 1 death every 34 seconds. Cardiovascular disease claims more lives each year than the next five leading causes of death combined, which are cancer, chronic lower respiratory diseases, accidents, diabetes mellitus, and influenza and pneumonia.

There are approximately 12,737 mortalities related to valvular heart disease and 90,000 hospital discharges[2]. Of these mortalities, 12,380 are aortic valve disorders, 2,865 are mitral valve disorders, 12 are pulmonary valve disorders, and 3 are tricuspid valve disorders. The National Heart, Lung, and Blood Institute's Framingham Heart Study reports that among people ages 26-84, the prevalence of a mitral valve disorder is 1-2% and equal between men and women[2].

Mitral valve prolapse (MVP) is the most common heart valve abnormality in the United States. Recent studies estimate that approximately 2 to 6% of the adult population in the United States has MVP[2]. The most common cause of chronic mitral regurgitation (MR) is MVP. Recent studies have found that 10% of healthy men and women between the

ages of 23 and 35 have some degree of MR, and 93% of these people have mild MR. Ten percent of those over age 65 have MR, and approximately 26% have moderate to severe regurgitation[2].

Surgery is often required for MR and is generally performed for MVP only when MR is present. Valve repair or replacement are the two types of surgery available to treat these conditions. Surgery for MVP is based upon the degree of valve or heart damage and whether the person with MVP also has severe MR, poor function of the lower left ventricle, and possibly symptoms of heart failure. Surgery for MR is recommended when the symptoms of heart failure are present, or when the ejection fraction drops below 60% and the left ventricle is larger than 45 mm at rest[2]. Repair is more successful if there is limited damage to the mitral valve leaflets or chordae tendineae. Replacement, however, is usually preferred for people who have a hard, calcified mitral annulus or widespread damage to the valve and surrounding tissue.

The question of repair versus replacement is a topic of discussion among many surgeons. Although most surgeons prefer repair, they are performing more replacements than repair due to the unknown mechanisms which cause complications such as ischemic mitral regurgitation. According to a study by Gillinov et al.[3] from 1985 through 1997, a total of 397 patients underwent valve repair and 85 patients underwent valve replacements for ischemic mitral regurgitation. Completion of the study revealed that most patients with ischemic mitral regurgitation benefited from mitral valve repair over replacement. However, patients with a high-risk setting attain the same survival rating regardless of repair or replacement.

A better understanding of mitral valve mechanics will help surgeons decide whether repair or replacement of the mitral valve is more beneficial to the specific patient. The complete understanding of the papillary muscles, the chordae tendineae, and the mitral apparatus is crucial to this understanding.

The studies presented in this thesis are designed to improve the understanding of the mitral apparatus. The Georgia Tech left heart simulator was used to isolate the effects of the different parts of the mitral apparatus. A new left heart model was created such that the effects of the chordae tendineae could be determined using dual camera stereo photogrammetry. This experimental method allowed the measurement of strain attained by the chordae tendineae during normal physiologic function. Uniaxial tests were conducted to determine the mechanical behavior of the chordae tendineae during physiologic loading conditions. Basic histology was performed on the chordae tendineae to determine the underlying microstructure and how this microstructure relates to the *in vitro* behavior. Verhoeff and van Gieson stains were performed on both radial and longitudinal sections of six different chordae tendineae to determine the collagen and elastin distribution of the chordae tendineae. The Verhoeff and van Gieson stains also allowed the observance of vascular structures. Immunohistochemistry of the von Wildebrand Factor was performed to verify the vascular structures. Hematoxylin and Eosin (H & E) stains were also performed on the same sections to determine the cellular distribution in the chordae tendineae. This research combines basic histology with standard mechanical tests to determine the functioning role of the chordae tendineae during the cardiac cycle.

CHAPTER 2

BACKGROUND

2.1 Anatomy of the Heart

The heart is one of the most important muscles in the body. The main purpose of the heart is to pump blood; which carries oxygen and nutrients to the other organ systems of the body. The heart is composed of four chambers, two atria and two ventricles. The right side of the heart, the right atrium and ventricle, receives deoxygenated blood from the systemic circulation and pumps it to the pulmonary circulation where the lungs replenish the oxygen in the blood. The left side of the heart, the left atrium and ventricle, receives oxygenated blood from the pulmonary circulation and pumps it to the systemic circulation. Figure 2.1 describes the heart anatomy and flow through the heart.

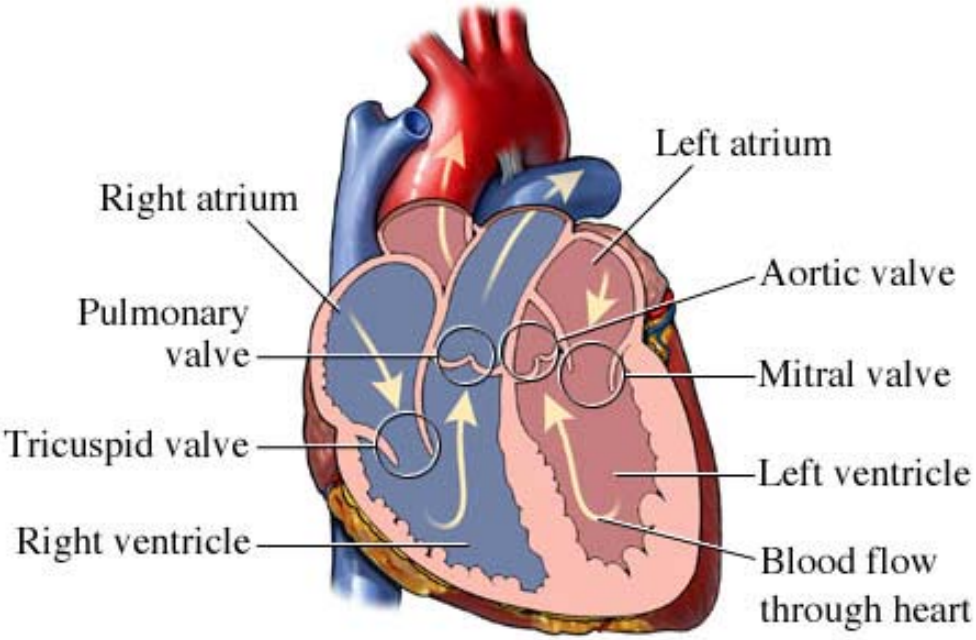

Figure 2.1: Diagram showing the anatomy of the heart. Illustrations copyright 2000 by Nucleus Communications, Inc. All rights reserved. http://www.nucleusinc.com

There are four valves located in the heart which separate each chamber. The right atrium and ventricle are separated by the right atrioventricular or tricuspid valve. This valve is composed of three fibrous flaps that are attached at the free edge to tendinous chords; which are attached to the heart wall by papillary muscles. During relaxation (ventricular diastole), the valve opens allowing the blood to drain directly from the inferior and superior vena cava, through the right atrium and into the right ventricle. However, during ventricular contraction (ventricular systole), the valve closes and prevents the backflow of blood into the atrium. The pulmonary semilunar valve consists of three semilunar cusps composed of thick connective tissue. During ventricular relaxation, this valve is closed such that blood cannot enter the right ventricle from the pulmonary trunk. When the ventricle contracts, the valve opens allowing the blood to flow into the pulmonary trunk, and beginning the pulmonary circuit.

The mitral or left atrioventricular valve consists of two cusps that prevent the backflow of blood into the left atrium during ventricular contraction. Tendinous connective tissue fibers called the chordae tendineae attach the free edges of the mitral valve to the papillary muscles. The papillary muscles are conical muscular projections that arise from the inner surface of the left ventricle. During ventricular contraction, the papillary muscles contract and tense the chordae tendineae preventing the mitral valve from prolapsing during ventricular contraction. The aortic semilunar valve is composed of three cusps that open during ventricular contraction allowing the left ventricle to pump the blood from the heart through the ascending aorta and to the systemic circulation. During relaxation, the three cusps are closed allowing the blood to pool in the left ventricle.

The function of the atrial chambers are to collect blood that is returning to the heart and deliver it to the attached ventricles. Due to the similarities in function of the two atrial chambers, they are similar in structure; however, the demands on the ventricles are much different and therefore they must have different structures. The right ventricle pumps blood to the pulmonary blood vessels which are thin and wide and hence provide little resistance to blood flow. Therefore, the right ventricle needs to create relatively low pressures to push the blood through the pulmonary circuit. The wall of the right ventricle is relatively thin, compared to the left ventricle, and acts like a bellows pump, squeezing the blood against the thick, muscular wall of the left ventricle. The left ventricle has to provide enough pressure to push the blood through the entire systemic circulation. When compared to the right ventricle, the left ventricle must exert six to seven times as much force to push the blood around the systemic circulation. The left ventricle has extremely

thick muscular walls and is round in cross sectional area. In order to generate enough force, the chamber squeezes and twists during contraction. This is a helical motion due to fiber arrangement. When squeezing, the distance between the base and apex decreases; when twisting, the diameter of the chamber decreases. By combining these two motions, the left ventricle is able to generate enough force to push the blood through the systemic circulation and also help the right ventricle push blood through the pulmonary circulation.

The heart wall is comprised of three distinct layers: the epicardium, the myocardium, and the endocardium. The epicardium is a serous membrane that covers the outer layer of the heart. This membrane is composed of an exposed mesothelium and an underlying layer of loose connective tissue that is attached to the myocardium. The myocardium is the muscular portion of the heart wall consisting of concentric layers of cardiac muscle tissue. The muscle bundles of the atrial myocardium wrap around the atria and form figure eights that pass through the interatrial septum. The muscle bundles of the ventricular myocardium wrap around both ventricles and spiral around the ventricles toward the apex. The endocardium covers the inner surface of the heart wall including the valves. The endocardium is composed of simple squamous epithelium that is continuous with the endolethium of the blood vessels.

2.2 Cardiac Cycle

The cardiac cycle includes alternating periods of contraction and relaxation that are divided into two phases: systole and diastole. During systole, the chamber contracts and pushes blood into another chamber or into an arterial trunk. During diastole, immediately

following systole, the chamber relaxes and fills with blood. The cardiac cycle consists of one cycle of atrial systole and atrial diastole. For a heart rate of 70 beats per minute, this cardiac cycle, or sequence of either atria or ventricle systole and diastole, lasts 860 ms. The movement of blood is influenced by the pressure induced in the chambers by systole and diastole which induces the opening and closing of the valves. Figure 2.2 shows the cardiac cycle.

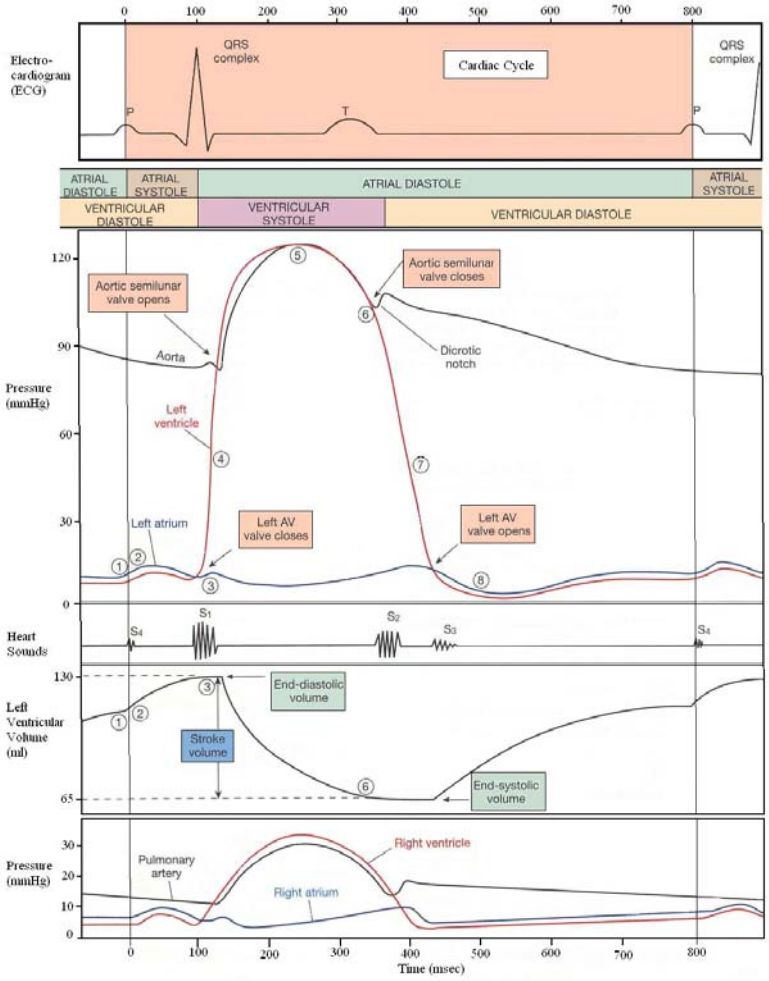

Figure 2.2: Pressure and volume relationships in the cardiac cycle.

The cardiac cycle starts with atrial systole, approximately 100 ms, in which rising pressure pushes blood from the atria to the ventricles through the open AV valves. Since the ventricles fill passively during the previous cardiac cycle, the ventricles are already filled with 70% of their capacity with blood. During atrial systole, the ventricle receives the remaining amount of blood to fill the ventricle; which is the maximum amount of blood that it will hold during the cardiac cycle called the end-diastolic volume. Ventricular systole occurs at the end of atrial systole and lasts for approximately 270 ms in a resting adult. As the pressure inside the ventricles surpasses that of the atria, the AV valve closes. A period called isovolumetric contraction occurs in which all the valves of the heart are closed and the pressure in the ventricles continues to rise as the ventricles contract isometrically. Ventricular ejection occurs when the pressure in the ventricles exceeds that of the pulmonary or aortic trunks. The aortic and pulmonary valves open and the ventricles contract isotonically pushing blood into either the pulmonary or systemic circulation. During this period of contraction, the ventricles expel approximately 70 ml of blood, or 5 L/min. This volume of blood is called the stroke volume and is 60% of the end-diastolic volume. At the end of ventricular systole, the pressure in the ventricles falls causing blood to flow back into the ventricles; however, the closure of the pulmonary and aortic valves prevents this backflow. The amount of blood remaining in the ventricle with the valves closed is the end-systolic volume. The ventricles then reach ventricle diastole when the muscle cells begin to relax. Since the pressure is still higher in the ventricle than the atria, the heart goes through a period called isovolumetric relaxation. As the ventricles relax to their resting state, the pressure

decreases rapidly. This causes the AV valves to open and blood to passively fill the ventricles and begin the cardiac cycle again.

2.3 Anatomy of the Mitral Valve

The mitral valve complex is composed of an annulus, the mitral valve leaflets, the chordae tendineae, two papillary muscles, and the underlying left ventricular myocardium. The mitral valve controls the flow of blood from the left atrium to the left ventricle. During ventricular systole, the mitral valve closes to prevent the backflow of blood into the left atrium and hence ensure the blood flows to the systemic circulation. The mitral leaflets are composed of three layers, the atrialis or spongiosa, the fibrosa, and the ventricularis. The mitral valve has also been shown to be a viscoelastic material.

The mitral valve can be decomposed into four sections: two commissural areas, anterolateral and posteromedial; and two leaflet areas, anterior and posterior. The commissural areas are defined by the insertion of the commissural chordae. The anterior leaflet is the largest leaflet with either a semicircular or triangular shape. The line of leaflet closure is defined by a distinct ridge that follows the rim of the leaflet, but is 0.8 to 1.0 cm from its free margin[4]. The rough zone of the leaflet tissue is distal to this ridge. During valve closure, the rough zones on both the anterior and posterior leaflet come into contact to form the closure line, line of coaptation. The majority of chordae tendineae insert into this rough zone on the leaflet. Between the rough zone and the annulus, the leaflet is membranous and normally free of chordae insertions. The posterior leaflet is the tissue posterior to the commissural areas. The posterior leaflet has a scalloped appearance with each scallop is semi-oval with either a smooth or a finely serrated free

margin. Three zones can be identified on the posterior leaflet: the rough zone, the membranous or clear zone, and the basal zone[4]. The rough zone is defined by the line of leaflet closure and its free margin. Figure 2.3 is a diagram representation defining the rough zone of the mitral valve.

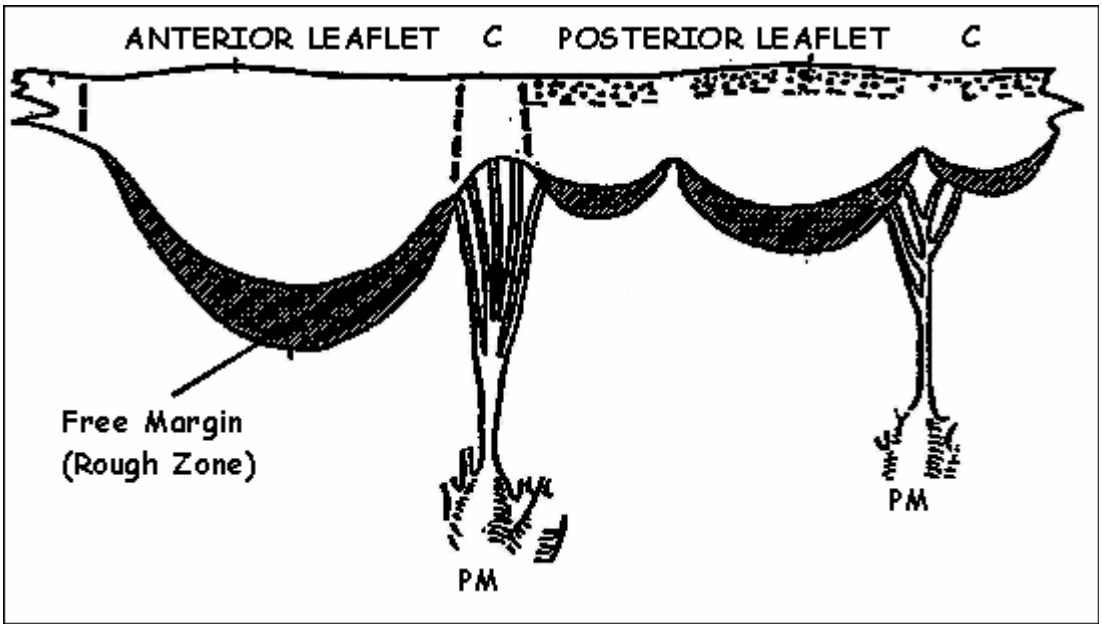

Figure 2.3: Diagram representation of the mitral valve (Ranganathan et al.[4]).

Under normal physiologic function, the mitral valve undergoes high fluid shear stresses, substantial hydrostatic pressures, and large in plane tensions. A study by Sacks et al.[5] was the first to complete a study of surface strains on the anterior leaflet of a functioning mitral valve. The central region of the anterior leaflet was found to experience large, anisotropic stretches during valve closure. However, after closure, further leaflet deformation ceased. This leaflet deformation was found to be reversed during valve opening. Even though the leaflet experienced large stretches, there was very little shear exerted during the cardiac cycle. It was also found that the peak stretch rates during the

closing and opening phases reached values as high as 500%-1000% per sec[5]. The leaflet appeared to stiffen when the areal strain plateaus. This is explained by the locking of the collagen fibers. This implies that the collagen fiber network of the valve allows for sufficient initial compliance to allow for adequate leaflet coaptation, followed by leaflet stiffening to prevent further deformation[5]. It was also concluded that the mitral valve has a finely tuned closing mechanism that works together with the chordae tendineae and the papillary muscles to ensure proper valve closure; hence, preventing regurgitation and mitral valve prolapse.

2.4 Anatomy of the Chordae Tendineae

The chordae tendineae of the mitral valve function to transmit the contractions of the papillary muscles to the leaflets of the mitral valve complex. They also serve to secure the leaflets to maintain valve closure and prevent mitral valve prolapse. In order to perform these functions, the chords must contain a high degree of elasticity, as well as considerable strength and endurance. These tendinous chords are composed of collagen and elastin fibers arranged in parallel. A study done by Millington-Sanders et al.[6] showed that the chordae tendineae are composed of multiple layers of elastic fibers, collagen, and an outer layer of endothelial cells. The outer layer of elastic fibers was found to be approximately 4μm thick, arranged at inclined angles to the axis of the chordae. The second layer of elastic fibers appeared to be arranged longitudinally. In the lower endocardium, there is a dense distribution of elastic fibers mixed with wavy collagen. Cross sectional views of the chordae revealed that the elastic fibers diminish

towards the interior of the chord while the amount of collagen increased. Figure 2.4 is a computer generated model of the chordae tendineae.

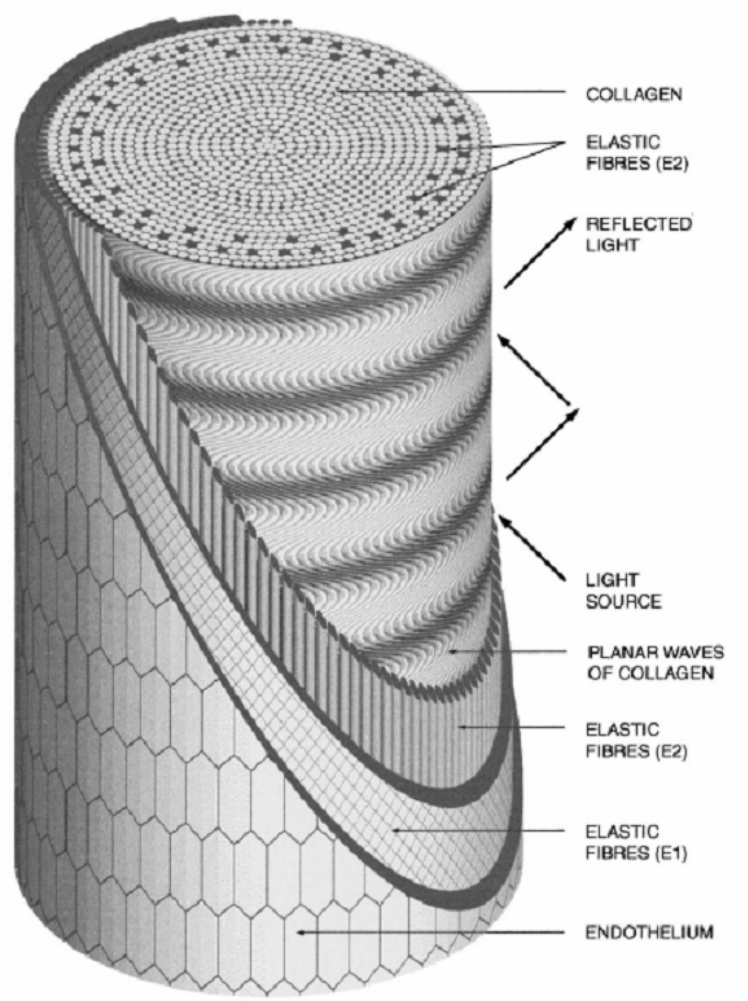

Figure 2.4: Computer generated model of the microsection of the chordae tendineae (Millington-Sanders et al.[6]). There are three layers: an inner collagen core, a middle elastin layer, and an outer endothelium layer.

The chordae must withstand the large repetitive forces that are encountered in the left ventricle. The arrangement of their elastic fibers and wavy collagen increases the mechanical properties of the chordae and allows them to withstand these forces. The wavy arrangement of collagen that is surrounded by elastic fibers is well adapted to the cyclic stresses to which the chordae are continuously subjected. This arrangement also

provides a mechanism for smooth transfer of forces to the valve leaflets thus protecting the structural components of the valve which have to withstand rapidly applied forces at systole. During stretching, when papillary muscle contraction straightens the chords, the collagenous wavy pattern disappears and transfers the peak stress during contraction to the leaflets. The sleeve-shaped elastic network which surrounds the internal collagen suggests that on relaxation of tension, the elastic fibers would tend to restore the collagen to their wavy configuration. This layer of elastic fibers also serves as a protective barrier between the collagen and the delicate layer of the endocardium.

The mitral valve consists of 8-12 chordae tendineae, 15-20mm long, and approximately 0.45mm in diameter before branching[6]. The chordae branch either soon after their origin in the papillary muscle, or shortly before they insert into the leaflet. The chordae insert into either the anterior leaflet, the posterior leaflet, or the commissural section. The chordae tendineae inserting into the anterior leaflet insert obliquely on either side of the anterior leaflet; however, those inserting into the posterior leaflet are aligned parallel to each other[7]. The arrangement and morphology of the chordae tendineae can be classified according to their insertion sites. The average number of chordae tendineae and their insertion locations presented by Lam et al.[7] are displayed in Table 2.1.1. The commissural chords branch radially immediately after extending from the papillary muscles and insert into the free margin of the commissural section. There are two commissural chords that insert into the anterior lateral commissural area or the posterior medial area. The commissural area is defined by the lateral spread of attachment of the branches of the commissural chordae. The average length and thickness of the commissural chordae recorded by Lam et al.[7] are displayed in Table 2.1.

The anterior leaflet has two types of chordae, the rough zone chordae and the strut chordae. The rough zone chordae insert into the rough zone of the anterior leaflet, and typically split into three chords soon after their origin in the papillary muscle. One chord inserts into the free margin of the valve leaflet, one into the intermediate area, and one beyond the free margin at the line of closure. These chords occasionally branch into secondary chords which insert into the same area as the parent chord. The two thickest and largest chordae originate from the tips of the anterior lateral and posterior medial papillary muscles and insert into the ventricular surface of the anterior leaflet near the line of closure between the 4 and 5 o'clock positions on the posterior medial side and between the 7 and 8 o'clock positions on the anterior lateral side[7]. These chords are termed the strut chords and are present in the majority (90%) of mitral valves. The average length and thickness of the chordae inserting into the anterior leaflet recorded by Lam et al.[7] are displayed in Table 2.1.

The posterior leaflet has three types of chordae, the basal chordae, the rough zone chordae, and the cleft zone chordae. The basal chordae; which are unique to the posterior leaflet, insert into the basal portion of the leaflet. These chordae are typically a single strand that extends from the papillary muscle and flares prior to its insertion in the leaflet. The rough zone chordae of the posterior leaflet has a morphology similar to that of the rough zone chordae of the anterior leaflet, but they are shorter and thinner than those inserting into the anterior leaflet. The cleft chordae insert into the free margin of the cleft in the posterior leaflet. These chordae have tiny radial branches like the struts of a fan. Two cleft chordae divide the posterior leaflet into three scallops. The average length and

thickness of the chordae inserting into the posterior leaflet recorded by Lam et al.[7] are displayed in Table 2.1.

Table 2.1: Average length, thickness, and insertion locations of chordae tendineae (Lam et al.[7]).

Site of insertion	Types of chordae	Length (cm)	Thickness (mm)
Anterior leaflet	Rough zone chordae	1.75 ± 0.25	0.84 ± 0.28
	Strut chordae	1.86 ± 0.43	1.24 ± 0.51
Posterior leaflet	Rough zone chordae	1.40 ± 0.08	0.65 ± 0.24
	Basal chordae	0.84 ± 0.21	0.40 ± 0.29
	Cleft chordae	1.30 ± 0.18	0.78 ± 0.15
Commissural areas	Anterior lateral commissural chordae	1.2 ± 0.31	0.70 ± 0.20
	Posterior medial commissural chordae	1.4 ± 0.40	1.0 ± 0.30

The chordae tendineae of the mitral valve can also be classified into first order (primary) chordae, second order (secondary) chordae, or third order chordae[7]. The primary chordae consists of the commissural chordae, the rough zone chordae of the anterior and posterior leaflets that insert into the free margin of the leaflets (marginal chordae), and the branches of cleft chordae of the posterior leaflet. The secondary chordae consists of the rough zone chordae of the anterior and the posterior leaflets that insert beyond the free margin, the strut chordae of the anterior leaflet, and the main stems of cleft chordae of the posterior leaflet. The third order chordae consist of the basal chordae of the posterior leaflet. Figure 2.5 is a diagram representation of the insertion locations of the chordae tendineae.

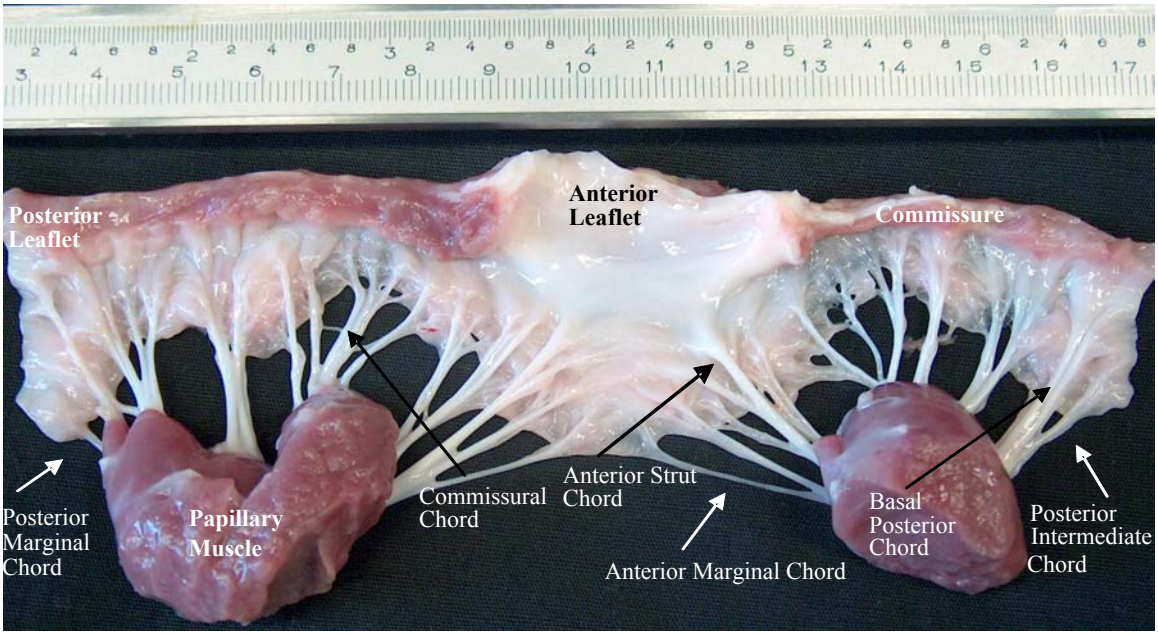

Figure 2.5: Diagram representation of the insertion locations of the chordae tendineae in the mitral valve. There are six primary chordae tendineae: anterior strut, anterior marginal, commissural, basal posterior, posterior intermediate, and posterior marginal.

2.5 Mechanical Properties of the Chordae Tendineae

The mechanical properties of the chordae tendineae have been shown to vary with chordal size and type. A study done by Liao et al.[8] postulated that when grouped according to cross-sectional area and according to chordal type, there is a clear relationship between chordal size, type, and mechanical properties. It was found that the thicker strut chordae were more extensible and less stiff than the thinner marginal chordae. These findings are described by Liao et al.[8] in Tables 2.2 and 2.3. The average collagen fibril crimp period showed a decrease in crimp period as the chordal diameter increased. Also, the marginal chordae consistently had smaller fibril diameters and a greater average fibril density than the basal and strut chordae. The extensibility of the mitral valve chordae tendineae increases with their diameter, while their tensile modulus decreases. The extensibility of the thicker chordae is due to the more highly crimped

collagen fibril and hence the smaller crimp period. All of these findings support the conclusion that the thicker strut chordae are more extensible than the thinner marginal and basal chordae. The findings by Liao et al.[8] are consistent with those of Lim et al.[9] and Kunzelman et al.[10].

Table 2.2: Comparison of mechanical properties of chordae according to their cross-sectional area (Liao et al.[8]).

Range of chordal area (mm^2)	0.1-0.5	0.5-1.0	1.0-2.0	2.0-3.0	Significance
Extensibility (% strain)	4.2±1.5	8.1±2.5	15.7±3.9	18.4±2.8	$p < 0.001$
Tensile modulus (MPa)	90.1±22.3	83.7±18.5	66.3±13.5	61.7±13.3	$p = 0.001$

Note: Values given as Mean ± S.D. Comparisons were made using one-way ANOVA. *p*-Values denote significant differences between groups.

Table 2.3: Comparison of mechanical properties of chordae according to chordal type (Liao et al.[8]).

Chordal type	Marginal	Basal	Strut	Significance
Extensibility (% strain)	4.3±1.6	8.5±2.0	17.5±3.3	$p < 0.001$
Tensile modulus (MPa)	84.4±21.2	86.1±20.9	64.2±13.5	$p = 0.002$
Average chordal size (mm^2)	0.38±0.18	0.71±0.25	2.05±0.40	$p < 0.001$

Note: Values given as Mean ± S.D. Comparisons were made using one-way ANOVA. *p*-Values denote significant differences between groups.

Lim et al.[11] report that the mitral valve chordae tendineae exhibit a nonlinear quasi-static elastic response. After removal of the outer elastin sheath, they demonstrated that the more readily extensible elastin layer cannot contribute to the nonlinear elastic behavior of the chordae tendineae. This further leads to the conclusion that the mechanical properties of this tissue are governed primarily by the behavior of the inner collagen core. As the chordae were stretched further, a force greater than the initial force was needed to strain the tissue. This further stretching involves the straining of the bonds and bond angels within the fibrils. This straining is evident in the observed nonlinear stress-strain curve. Lim et al.[11] also reported that the initial segment of the nonlinear stress-strain curve could not be attributed to the presence of the more extensible elastin. This is in contrast to the properties of arteries, which contain the same structural components as the chordae, but have an elastic response which cannot be explained by the same theory.

Failure mechanisms of the chordae tendineae have been examined by Sedransk et al.[12]. It was observed that the marginal chordae and posterior leaflet chordae were thinner and required less strain and load to fail than basal chordae and anterior leaflet chordae, respectively. These findings are in agreement with those found earlier, Lim et al.[11], which concludes that the marginal chordae have a decreased extensibility in comparison to the thicker strut and basal chordae. It was also concluded that the failure strength and the failure strain of the chordae depend primarily on the insertion position (marginal or basal/strut) and less on the particular leaflet (anterior or posterior).

An *in vitro* study conducted by Jimenez et al.[13] indicates the importance of annulus configuration on chordal force distribution. It was concluded that when comparing the dynamic changes in tension on the chordae, the secondary chords bore the larger loads on each of the leaflets when compared with the primary chords. The anterior strut chord had a tension 0.74 ± 0.46 N higher than the anterior marginal chord. The load on the posterior intermediate chordae was 0.18 ± 0.16 N higher than the load on the posterior marginal chordae. The average forces on the chordae found by Jimenez et al.[13] are displayed in Table 2.4. This force distribution is consistent with the results found by Sedransk et al.[12] and Lim et al.[11]; which conclude that the secondary chordae are thicker and have a larger failure strength and failure strain than the primary chordae.

Table 2.4: Force distribution of the chordae tendineae (Jimenez et al.[13]).

Chord	Number of Specimens	Tension Flat (N)	Tension Saddle (N)	Percentual Difference (%)	Statistical Significance
Anterior Strut	6	1.22±0.52	0.95±0.35	18.5±16.1	0.018
Posterior Intermediate	5	0.25±0.14	0.30±0.18	-22.3±17.1	0.022
Posterior Marginal	4	0.03±0.04	0.06±0.05	-137.8±188.6	0.12
Basal Posterior	6	0.19±0.10	0.31±0.25	48.5±89.9	0.122
Anterior Marginal	6	0.31±0.17	0.35±0.16	-58.5±111.4	0.145
Commissural	5	0.17±0.18	0.11±0.20	59.0±32.3	0.008

2.6 Mitral Valve Pathologies

The World Health Organization reports that 16.6 million people die each year to cardiovascular diseases[1]. In 2001, one-third of all deaths were related to cardiovascular diseases, and by 2020, the World Health Organization estimates that approximately 25 million people will die each year from cardiovascular diseases.

Mitral valve prolapse (MVP) is the most common heart valve abnormality in the United States. Recent studies estimate that approximately 2 to 6% of the adult population in the United States have MVP[2]. Mitral valve prolapse is a condition in which the mitral valve leaflets prolapse upward into the left atrium rather than forming a line of coaptation as the heart contracts. Figure 2.6 is a diagram representation of a normal valve and a valve with mitral valve prolapse. The most common cause of chronic mitral valve regurgitation (MR) is MVP.

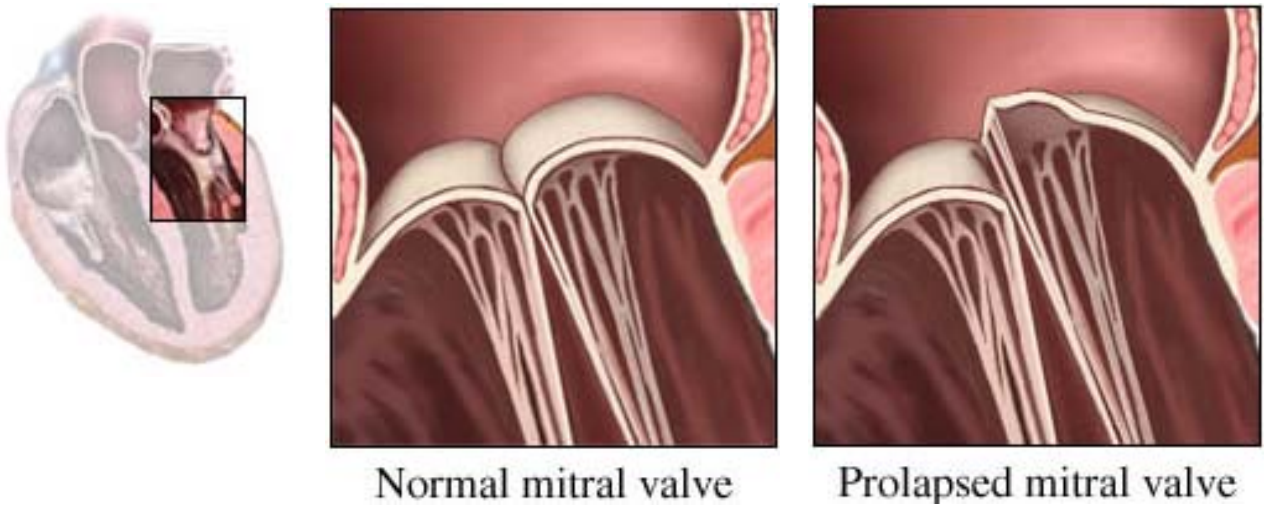

Figure 2.6: Diagram representation of a normal and prolapsed mitral valve. Image copyright 2000 by Nucleus Communications, Inc. All rights reserved. http://www.nucleusinc.com.

Mitral valve regurgitation occurs when the flow proceeds in the reverse direction through the mitral valve during ventricular contraction. Chronic MR is a common disorder, although the exact number of people affected by the condition is difficult to estimate due to the presence of murmurs in many adults and the small amount of regurgitation detected in 80% of adults[2]. Mitral valve regurgitation can develop suddenly known as acute MR. Symptoms of acute MR include sudden heart failure, fluid in the lungs, and chest pain. Acute MR requires urgent surgery to repair or replace the mitral valve. Recent studies have found that 10% of healthy men and women between the ages of 23 and 35 have some degree of MR, and 93% of these people have mild MR[2]. Ten percent of those over age 65 have MR, and approximately 26% have moderate to severe regurgitation[2]. There are three risk factors associated with MR. The age of the patient increases mechanical stress, wear and tear of the mitral valve over time, and increases the likelihood of blood leaking back into the atrium. During high blood pressure, the left ventricle encounters greater resistance as it pumps blood to the body. The increase in resistance ultimately places greater strain on the mitral valve and could cause leakage.

Chronic MR can result from many pathologies of the heart. The most common cause of chronic MR is MVP. Calcification of the annulus prevents the mitral valve leaflets from closing completely and therefore, blood leaks backward into the left atrium. Congenital heart disease, an abnormality of the heart valve that developed before birth, can lead to MR. Endocarditis can cause scarring of the heart valves that can lead to chronic MR. Another common cause of MR is damage to the heart muscles of the chordae tendineae. Myocardial infarctions or coronary artery disease can lead to an enlarged left ventricle,

damage to the heart muscles or the chordae tendineae which control movement of the mitral valve.

Acute MR can result from three causes. Rupture of the chordae tendineae is most commonly seen in middle-aged and older men and can be caused by endocarditis or trauma. Rupture of the papillary muscles can be caused by a myocardial infarction or by trauma. Also, problems associated with a prosthetic valve can lead to acute MR.

Once MR develops, little can be done to prevent its progression. Due to the quick onset of acute MR, treatment must be immediate. Vasodilators such as nitroprusside help reduce the amount of blood flowing back into the left atrium and left ventricle. An intro-aortic balloon counterpulsation device is used if the condition is not stabilized with medications. Surgery to repair or replace the valve is generally necessary. Additional surgery to correct the underlying cause of MR may also be necessary.

Surgery is often required for MR and is generally performed for MVP only when MR is present. Valve repair or replacement are the two types of surgery available to treat these conditions. Surgery for MVP is based upon the degree of valve or heart damage and whether the person with MVP also has severe MR, poor function of the lower left ventricle, and possibly symptoms of heart failure. Surgery for MR is recommended when the symptoms of heart failure are present, or when the ejection fraction drops below 60% and the left ventricle is larger than 45 mm at rest[2]. Repair is more successful if there is limited damage to the mitral valve leaflets or chordae tendineae. Replacement, however, is usually preferred for people who have a hard, calcified mitral annulus or widespread damage to the valve and surrounding tissue.

There are three different heart valve repair procedures which include reshaping of the valve by removing excess valve tissue, adding support to the valve ring by adding tissue or an annulus ring, or attaching the valve to nearby heart chordlike tissues, chordal transposition.

Heart valve replacement surgery involves the removal of the badly damaged valve. The valve is replaced with a plastic or metal mechanical valve, or a bioprosthetic valve usually made from pig tissue. People who receive a mechanical heart valve are more likely than those who receive a bioprosthetic heart valve to develop blood clots in the heart that may break loose, travel to the brain, and cause a stroke. Therefore, lifelong anticoagulant therapy is necessary for the rest of the patient's life. There are many risks associated with heart valve replacement. Effects from the operation, such as bleeding, infection, and risks associated with anesthesia are often low risks, but often include a psychological component. Blood clotting caused by the new valve, infection in the new valve, and failure of the new valve are all risks associated with heart valve replacement, but are significantly lower with heart valve repair.

Mitral valve stenosis is an uncommon heart condition that develops when the mitral valve fails to open as wide as it should. Although this has no immediate effect on health, it can eventually disrupt normal heart function and lead to heart failure, abnormal heartbeat, and other heart conditions. Most cases of mitral valve stenosis were reported to be caused by rheumatic fever; however, 60% of the people with mitral valve stenosis do not report a history of rheumatic fever[2]. It is unknown how many people have mitral valve stenosis. Most people do not have symptoms until after age 40, with symptoms appearing in people who are in their 50s and 60s. People in this age group often have more than one

heart problem, which can make it more difficult to diagnose and treat mitral valve stenosis. Figure 2.7 is a diagram representation of a normal and stenosed mitral valve.

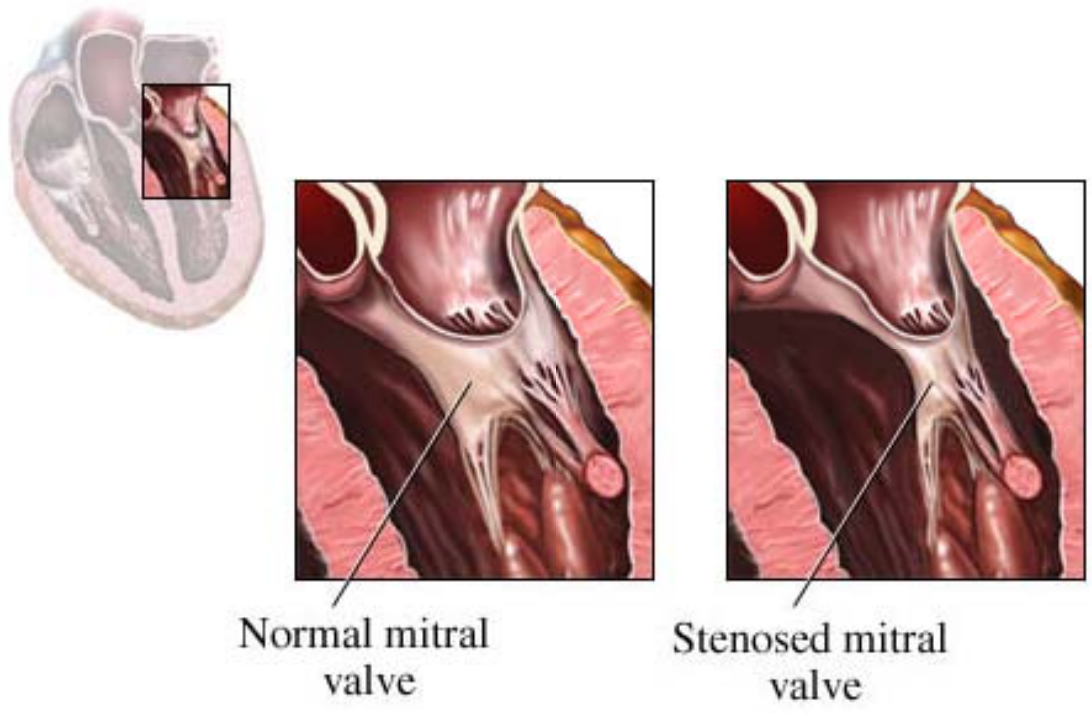

Figure 2.7: Diagram representation of a normal and stenosed mitral valve. Image copyright 2000 by Nucleus Communications, Inc. All rights reserved. http://www.nucleusinc.com.

Treatment of mitral valve stenosis focuses on managing symptoms and preventing complications. Medication can help manage symptoms and related complications such as heart failure. Balloon valvotomy or valve surgery may be done to repair or replace the damaged mitral valve. Balloon valvotomy is the method of choice for treating mitral valve stenosis due to the quicker recovery time than open heart surgery. Complications of mitral valve stenosis, including heart failure, arrhythmias, and endocarditis, can greatly affect the quality of life.

There are two situations where surgery is recommended, when symptoms are severe, or there are no symptoms, but high blood pressure in a pulmonary artery, pulmonary edema,

atrial fibrillation, thromboembolism, or severe mitral valve stenosis. For mitral valve stenosis, the American College of Cardiology and the American Heart Association (ACC/AHA) guidelines recommend having the mitral valve replaced once the valve area drops below 1.5 cm^2 and is accompanied with serious, life limiting symptoms[2].

Although there are solutions to these mitral valve pathologies, the solutions have inherent problems such as lifelong anticoagulant therapy. Most surgeons today perform mitral valve repair instead of mitral valve replacement. However, many surgeons have suggested many repair procedures that require further research before worldwide clinical implantation.

CHAPTER 3

HYPOTHESES AND SPECIFIC AIMS

3.1 Hypotheses

3.1.1 Hypothesis 1

The chordae tendineae exhibit specific, finely tuned mechanical responses that enhance mitral valve function, and are thus not simple struts.

3.1.2 Hypothesis 2

The underlying basis for their unique specific behaviors lies in their unique structure. Therefore, structural characterization and architecture of mitral valve chordae tendineae will provide additional understanding of their mechanical function.

3.2 Specific Aims

3.2.1 Specific Aim 1 – Hypothesis 1

Specific aim 1 was to investigate the dynamic strain response exhibited by the chordae during normal physiologic function. Dual camera stereo photogrammetry was used to measure the displacement of small graphite markers that were adhered to the central region of the chordae. The mitral valve was placed in a left heart simulator with physiologic flow and pressure waveforms. A left heart model was designed such that visualization of all six types of chordae was possible with both cameras during the entire cycle time. Images were taken with a sampling rate of 500 frames per second. The

images were then digitized and the displacement of the markers determined. From the resulting marker displacement, the uniaxial strains along the chordae were computed over the cardiac cycle.

3.2.2 Specific Aim 2 – Hypothesis 1

In specific aim 2, we investigated the load/strain behavior of the chordae during uniaxial testing. To obtain load/strain information, elongations from the testing device actuator (cross-head displacement) and non-contact optical methods were employed and compared. A single high speed camera was set up perpendicular to the chordae in order to measure the displacement of the markers on the chordae during uniaxial testing. This is in contrast to earlier studies which have only used the cross-head displacement to measure elongations of the chordae. After appropriate preconditioning, the chordae were loaded and unloaded at physiologic loading rates, 40% strain per second, to 2 N of force for five cycles. Images were recorded at 45 frames per second, which was a limitation set by the uniaxial machine. A trigger signal was designed to couple the cameras and the uniaxial machine such that the data were recorded simultaneously. The load from the uniaxial machine and the strain measured with the cameras were synchronized and a final load/strain curve was generated.

3.2.3 Specific Aim 3 – Hypothesis 1

Specific aim 3 was to combine the information from the uniaxial studies with the *in vitro* flow loop data. The strain determined using the *in vitro* flow loop was compared to the strain found during the uniaxial tests. The strain from the *in vitro* flow loop could then be correlated with a known load. If this procedure is completed for all data points collected

from the *in vitro* flow loop, the outcome would be a load/time curve which correlates to the dynamic environment the mitral valve chordae experiences during the cardiac cycle.

3.2.4 Specific Aim 4 – Hypothesis 2

Specific aim 4 was to characterize the structure and composition of the chordae. The chordae were examined using standard histological staining techniques. Collagen and elastin components were examined to determine if there was a structure function relationship between the compositional makeup of the chordae and their function in the cardiac cycle. A hematoxylin and eosin stain was observed under brightfield and fluorescent microscopy to visualize cell placement in the chordae. A Verhoeff and van Gieson stain was used to determine the collagen, elastin, and cellular distribution in the chordae. A Verhoeff and light green stain allowed for observing elastin distribution. Immunohistochemistry was performed on all six types of chordae tendineae in the radial direction to verify the finding of vasculature. Assays were performed on all six chordae tendineae to quantify the amount of DNA, collagen, and elastin contained in each of the different chordae.

CHAPTER 4

MATERIALS AND METHODS

4.1 Mitral Valve Preparation

For this study, fresh porcine mitral valves were used. Fresh porcine hearts were attained from a local abattoir; the mitral valves were extracted and stored in 0.9% saline solution. The protocol for extraction of the mitral valves can be found in Appendix A. The sizes of the mitral valves were determined using an annuloplasty ring sizer (Edwards Life Sciences, CA, USA). Mitral valves with similar chordae insertion patterns and similar orifice size, commissural-commissural sizes of 34 mm, were used. Figure 4.1 shows the intact mitral valve after extraction.

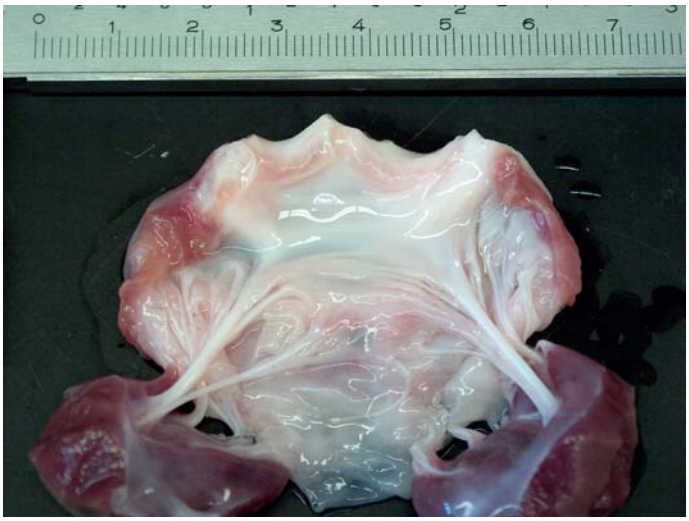

Figure 4.1: Intact mitral valve after extraction.

3.2 Chordae Tendineae Marker Technique

3.2.1 *In Vitro* Flow Loop

All experiments were completed in the modified Georgia Tech left heart simulator. The simulator is controlled by a pressure driven, compressible bladder pump, which uses a pulse generating computer system to control and synchronize the pump. Compressed air is fed to the system at 40 Psi by a portable compressor (Thomas Ultra Air Pac Model T-2820, Thomas Compressor and Vacuum Pumps, WI, USA). Solenoid valves, which are synchronized using a generic driver and pulse timer (TeleVideo Model 910, Televideo Inc., CA, USA), control the air supply to cyclically compress the silicon bladder in order to provide the driving force for the loop simulating ventricular pressure. By synchronizing the solenoid valves, a total cycle time of 860 ms, with a systolic duration of approximately 300 ms and a diastolic duration of 560 ms, was maintained.

Trans-mitral and ventricular pressures were measured using a differential pressure transducer (Model DP15-24 T1, Valydine Inc., Northridge, CA, USA) coupled to an amplifier/signal conditioner (Model CD23, Validyne Inc., Northridge, CA, USA). The trans-mitral flow rate was measured upstream from the valve using an electromagnetic flow probe (Model EP 680, Carolina Medical Instruments Inc., King, NC, USA) connected to an analog flow meter (Model FM501, Carolina Medical Instruments Inc., King, NC, USA).

The left heart simulator is composed of a gravity feed reservoir, an atrial chamber, and a ventricular chamber and bladder. Resistance and connective tubing were used to better generate physiologic flow conditions. Figure 4.2 is a schematic diagram of the left heart simulator. The system is filled with 0.9% saline solution as a blood analogue. The atrial

chamber is filled from the reservoir by gravity. The fluid then flows through the atrial chamber into the ventricular chamber through the native mitral valve. The compressible bladder pump creates increased pressure in the ventricular chamber causing the mitral valve to close, and the fluid to flow out through the aortic valve. Immediately following the aortic valve are sections of compliant tubing to simulate the aorta. Resistance is controlled using a manual clamp simulating circulatory systemic resistance. After this section of resistance and compliance tubing, the fluid returns to the reservoir to initiate the next cycle. This system is capable of physiologic and pathophysiologic flow and pressure waveforms. The Georgia Tech modified left heart simulator has been described in previous documents[14,15,16].

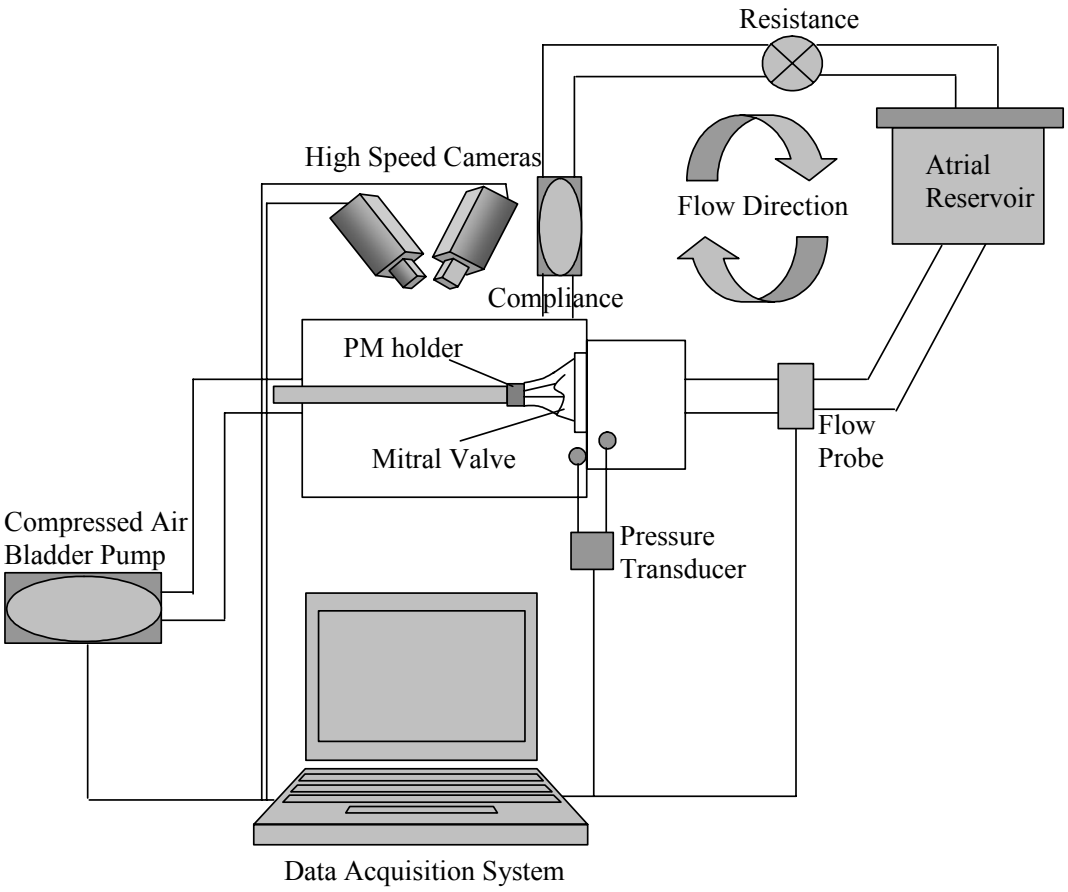

Figure 4.2: Schematic diagram of the Georgia Tech left heart simulator.

4.2.2 Left Ventricle Model

The left ventricle chamber is an octagon shaped acrylic chamber, Figure 4.3. The sides of the model are arranged at 60° angles to each other such that the cameras could be arranged perpendicular to the surface of the model in order to reduce the effects of refraction. The front section of the chamber, which holds the aortic valve, forms a 135° angle with the frontal face of the chamber to ensure geometrical positioning of the mitral and aortic valves. A 25 mm tilting disk mechanical valve (Omnicarbon 3523, MedicalCV Incorporated, USA) is used in the aortic position. Two syringes, connected through luers on the top of the ventricle chamber, are used as compliance in order to reduce fluctuations in the pressure waveforms. Detailed drawings of the ventricle chamber are located in Appendix B.

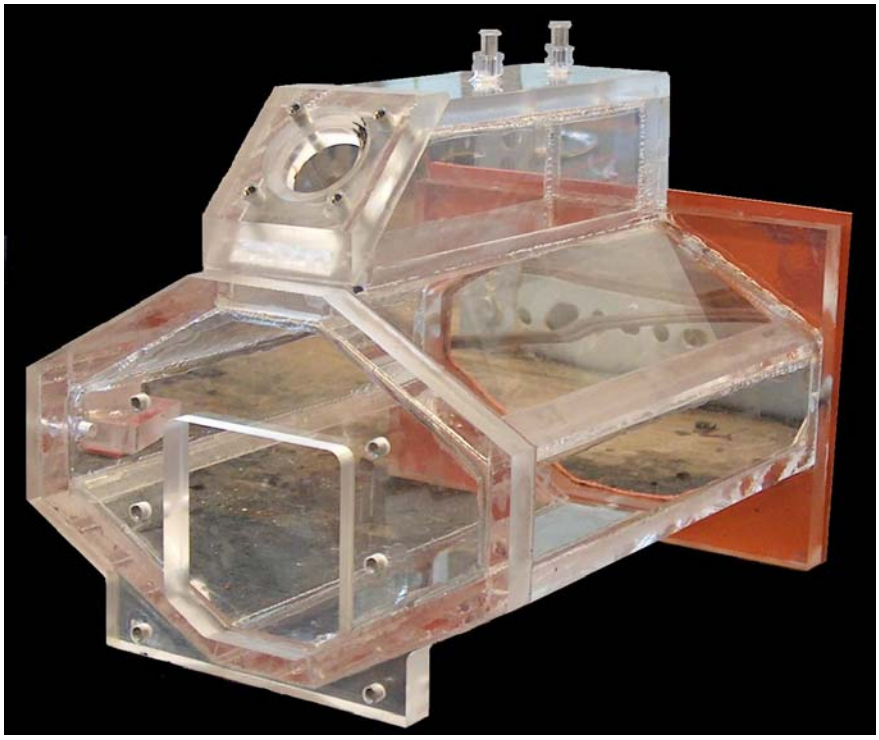

(a)

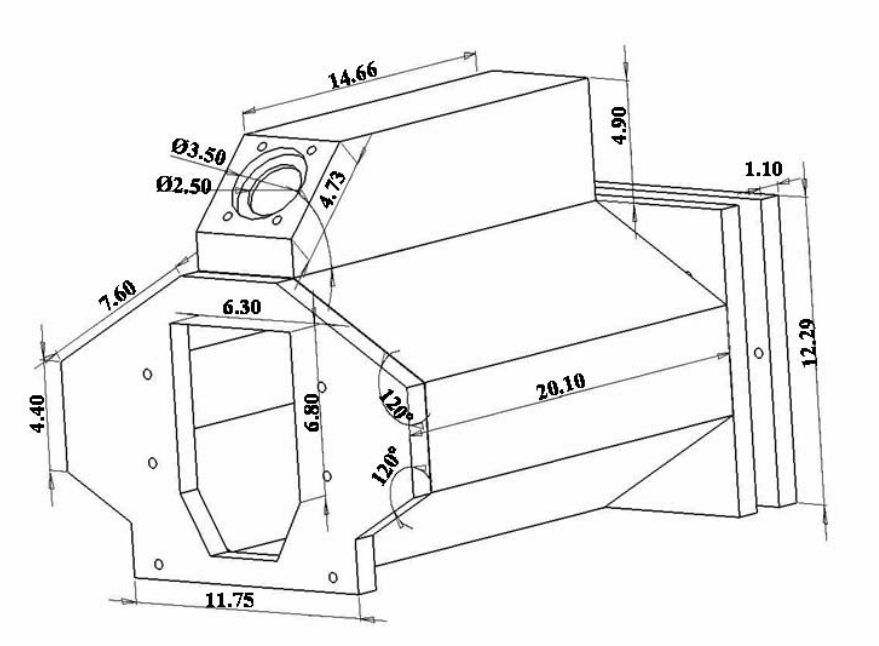

(b)

Figure 4.3: Model (a) and schematic (b) of the left ventricle.

A papillary muscle holding system was designed which allows three dimensional displacements of each papillary muscle individually, Figure 4.4. This allows the papillary muscles to be positioned in both physiologic and pathophysiologic conditions. The papillary muscles can be moved in the anterior/posterior, septal/lateral, and apical/basal positions independently. The papillary muscles are attached to holding disks, which are then attached to force rods as described in previous documents[14,16]. The forces rods are attached to the screw driven rod at 90°. This rod is attached through gears to the rod that goes through a tight fitting hole in the back of the ventricle chamber. The apical/basal position is determined using a caliper to measure the movement of the rod with respect to the back plate. The rotation of the outer rod allows measurement of the septal/lateral positions. The rotation of the inner rod moves the force rod along the elevator to measure the anterior/posterior position. Using this new system, exact displacements can be determined from a reference position without movement of the mitral valve, or opening of the ventricle chamber. Schematic drawings of the papillary muscle holding system are given in Appendix B.

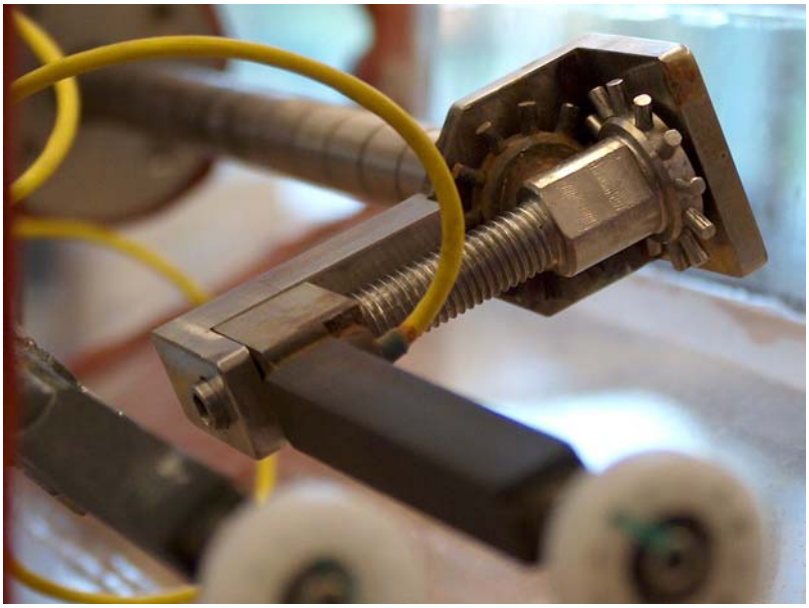

Figure 4.4: Picture of the papillary muscle holding system. The papillary muscles are sutured to the white holding disks. The position of the papillary muscle can be modified by: 1) movement of the green force rod along the length of the screw allows measurement of the anterior/posterior position; 2) movement of the rod with respect to the back plate for measurement of the apical/basal position; and 3) rotation of the outer rod allows measurement of the septal/lateral position.

4.2.3 Annulus Chamber and Board

The atrial chamber for the Georgia Tech left heart simulator has a rectangular volume of 229 cm^2 and a 2.5 cm diameter inlet, Figure 4.5. A cylinder attached to the top of the atrial chamber is used as air compliance to create physiologic pressure waveforms. A stopcock on the top of the chamber allows the extraction of air during setup. The exit orifice diameter is 4.5 cm, which attaches to the annular board. A stopcock on the right lateral wall is used to connect the pressure transducer. The annular board contains a flat annulus ring back plate which the mitral annulus was sutured. Details on the annulus chamber and board construction and geometry are available in a previous publication[14].

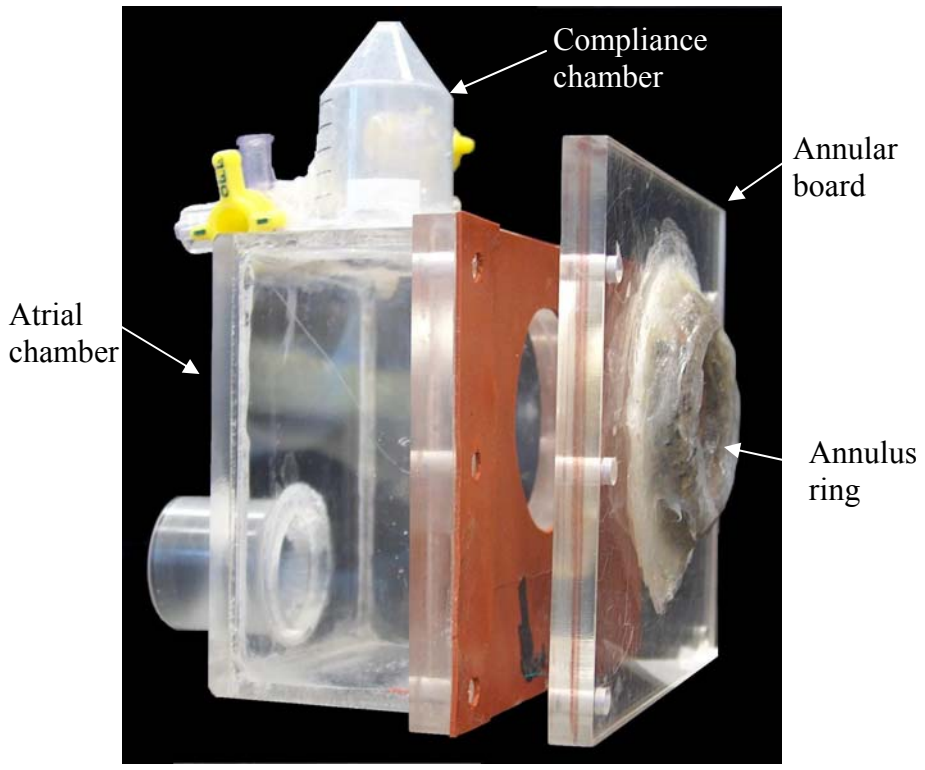

(a)

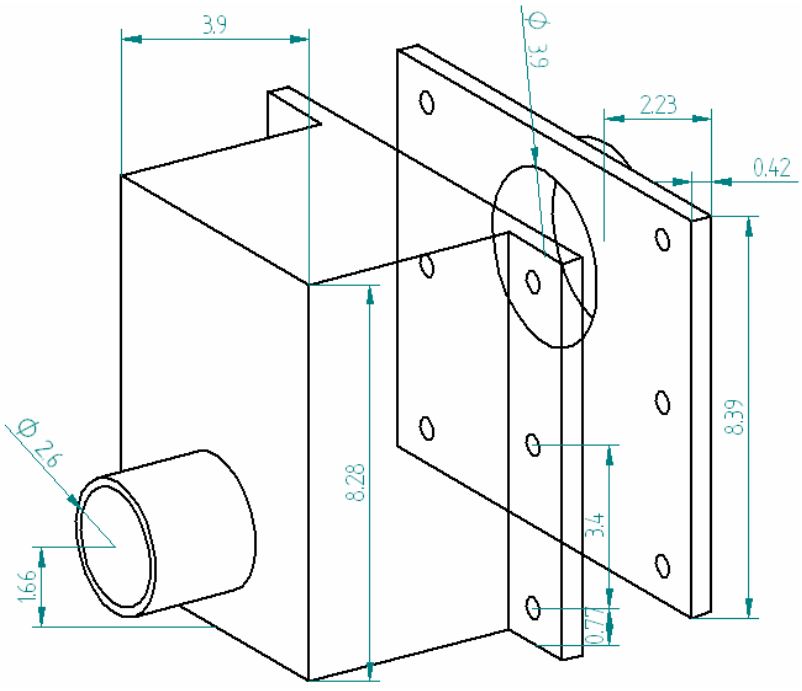

(b)

Figure 4.5: Left atrium model and rigid annulus ring. The valve is sewn using sutures to the rigid annulus ring. The annulus ring and atrial chamber are then connected to the ventricle model.

4.2.4 Instrument Calibrations

The trans-mitral and ventricular pressure transducers were calibrated using a differential water column. The positive and negative terminals of the transducer were calibrated independently. The voltage output of the pressure transducer amplifier was measured with a voltmeter and was recorded and plotted against the water column differential pressure to obtain the sensitivity of the system. An example of the calibration curve for the pressure transducer is shown in Figure 4.6.

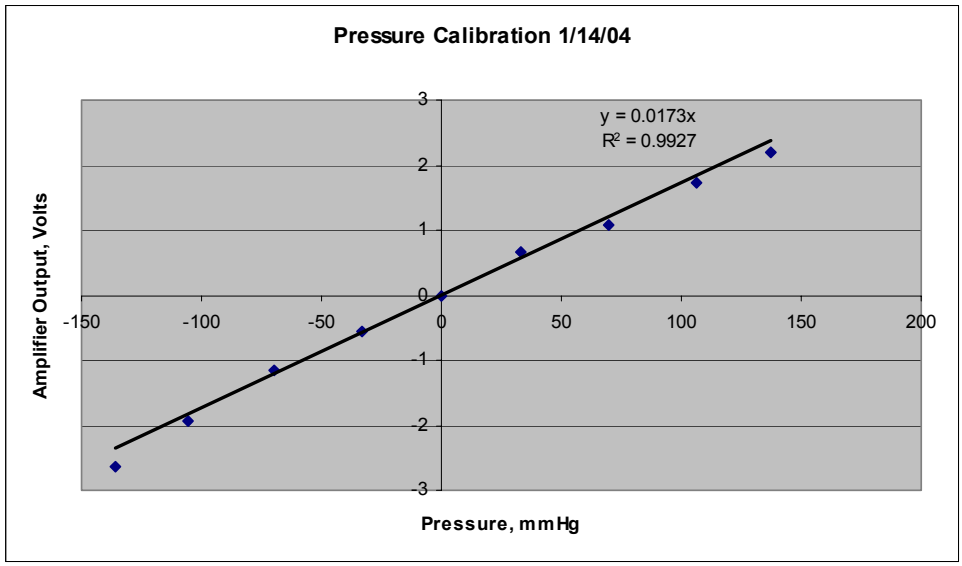

Figure 4.6: Calibration curve for the pressure transducer.

The flow probe was calibrated using a precision flow rotometer. The flow rotometer and the flow transducer were connected in series to a steady flow pump. The average flow in the loop was varied, and the output of the voltage of the flow amplifier and the rotometer flow were measured with a voltmeter and were recorded. An example of the calibration curve for the flow probe is shown in Figure 4.7. Detailed calibration procedures for both the flow probe and the pressure transducer are discussed in a previous document[14].

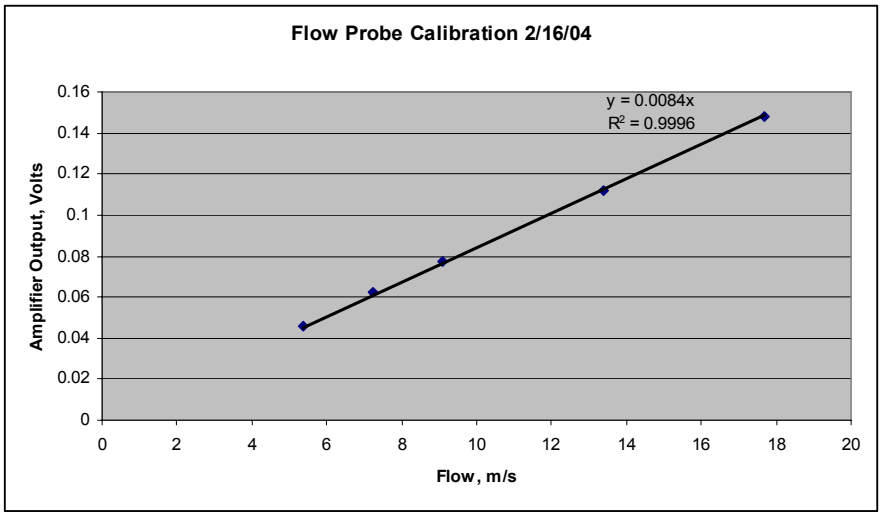

Figure 4.7: Flow probe calibration curve.

4.2.5 Graphite Markers

Graphite markers, approximately 0.368 mm in diameter were affixed to the desired chordae tendineae using super glue (Krazy Glue, Elmer's Products Inc., USA). Four graphite markers were affixed to the central region of the chordae where no branching was observed. Preparation of the graphite markers began by depositing a single drop of adhesive onto a plastic sheet. A suture needle held with forceps was dipped into the adhesive. A graphite particle was then picked up with the suture needle and placed in the adhesive until coated. The particle was then put on a clean sheet of paper to remove excess adhesive, leaving only a coating around the graphite marker. The particle was picked up with the suture needle and attached to the chordae. Care was taken to ensure that excess adhesive did not come in contact with the chordae. Four graphite markers were affixed to the central region of the anterior strut chordae where no branching was observed approximately 2 mm apart, 10 mm from the papillary muscle, and 12 mm from

the insertion into the anterior leaflet. Figure 4.8 depicts the correct placement of the graphite markers.

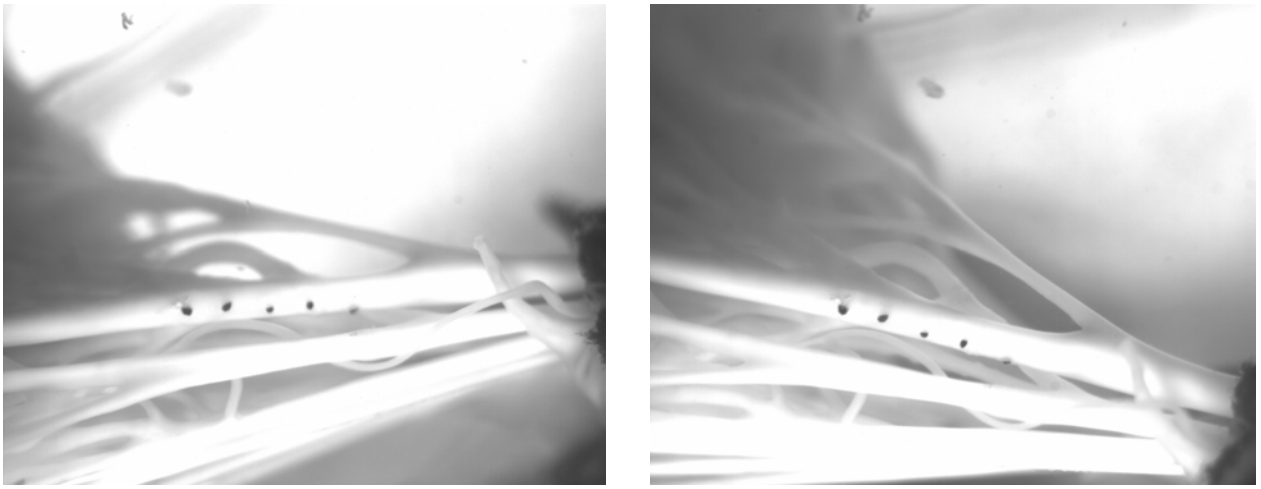

Figure 4.8: Pictures from cameras A and B showing the correct placement of the graphite markers.

4.2.6 Dual Camera Stereo Photogrammetry

Dual camera stereo photogrammetry was used to obtain pictures of the chordae tendineae during the cardiac cycle. Two high speed, high resolution cameras (Basler a504k, Basler Vision Technologies, PA) were positioned on tripods approximately 0.5 m from the ventricle chamber and 30° relative to each other. Figure 4.9 is a schematic showing the position of the cameras relative to the left ventricle model. Both cameras were positioned such that they were centered on the desired chordae, and light and lens (105mm f/2.8D AF Micro-Nikkor, Nikon, USA) were adjusted to achieve maximum contrast between the markers and background as seen in Figure 4.8 above.

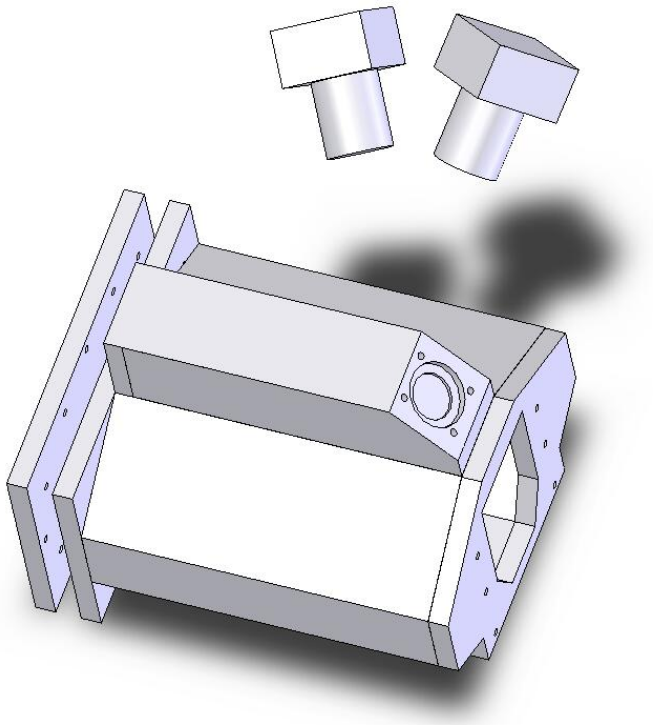

Figure 4.9: Schematic depicting the correct placement of the cameras.

Each camera was connected to an individual EPIX high speed frame grabber card (PIXCI CL3SD Frame Grabber, EPIX Inc., USA) which were synchronized using the EPIX software. Images were recorded simultaneously at 500 frames per second with an 8 bit gray-scale and a resolution of 1280 × 1023 pixels. A trigger signal was sent to a TTL module to ensure that the cameras and pressure data were recorded in synchronization.

4.2.7 Extension Tubes

Extension tubes (Vivitar Extension Tube Set f/Nikon AIS, Vivitar, USA) were attached to the end of both cameras to increase the resolution of the camera system. One extension tube was attached to each camera to increase the focal length an additional 36 mm. The increase in magnification can be determined using the following equation:

$$\frac{focal\ length}{sensorsize} = magnification$$

$$\frac{105mm + 36mm}{35mm} = 4.03$$

With the 36 mm extension tube, the markers had an average diameter of 11 pixels, which gave an average of 0.37 mm in diameter. The total magnification achieved with the extension tube was 4X. Figure 4.10 depicts the camera with the 36 mm extension tube and lens attached.

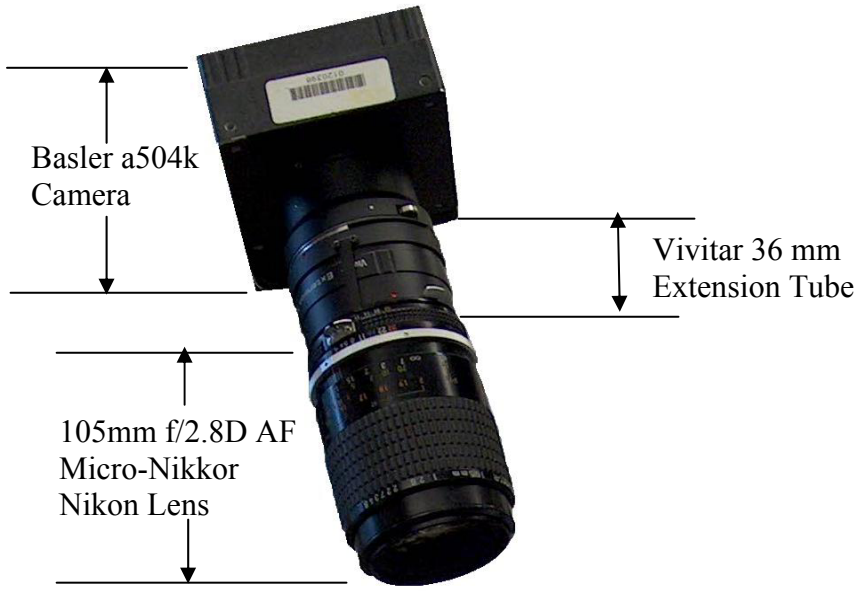

Figure 4.10: Diagram of the Basler camera with the Vivitar 36mm extension tube and micro-Nikkor Nikon lens attached.

4.2.8 Experimental Protocol

After valve extraction, detailed in Appendix A, the papillary muscles were wrapped in Dacron cloth and attached to the papillary muscle holding disks described earlier. The mitral valve was then sutured to the annular board described earlier using 3-0 sutures (braided silk, Ethicon, NJ, USA). After suturing, the annular board was inserted into the left heart simulator. The papillary muscles were attached to the force rods. After filling the loop with 0.9% saline solution, the flow probe and pressure transducer were zeroed. The valves were then placed in the defined normal position[17]:

- *Apical-Basal location*: The papillary muscle rods were moved towards the annulus to a point where slack was observed in all the chordae tendineae. The papillary force rods were zeroed at this location. Each force rod was pulled backwards until a change in voltage of 0.02 volts (0.09 Newtons) was achieved for that particular rod. This was the minimal significant change that may be observed by the system. This defined a position with no slack or apparent tension on the chordae tendineae.
- *Lateral location*: The papillary muscles arranged parallel to each other and directly aligned with the valve's annulus on each commissure. The commissural chords inserting in the annulus were vertically perpendicular to the annular plane.
- *Septal-lateral location*: The rods were moved septal laterally until an even extension of the commissural chords inserting into the annulus was observed. Normally, this point was a couple of millimeters below the annular height midpoint.

The two high speed, high resolution cameras were setup to capture images of the desired chordae as detailed in section 4.2.6. The cameras were set up 30° relative to each other and perpendicular to the surface of the ventricle chamber as described above. Light and lens were adjusted such that the markers could be clearly seen with both cameras as shown in Figure 4.8 above.

The simulator was run under physiologic flow and pressure conditions with the valve in the normal position (cardiac output: 5 L/min, peak trans-mitral pressure: 120 mmHg, heart rate: 70 BPM, systolic duration: 300 ms). Flow and pressure curves were saved on a laptop computer for offline processing.

Digital images were taken at 500 frames per second with a resolution of 1280 × 1023. The images were acquired as a sequence of TIFF images. The cameras were setup with a trigger system such that the cameras recorded images simultaneously and in sequence with the flow and pressure waveforms. A 5 volt signal sent from the waveform generator was split between the PCMCIA data acquisition card (Daq-card 1200, National Instruments, TX, USA) and the TTL module connected to the EPIX high speed frame grabber cards (PIXCI CL3SD Frame Grabber, EPIX Inc., USA). The DAQ-ANAL and EPIX software allowed collection of data at the beginning of the 5 volt trigger signal. This allowed the pressure, flow, and camera images to be recorded in synchrony. The images were processed offline. After collecting the data, a calibration cube 10 mm on edge was positioned in the area of the markers such that seven corners of the cube could be clearly seen with both cameras. The images of the cube were taken with both cameras, digitized, and used later for direct linear transformation (DLT).

4.2.9 Data Collection

The signal from the flow probe and pressure transducers is sent through a PCMCIA data acquisition card (Daq-card 1200, National Instruments, TX, USA). This card has eight different channels, which may be synchronized by a trigger. The flow and pressure data were recorded onto a laptop computer using DAQ-ANAL 2.1, an in house data collection program based on LabVIEW 5.0. Ten cardiac cycles are automatically stored for both flow and pressure data. The curves for the ten stored cardiac cycles were averaged and analyzed offline using Microsoft Excel. After deletion of deficient data, Excel was used to plot and store the averaged curves. The data acquisition system and the DAQ-ANAL 2.1 software have been described in detail in a previous document[14].

Dual camera stereo photogrammetry was used to obtain pictures of the chordae tendineae during the cardiac cycle. Each camera was connected to an individual EPIX high speed framegrabber cards (PIXCI CL3SD Frame Grabber, EPIX Inc., USA) which were synchronized using the EPIX software. Images were recorded simultaneously at 500 frames per second with an 8 bit gray-scale and a resolution of 1280 × 1023 pixels. A trigger signal was sent to a TTL module to ensure that the cameras and pressure data were recorded in synchronization.

4.2.10 Autotracking Code

The autotracking code was developed in house, and contains two different m-files written in Matlab, autotracking.m and marker_check.m. The first m-file, autotracking.m, requires four different inputs from the user; location of the image files, the first frame number to be tracked, the last frame number to be tracked, and the total number of markers to be tracked. The first image is displayed and the user must choose regions of

interests around each of the markers desired to be tracked. The program then crops the image to the region of interest, and blurs the image to reduce the impact of noisy pixels. A set threshold chooses the darkest 10% of the pixels and calculates their centroid. For the first three frames, the centroid of the marker defined in the first frame is used as the center of the search box. After the first three frames, the program estimates marker position using position, velocity, and acceleration calculations from the three previous frames. The center of the search box is then located at this new position.

After the autotracking has finished, the user then utilizes the marker_check.m file to check the position of the centroid of the markers and to generate a text file to be imported into the 3D reconstruction software. The autotracking.m and marker_check.m files are located in Appendix C.

The largest difference between five autotracked marker centroids was two pixels. For manual tracking, this difference increased to a five pixels difference. The position variation is due to the size of the search box and the number of pixels included for the adaptive threshold.

4.2.11 Direct Linear Transformation Code

Direct linear transformation method was used to transform the 2D pixel coordinates to 3D spatial coordinates. The program SW3D6.m, written in Matlab, was used to compute the 3D coordinates and is detailed in previous publications. This program utilizes the function dltfu.m and reconfu.m originally written by Christoph Reinschmidt from the University of Calgary. This program has four different phases: loading of the 2D data sets, calibrating camera coordinates, computing the 3D coordinates, and writing the output text file. When loading 2D data sets, the program will ask for two filenames,

these are where the 2D coordinates are stored for each camera. For calibrating the camera coordinates, the program will ask for three filenames. These are where the 2D coordinates of the cube corners and the known 3D coordinates of the cube, reference, are stored. When computing the 3D coordinates, the x, y, and z coordinates are calculated using the least squares method. After computation of the 3D coordinates, the output file is written. The program will ask for two pressure files (ventricular and trans-mitral) to synchronize the pressure data with the image data. The output is in the following format:

Row 1: number of frames, number of markers

Row n: frame number, time, ventricle pressure, trans-mitral pressure

Row n+1: X,Y,Z coordinates

The SW3D6.m code and the supporting m-files are located in Appendix C.

4.2.12 Strain Code

The strain was calculated using the infinitesimal strain definition. This has been proven to approximate the strain for soft tissue mechanics if the strains are small.

The strain.m algorithm written in Matlab takes the text file output from SW3D6.m and calculates the distance between each marker and the total distance between markers one and three. After calculating the total distance, the program will ask for one input, the reference distance. The strain is then calculated using the infinitesimal strain definition.

The reference frame for the strain calculations was determined during the cube calibration. With no pressure on the valve, the valve was defined to be in a relaxed state during calibration. This relaxed state was used as the zero strain reference. A wire of known spatial length was used as a ruler, and positioned parallel to the maker placements on the chordae during the calibration to obtain pictures of the chordae in the relaxed state.

Pictures were obtained for both cameras and subsequently imported into Sigma Scan Pro (Jandel Scientific, San Rafael, CA, USA), and the distance between each centroid of the markers was recorded.

The output from strain.m has the following form: frame number, time (assuming 500 fps), ventricular pressure, trans-mitral pressure, distance between markers 1 and 2, distance between markers 2 and 3, total distance between markers 1 and 3, and the strain. This text output is formatted to be inputted into Microsoft Excel for further analysis. The algorithm for strain.m is located in Appendix C.

4.3 Uniaxial Test

4.3.1 Specimen Preparation

The uniaxial tests were performed no more than 24 hours after the *in vitro* flow loop experiments using a Test Resources servohydraulic testing machine (model 650R, Shakopee, MN). The same chordae and the same markers were utilized for both experiments. The chordae were extracted from the mitral valve and separated into chordal type by insertion location. During specimen preparation, a section of leaflet tissue 5 mm above the insertion location into the leaflet was left intact. A section of papillary muscle tissue, approximately 8 mm in diameter, was left intact where the chordae and the papillary muscle connect. The leaflet tissue was inserted between two clamps and positioned into the upper grip of the machine. The clamps were constructed out of aluminum with teeth spaced 0.5 mm apart, Figure 4.11. The teeth allowed secure clamping of the tissue without slippage which occurred during testing with other clamping mechanisms. The cross head was then jogged until the papillary muscle could be placed in the lower grips of the machine. This preparation technique allowed the

clamping mechanisms to not come in contact with the chordae. This was used to reduce grip and end effects that occur during tension testing. The sample was placed in the clamps as shown in Figure 4.11. The clamping mechanism held the papillary muscle below the point of chordae insertion and the leaflet tissue above the point of insertion such that the chordae were not gripped by the clamps during testing.

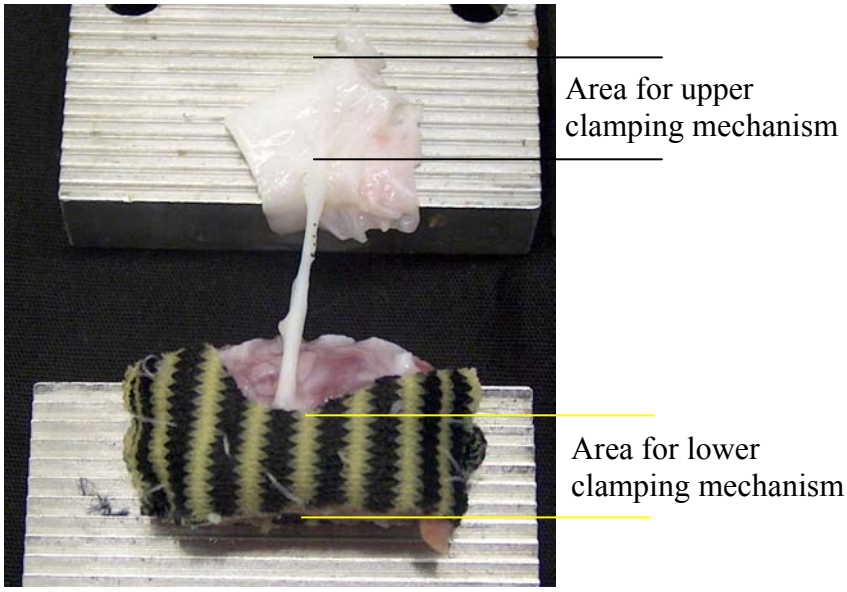

Figure 4.11: Chordae placed in the uniaxial clamps. The clamps were constructed out of aluminum with teeth spaced 0.5 mm apart. A section of leaflet tissue 5 mm above the insertion location into the leaflet was left intact. A section of papillary muscle tissue, approximately 8 mm in diameter, was left intact where the chordae and the papillary muscle connect. The leaflet tissue was inserted between two clamps and positioned into the upper grip of the machine.

Preliminary experiments were conducted to determine the best method of specimen insertion in the testing machine. If the chordae were extracted from the leaflet and papillary muscle and placed in a clamping mechanism such that the chordae was clamped, as previous investigators have done, major grip and end effects would occur and cause higher stress concentrations on the ends of the tissue. The ends of the chordae in the clamps would also plastically deform during testing. Therefore, the leaflet tissue

above the insertion site and the papillary muscle around the insertion site should be left intact and used during clamping. This is similar to clamping mechanisms used to perform tendon testing in which the muscle and bone surrounding the ends of the tendon are left intact and placed in the clamping mechanism. Various clamping mechanisms were also investigated during these preliminary experiments. Standard soft tissue testing typically utilizes high grade sandpaper to be placed between two metal clamps to provide friction during testing. However, during these experiments, slippage occurred when using sandpaper or sandpaper and superglue to clamp the specimen. It was found that the metal teeth provide the best stability during uniaxial testing. If the clamps are placed correctly in the machine, it was found that no slippage, tearing, or deformation of the tissue occurred.

Since this test was uni-directional, only one high speed, high resolution camera was setup perpendicular to the test. Figure 4.12 shows the setup of the camera for the uniaxial test. Three extension tubes, for an increased focal length of 68 mm, were used with the camera.

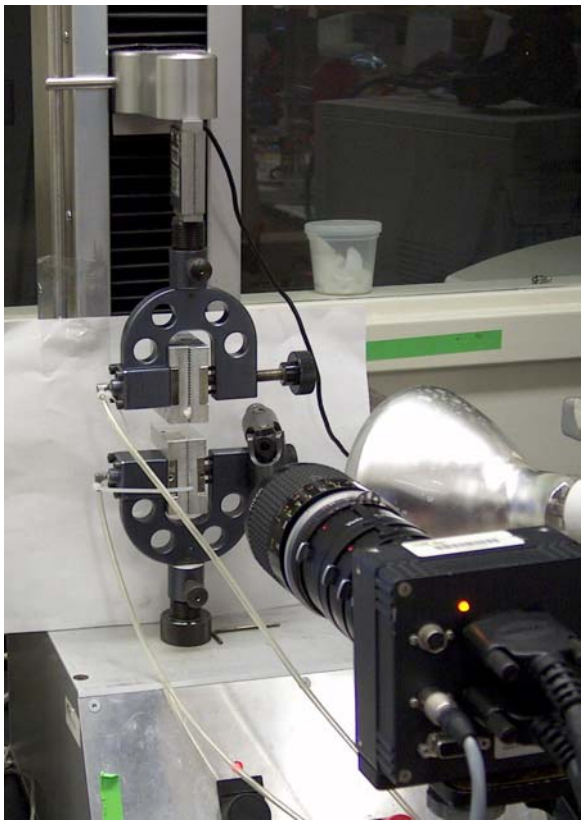

Figure 4.12: Picture depicting the uniaxial test setup. One high speed, high resolution camera was set up perpendicular to the movement of the test specimen. A light was placed beside the camera to enhance the contrast of the specimen against the background.

4.3.2 Experimental Protocol

The chordae were inserted into the uniaxial machine and were unloaded until the chordae was slack. A calibration picture of the chordae and a millimetric ruler was taken to determine the millimeter to pixel conversion. Using Sigma Scan Pro, the distance between the markers was determined in millimeters. This calibration allowed the loading rate to be set at 40% per second of the distance between the markers for the chordae. The chordae were preloaded at a 40% strain per second rate up to 2 N force for 25 cycles. This force was chosen since previous studies have shown that the strut chordae withstand a force of approximately 1.5 N during the cardiac cycle[17]. After appropriate preloading,

when the loading and unloading curves were repeatable, typically 20 cycles, the chordae were immediately loaded with the same parameters (40% strain per second up to 2 N force) for five cycles. The camera and testing machine were set to a frame rate of 45 frames per second. This was the highest frame rate that the testing machine could record. In order to ensure synchronization between the testing machine and the camera, the signal from the computer sent to an external interface box was split between the two systems. The signal is then sent from the I/O channel to the machine. Pin 16 from the digital input-output port on the external interface box controls the machine as to when to start the test. This is achieved by sending a 5 volt signal through this pin. In order for the machine and the camera computer to begin recording at the same time, this 5 volt signal was split from pin 16. All the other pins remained the same and were sent to the machine. Pin 16 and pin 1, digital ground, were split and sent to the machine and to the TTL module on the camera computer. This 5 volt signal was sent from the Mtest WR software to the external interface box which was then split to the camera computer and the machine such that the data could be synchronized.

4.3.3 Data Analysis

The pictures of the uniaxial test were processed with the same protocol as the *in vitro* flow loop picture files. The uniaxial data was processed using the autotracking code to track the same markers as those recorded during the *in vitro* experiments. Using the calibration picture taken before the test as described above, the pixel coordinates were transferred to spatial coordinates. In order to have the same definition for infinitesimal strain, the initial length used for the *in vitro* experiments was used as the initial length for the uniaxial data. The load data obtained from the force transducer was then correlated

with the strain data captured with the camera. Because the camera and the testing machine were synchronized with a trigger signal, there was a one-to-one correspondence between the load data and the strain data. The load-strain data were then fitted with a mixed linear-exponential curve.

4.4 Chordae Force Marker Technique

After data collection from the *in vitro* flow loop and the uniaxial test, load versus strain and stress versus strain curves can be generated. The data from the uniaxial test must be curved fitted in order to generate a relationship between the load and strain. Due to the shape of the uniaxial data, a linear and exponential curve fit is necessary.

The curve fits were then used with the strain data from the *in vitro* flow loop data. The strain from the flow loop data was put into the correct equation and the corresponding load was calculated. Then, a load versus time curve was generated for the *in vitro* flow loop. This curve could also be plotted with trans-mitral pressure to indicate at which point in the cardiac cycle the maximum load was attained.

4.5 Histology and Biochemical Composition

4.5.1 Tissue Processing

Chordae tendineae were dissected from fresh porcine mitral valves according to insertion location. Figure 4.13 is a schematic diagram of the chordae tendineae classified by their insertion into the leaflets. After extraction, the chordae tendineae were fixed in 10% neutral buffered formalin for 24 hours. The chordae tendineae were transferred to 70% ethanol until tissue processing. The tissue was processed in paraffin using the Shandon Pathcentre. After tissue processing, the chordae tendineae were embedded in paraffin

wax in both the longitudinal and radial directions. This allowed the tissue to be cut into 5 micron sections with a Microtome Microm HM355S and placed on specially treated slides (Superfrost, Plus, Shandon). The tissue sections where dried overnight in a 37°C incubator, and then utilized for different staining protocols. Standard deparaffinization was performed on each slide before staining. Deparaffinization was completed with xylene, descending grades of alcohol, and finally to deionized water.

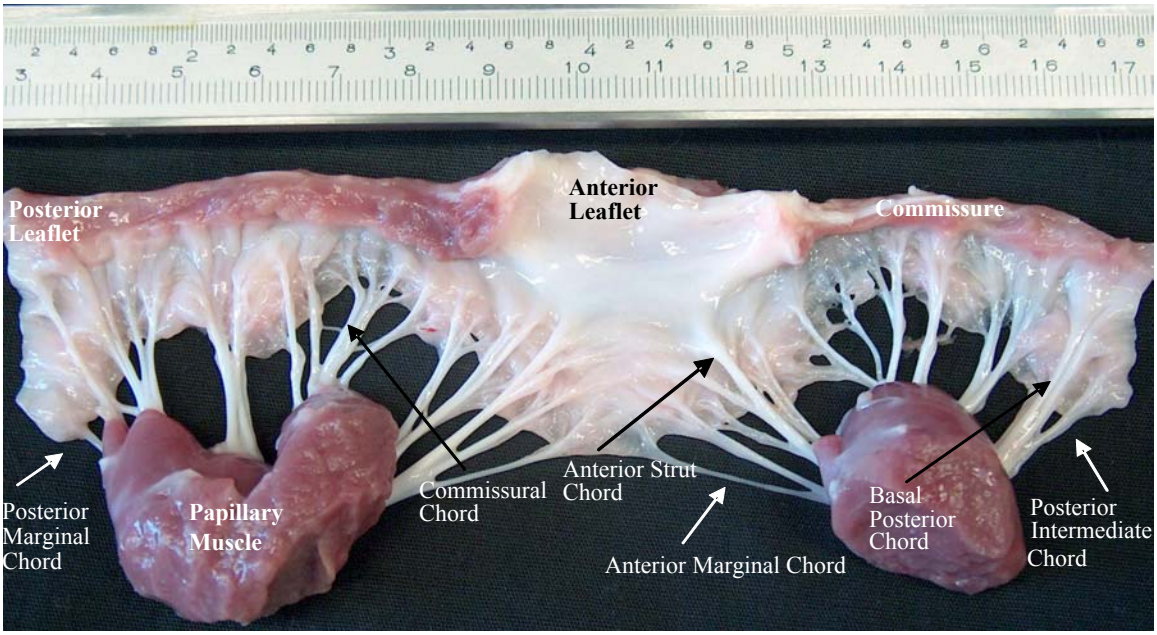

Figure 4.13: Diagram showing the chordae insertion pattern of the mitral valve. The valve was cut along the posterior leaflet. Six different types of chordae are shown. The histology studies focused on all six chordae. The *in vitro* tests focused on the anterior strut chord.

After staining, all slides were observed with either conventional brightfield microscopy or a 100 Watt mercury lamp fluorescence light source using the Nikon Eclipse E600 microscope/imaging system. Images were recorded with a high-resolution CCD camera (Quantix, Photometrics) using Quantum Image (Release 4.0) software. All images had a final image resolution of 1280 X 1024 and a 48 bit intensity resolution.

4.5.2 Hematoxylin and Eosin Stain

A standard hematoxylin and eosin (H & E) stain was performed to determine cellular distribution. After deparaffinization, the tissues were stained with hematoxylin to stain the cell bodies black and eosin to stain the surrounding tissue pink. The deparaffinization and H & E stain were performed with a Leica Autostainer XL following a standard H & E protocol which can be found in Appendix D. Coverslips were mounted over the sections with Permount and air dried overnight. The H & E sections were viewed with both brightfield microscopy and fluorescence with the Nikon Eclipse E600 microscope.

4.5.3 Verhoeff and van Gieson Stain

A standard Verhoeff stain followed by a van Gieson stain was performed to determine collagen, elastin, and cellular distribution. After deparaffinization, the sections were stained for 20 minutes in Verhoeff's elastic stain. The sections should appear jet black after this stain. Microscopic differentiation was carried out in 1% ferric chloride until the background tissue was colorless and the elastic fibers were black. If sections were over differentiated, they were replaced in the Verhoeff's elastic stain and microscopic differentiation was carried out again. After rinsing in distilled water, the sections were place in sodium thiosulfate for 1 minute to remove the iodine. After rinsing in running tap water, the sections were stained in a van Gieson solution for 1 minute. The sections were dehydrated through ascending grades of alcohol, cleared in xylene, and cover slips where mounted with Permount. Arterial cross sections were used as a control during the staining process.

During the Verhoeff stain, the elastin and cell bodies are stained black. The iodine in the Verhoeff solution may act as a trapping agent for the cationic dye, facilitation staining of

elastic fibers and retarding the extraction of stain from elastic fibers during differentiation. The dilute ferric chloride solution used for differentiation is used to break the tissue dye complex. Also note that the picric acid in the van Gieson stain will also act as a differentiation agent. The van Gieson stain is used to differentiate the collagen from the other tissue. The collagen appears red, while the other tissue remains yellow. The Verhoeff and van Gieson stain was observed using brightfield microscopy with the Nikon Eclipse E600 microscope.

4.5.4 Verhoeff and Light Green Stain

A standard Verhoeff stain followed by a light green stain allowed for observing elastin distribution. Due to the picric acid contained in the van Gieson solution, the continued differentiation of the elastin fibers caused them to release the dye making it difficult to delineate the elastin fibers in the tissue. Therefore, by using a light green stain as a counterstain to the Verhoeff, the elastin maintained the cationic dye. The procedure followed was similar to the Verhoeff and van Gieson stain; however, in place of the van Gieson stain, a light green stain was used. The same clearing and mounting procedure was used as before. The protocol is located in Appendix D. The elastin and cell nuclei stain black and the remaining tissue stains light green. The Verhoeff and light green stain was observed using brightfield microscopy with the Nikon Eclipse E600 microscope.

4.5.5 Immunohistochemistry

Immunohistochemistry was performed on all six chordae tendineae in the radial direction to verify the finding of vasculature. After standard deparaffinization and rehydration to water, the sections were washed in 1X PBS for five minutes. This wash in PBS stabilizes

the antigen-antibody interactions. The sections were pretreated with 100 μg/ml of protease for 10 minutes in order to better expose the antigen of interest. During pretreatment, the sections were incubated in a humid container. Sections were washed in 1X PBS to remove the excess enzyme. Endogenous peroxidase, false positives, was blocked using 0.3% H_2O_2 in methanol for 15 minutes. After rehydration in 1X PBS, the tissue was blocked with 1% gelatin/PBS mixture to neutralize the tissue to prohibit non-specific binding. The first antibody, rabbit α-vWF, was applied and the sections placed in a humid chamber for 1 hour. After washing in 1X PBS, a biotinylated secondary antibody, goat anti-rabbit IgG, was applied and the sections were incubated for 30 minutes in a humid chamber. Once the slides were washed in 1X PBS, the ABC mixture, avidine-biotin-peroxidose, was applied to the slides and incubated in a humid chamber for 1 hour. The avidine binds with the biotin which was contained in the second antibody. After washing in 1X PBS and deionized water, diaminobenzidine, DAB, was applied to each section for 4 minutes. The sections were then counterstained with hematoxylin, dehydrated through graded alcohols, xylene, and coverslipped with Permount. The sections were observed using brightfield microscopy with the Nikon Eclipse E600 microscope. The exact protocol is located in Appendix D.

4.5.6 DNA, Collagen, and Elastin Assays

Assays were performed on all six chordae tendineae to quantify the amount of DNA, collagen, and elastin contained in each of the different chordae. After dehydration for 48 hours, the tissue was then digested according to the specific assay. For the DNA and elastin assays, the tissue was digested for approximately 6 days with proteinase K, incubated in a water bath at 55°C. Since the chordae contain soluble and insoluble

collagen components, two digestion processes were utilized. For the collagen assay, the tissue was digested for approximately 24 hours with pepsin to digest the soluble collagen and then placed in a water bath at 80°C to dissolve the insoluble collagen. The protocols for the DNA, collagen, and elastin assays are given in Appendix D.

4.6 Statistical Analysis

All mechanical (flow loop and uniaxial) and biological (histology and biochemical) data are reported as mean ± one standard deviation unless otherwise stated. Means were compared using t tests for paired comparisons. A p-value less than 0.05 was considered significant. Statistical analysis was computed using Minitab (version 14) software.

CHAPTER 5

RESULTS

5.1 Overview

The results for this study are divided into four main sections. Section 5.2 contains the results for the anatomical measurement of the anterior lateral and posterior medial strut chordae study. Section 5.3 contains the results for the *in vitro* flow loop studies. All data for this study are included in the results chapter. Section 5.4 contains the results for the uniaxial test completed on all eleven strut chordae. All raw and processed data for this study are included in the results chapter. Section 5.5 contains the results for the histological and biochemical composition of the chordae tendineae. All processed data are included in the results chapter. All raw data for the biochemical assays can be found in Appendix E. Additional histological pictures not shown in the results chapter can be found catalogued on CD1.

5.2 Anatomical Measurements

Measurements of the diameter and length from the origin in the papillary muscle to insertion point on the anterior leaflet were taken of both the anterior lateral and the posterior medial strut chordae. The strut chordae which inserted in the posterior medial papillary muscle had a diameter of 1.68 ± 0.22 mm and a length of 36.29 ± 3.23 mm. The strut chordae which inserted in the anterior lateral papillary muscle had a diameter of 1.47 ± 0.12 mm and a length of 29.82 ± 5.18 mm. It was found that there was a

significant difference ($p<0.02$) between the diameter and lengths of the two strut chordae, shown in Figure 5.1.

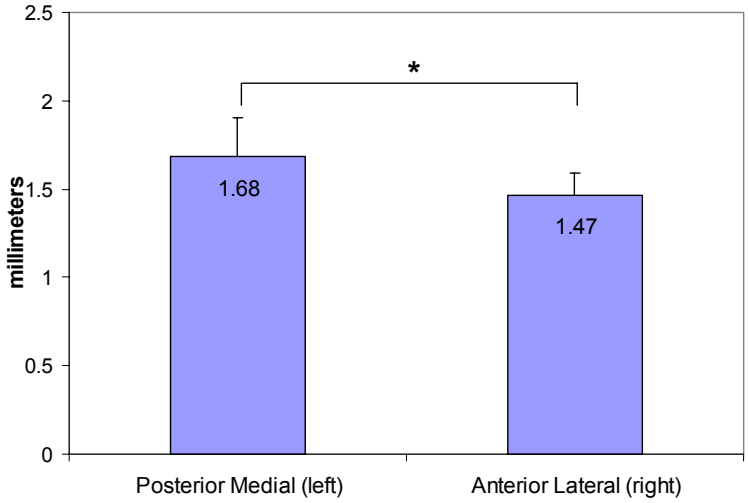

(a)

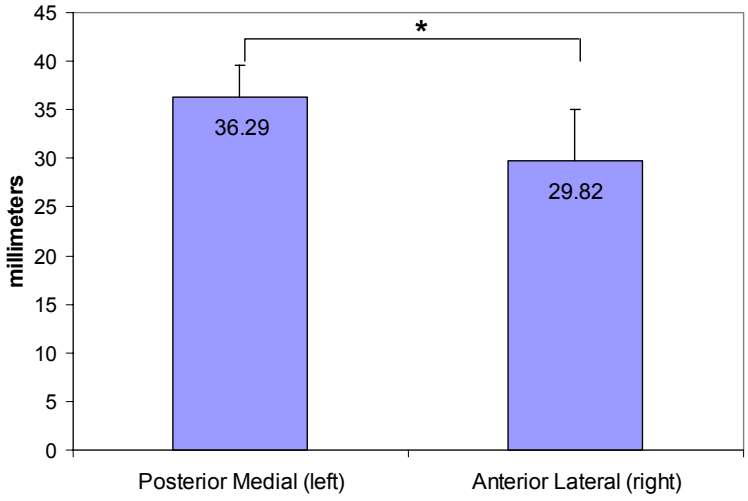

(b)

Figure 5.1: Geometrical differences between the posterior medial and anterior lateral strut chordae in (a) diameter and (b) length (* indicates $p< 0.05$). It was found that there was a significant difference ($p<0.02$) between the diameter and lengths of the two strut chordae. The strut chord which inserted into the posterior medial papillary muscle was significantly longer and thicker than the strut chord which inserted into the anterior lateral papillary muscle.

Table 5.1 below contains the values of the diameter and length for all posterior medial and anterior lateral strut chordae measured.

Table 5.1: Diameter and length measurements for both strut chordae. It was found that there was a significant difference ($p<0.02$) between the diameter and lengths of the two strut chordae. A p-value less than 0.05 was considered significant.

	Diameter (mm)		Length (mm)	
Specimen	*Posterior Medial*	*Anterior Lateral*	*Posterior Medial*	*Anterior Lateral*
1	1.826	1.505	37.304	28.109
2	2.060	1.471	39.544	39.544
3	1.481	1.526	38.455	25.822
4	1.610	1.638	29.359	26.953
5	1.351	1.293	35.423	24.525
6	1.576	1.302	39.136	34.555
7	1.611	1.391	33.786	31.715
8	1.759	1.445	35.486	24.357
9	1.887	1.631	38.150	32.797
Average	1.685	1.467	36.294	29.820
Std. Dev	0.219	0.125	3.232	5.178
p-value	0.020		0.006	

5.3 Flow Loop Experiments

A total of six valves and eleven strut chordae were examined during this study. Figures 5.2 a-k depicts the strain experienced during the cardiac cycle under physiologic flow conditions for all eleven strut chordae examined. The valves were tested at a peak trans-mitral pressure of 106.1 ± 7.7 mmHg and mean cardiac flow of 5.41 ± 0.35 L/min. When tested under the defined normal position[13,17], the valves coapted well with no regurgitant orifices.

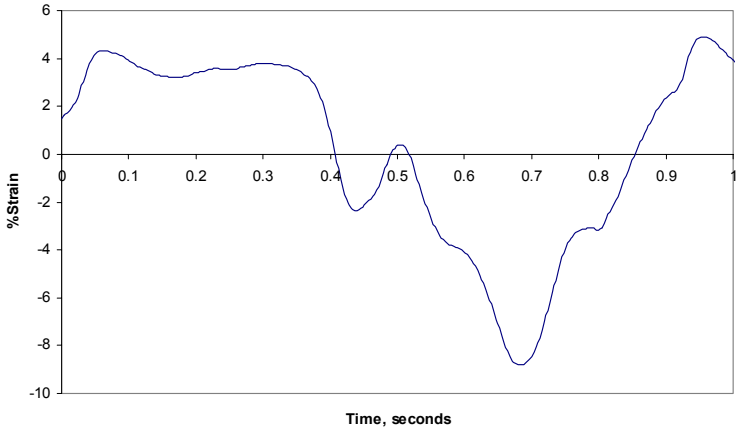
%Strain
Time, seconds

(a)

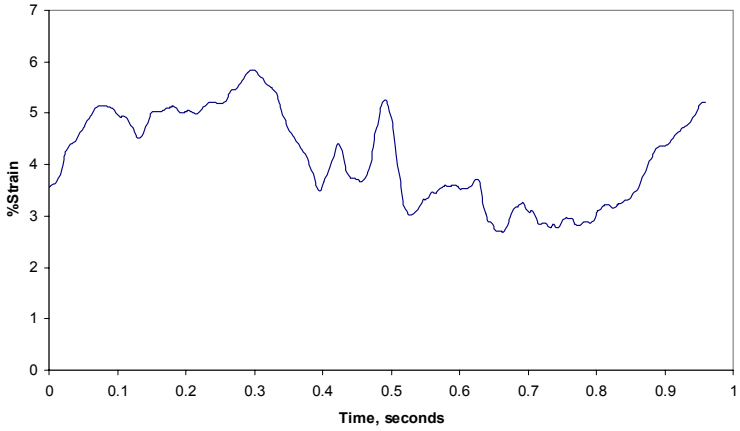
%Strain
Time, seconds

(b)

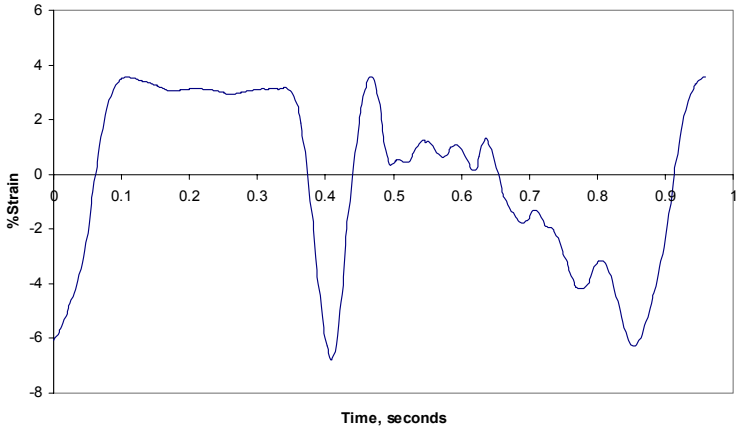
%Strain
Time, seconds

(c)

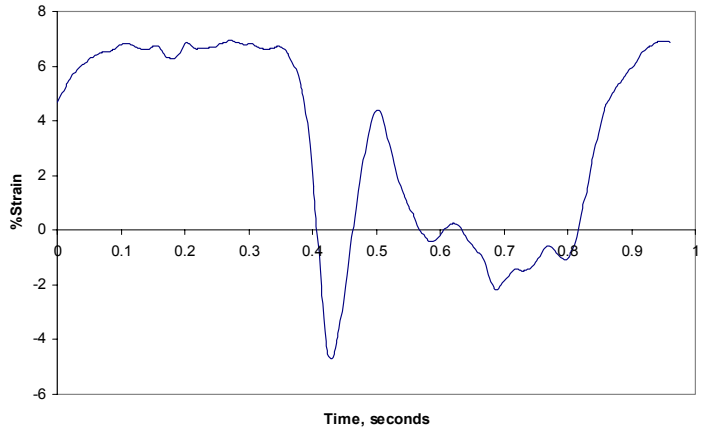
%Strain
Time, seconds

(d)

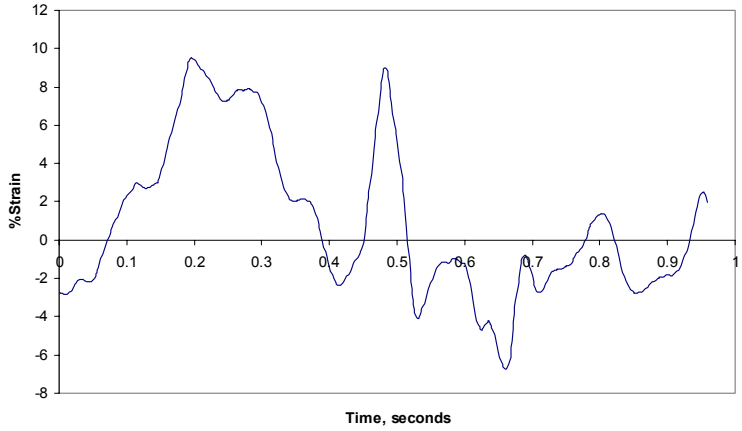
%Strain
Time, seconds

(e)

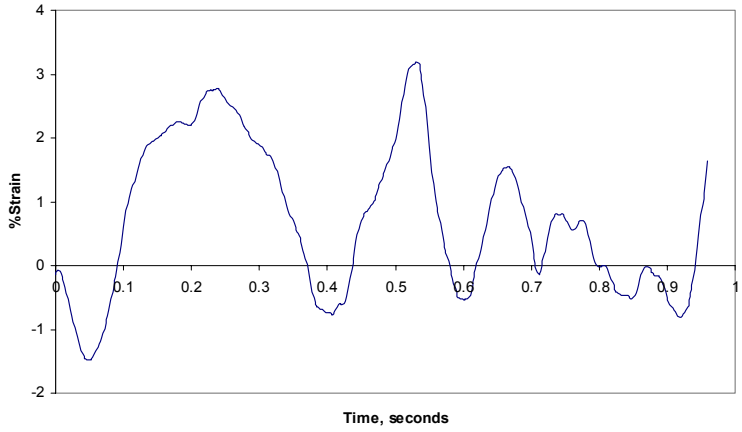
%Strain
Time, seconds

(f)

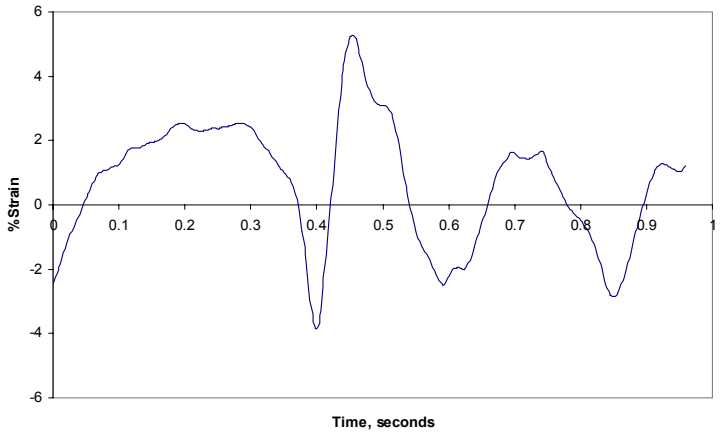
%Strain
Time, seconds

(g)

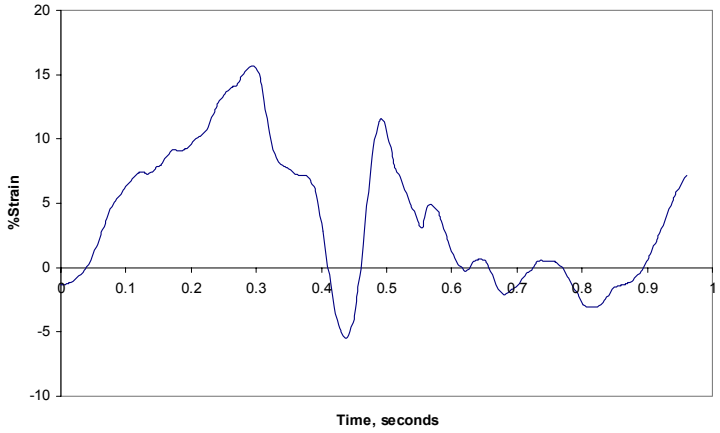
%Strain
Time, seconds

(h)

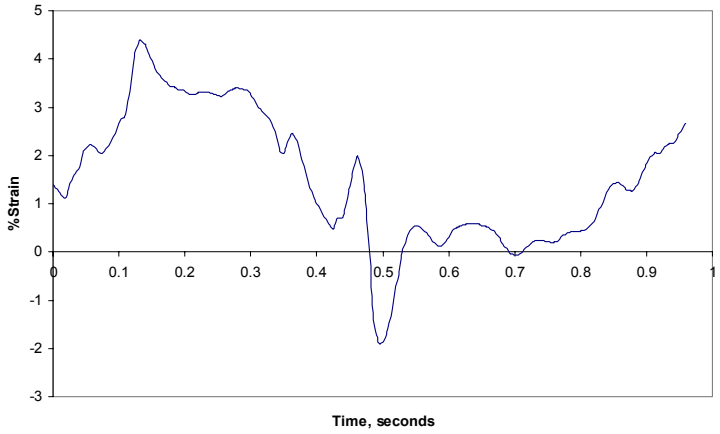
%Strain
Time, seconds

(i)

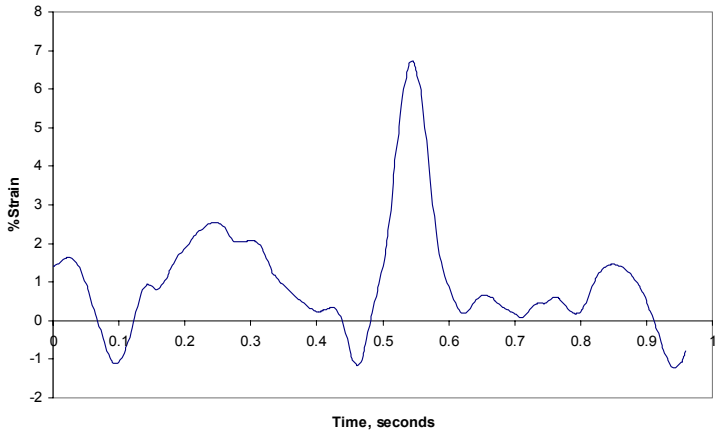

(j)

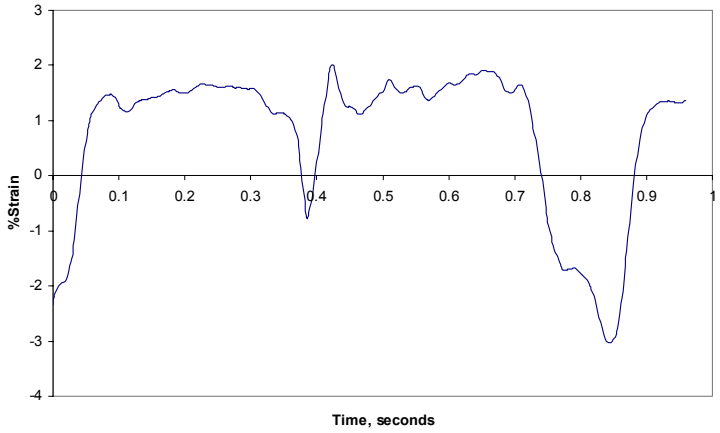

(k)

Figure 5.2: Strain data from eleven strut chordae from the flow loop experiments. Anterior lateral strut chordae (a, c, e, g, i) and posterior medial strut chordae (b, d, f, h, j, k).

Figure 5.3 describes the cardiac cycle with 0 msec representing when the mitral valve begins to close. All subsequent time references correspond to the time in the cardiac cycle as described in Figure 5.3.

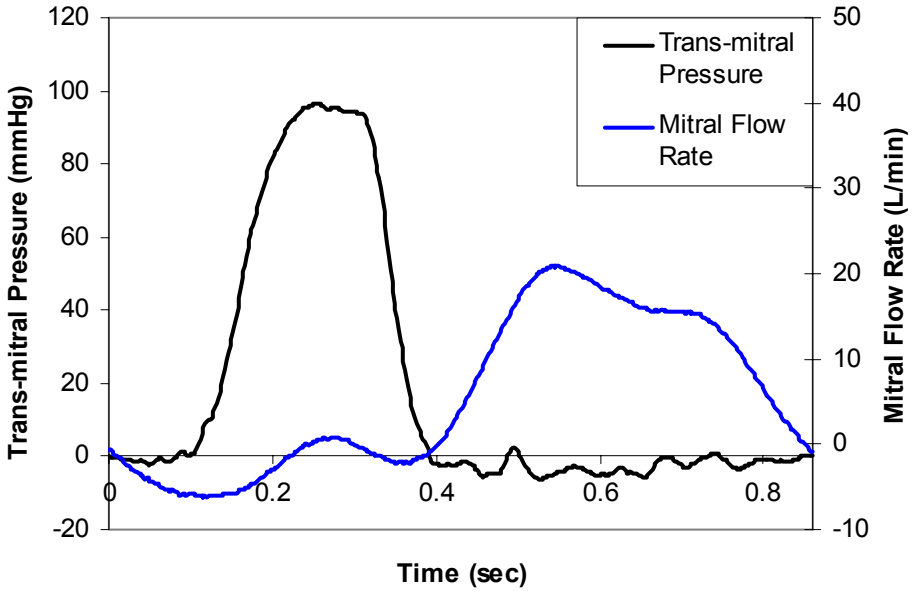

Figure 5.3: Pressure and flow curves from the Georgia Tech left heart simulator. The valves were tested at a peak trans-mitral pressure of 106.1 ± 7.7 mmHg and mean cardiac flow of 5.41 ± 0.35 L/min.

The average strain experienced on the chordae is given in Figure 5.4. The maximum strain experienced during the cardiac cycle was 4.43% ± 3.43% and was experienced at 249 msec after the start of valve closure. The valve closed between 14 and 150 msec with a strain rate of approximately 75.3% ± 48.6% strain per second on both strut chordae. It was also found that the strain increases in both strut chordae after the start of valve closure and plateaus before the trans-mitral pressure increases at valve closure; hence the trans-mitral pressure and chordae strain increases are not synchronized. There is a strain plateau after the start of valve closure between 192 and 298 msec. The valve opened between 320 and 420 msec with a strain rate of approximately -54.8% ± -56.6% strain per second on both strut chordae. Between 420 and 486 msec, the anterior leaflet opened to its maximum. After 486 msec, the valve remained open until 860 msec, when

the next cycle begins. Immediately after opening, there is a small negative strain on the strut chordae which occurs when the strut chordae and the anterior leaflet are parallel to each other, causing a no strain situation on the chordae. Immediately after this negative strain, when the anterior leaflet continues to open, there is a large peak in strain at 486 msec which corresponds to the maximum leaflet opening. The chordae then pulls the anterior leaflet back to a situation of little or no strain. Small oscillations in the chordae occur when the valve is open and the fluid flows from the atrial chamber through the mitral valve and into the left ventricle chamber.

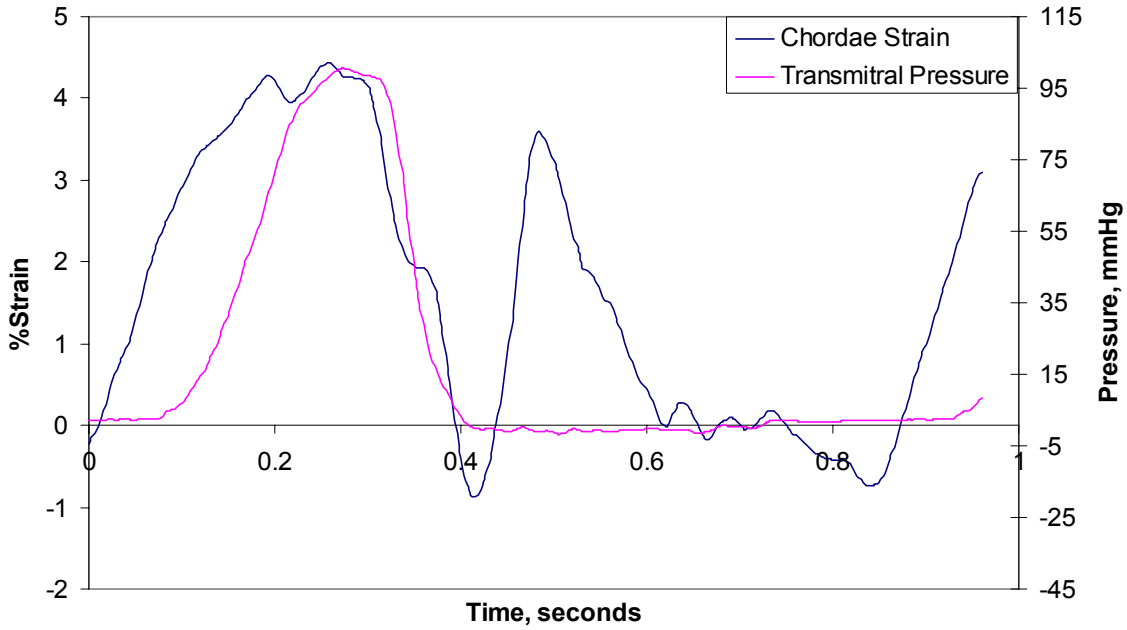

Figure 5.4: An example of strain versus time relationship for the in vitro measurements of strain using dual camera stereo photogrammetry. The maximum strain experienced during the cardiac cycle was 4.43% ± 3.43% and was experienced at 249 msec after the start of valve closure. The valve closed between 14 and 150 msec with a strain rate of approximately 75.3% ± 48.6% strain per second on both strut chordae. The valve opened between 320 and 420 msec with a strain rate of approximately -54.8% ± -56.6% strain per second on both strut chordae.

The maximum strain, loading rates, and unloading rates are given in Figure 5.5. As can be seen, there is no significant difference between the loading and unloading rates. The loading rate (valve closure) was slightly higher at 75.3% ± 48.6% strain per second than the unloading rate (valve opening) at -54.8% ± -56.6% strain per second. Table 5.2 below contains the values of the maximum strain, loading rates, and unloading rates for all posterior medial and anterior lateral strut chordae measured.

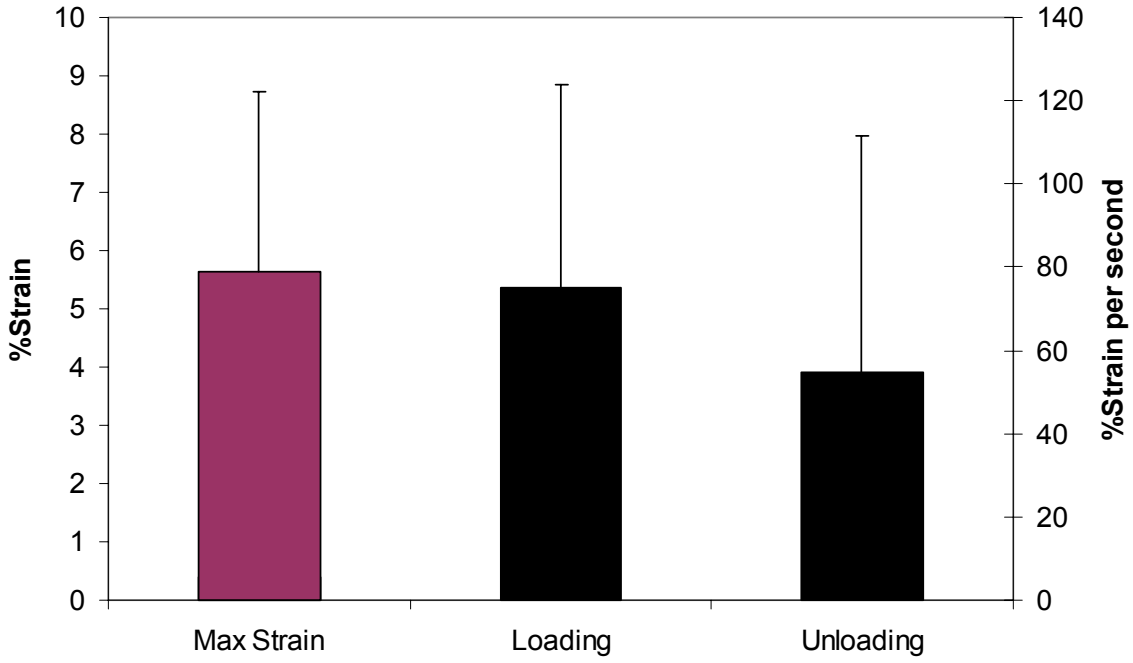

Figure 5.5: Maximum strain, loading and unloading rates for the strut chordae from the flow loop experiments. The maximum strain uses the vertical axis on the left (%strain). The loading and unloading rates use the vertical axis on the right (%strain per second). There was no significant difference between the loading and unloading rates. The loading rate (valve closure) was slightly higher at 75.3% ± 48.6% strain per second than the unloading rate (valve opening) at -54.8% ± -56.6% strain per second.

The maximum strain, loading, and unloading rates for the two strut chordae were also compared, as seen in Figure 5.6. There was no significant difference in the strain, loading rates, or unloading rates between the two strut chordae. The strut chordae which inserted into the anterior lateral papillary muscle had a slightly higher maximum strain (5.7% ± 3.8%) and loading rate (80.5% ± 51.9% strain per second) than the strut chordae which inserted into the posterior medial papillary muscle (5.5% ± 2.3% and 68.1% ± 48.3% strain per second). The strut chordae which inserted into the posterior medial papillary muscle had a higher unloading rate (-68.5% ± -59.1% strain per second) than the strut chordae which inserted into the anterior lateral papillary muscle (-44.9% ± -57.2% strain per second).

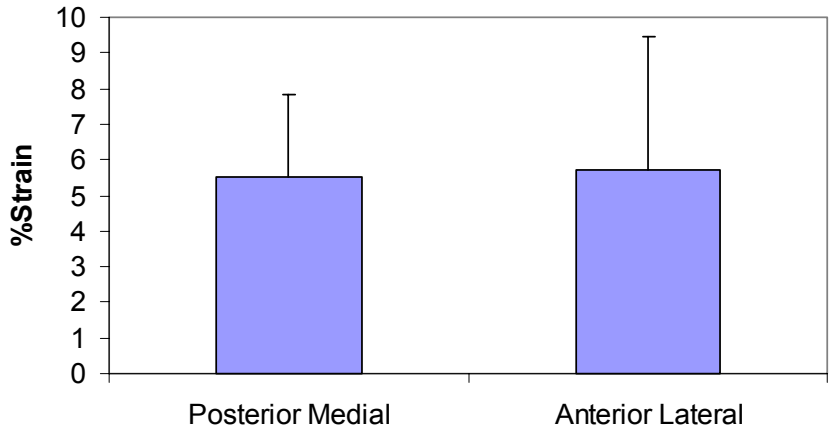

(a)

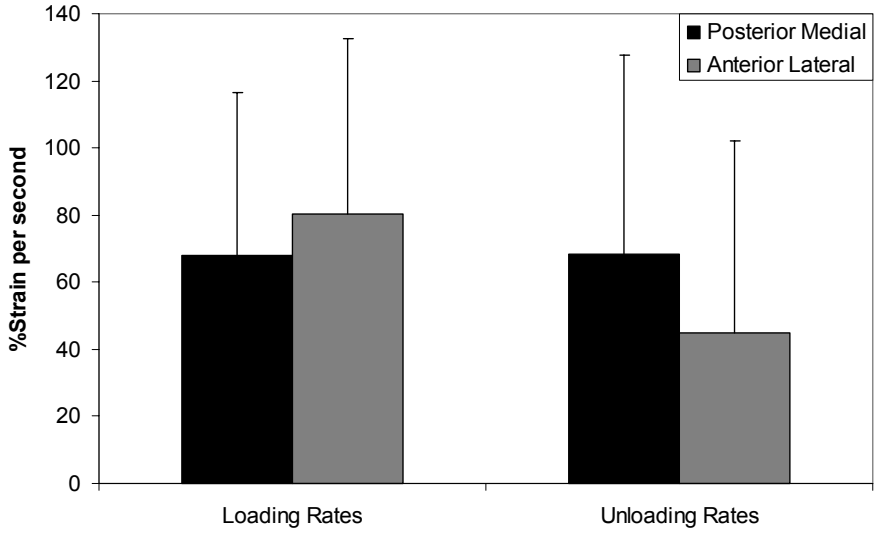

(c)

Figure 5.6: Comparison of (a) max strain, (b) loading and unloading rates for the two strut chordae for the flow loop experiments. There was no significant difference in the strain, loading rates, or unloading rates between the two strut chordae.

Table 5.2 below contains the values of the maximum strain, loading rates, and unloading rates for all posterior medial and anterior lateral strut chordae measured.

Table 5.2: Maximum strain, loading, and unloading rates determined for both strut chordae during the flow loop experiments. There was no significant difference in the strain, loading rates, or unloading rates between the two strut chordae. A p-value of less than 0.05 was considered significant.

	Maximum Strain (%Strain)		Loading Rate (%Strain per second)		Unloading Rate (%Strain per second)	
Specimen	*Posterior Medial*	*Anterior Lateral*	*Posterior Medial*	*Anterior Lateral*	*Posterior Medial*	*Anterior Lateral*
1	4.907	5.838	39.423	137.920	-102.730	-24.293
2	3.582	6.960	139.480	149.500	-5.464	-28.276
3	9.523	3.190	95.904	47.876	-72.869	-24.947
4	5.271	12.842	40.856	106.230	-146.050	-172.850
5	4.388	6.725	24.616	24.474	-15.612	-14.861
6		2.004		73.713		-9.430
7		2.339		23.609		-40.315
Average	5.534	5.699	68.056	80.475	-68.545	-44.996
Std. Dev	2.318	3.762	48.279	51.971	59.109	57.230
p-value	0.933		0.684		0.504	
			0.352			

5.4 Uniaxial Tests

Preliminary experiments were conducted to determine the necessity of using a camera system to measure strains in a localized region. Figure 5.7 shows the difference in load-strain behavior between the uniaxial testing machine and the marker displacement recorded by the camera system. When calculating the strain using the uniaxial testing machine, the lengths are determined by the distance between the clamps (cross-head displacement). When calculating the strain using the camera, the lengths are determined by using a non-contacting optical method, i.e. tracking the displacement of the markers on the chordae. The distances between markers located on the central region of the chordae are recorded using a high speed camera system. The difference at mid-load (1

N) between the high speed camera system and the cross-head displacement was 46.2%. The strain calculated at mid-load (1 N) using the cross-head displacement would be approximately 46% higher than the strain calculated at mid-load using the high speed camera system.

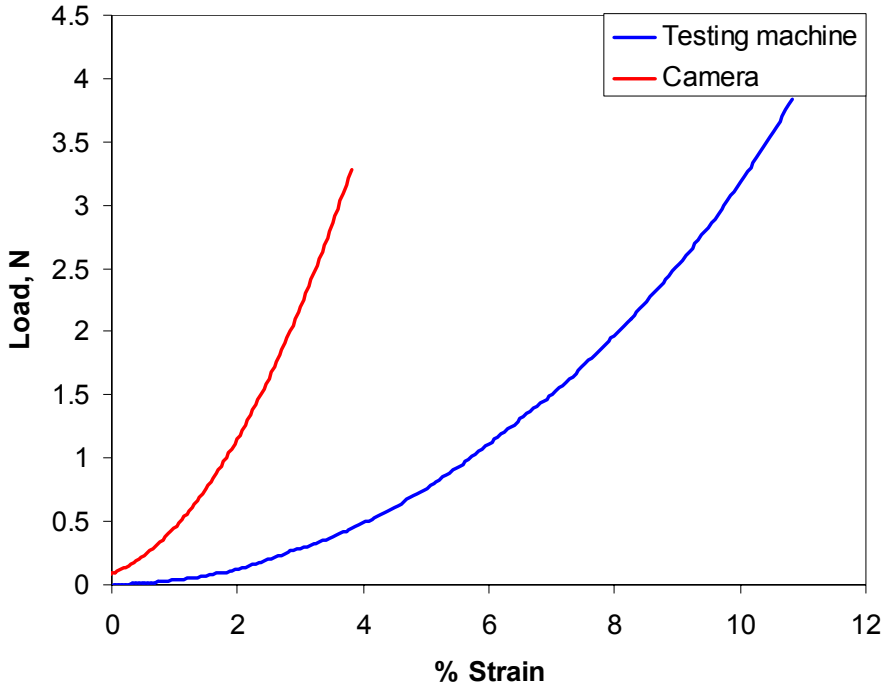

Figure 5.7: Uniaxial test results comparing the camera system and the cross head displacement strain. The difference at mid-load (1 N) between the high speed camera system and the cross-head displacement was 46.2%. The strain calculated at mid-load (1 N) using the cross-head displacement would be approximately 46% higher than the strain calculated at mid-load using the high speed camera system.

The same eleven strut chordae were examined during the uniaxial tests no more than 24 hours after the flow loop experiments. Figure 5.8 below shows the raw, unfit data for the eleven strut chordae used during this study. Three features can be taken from the uniaxial tests: a non-linear load-strain relationship, a hysteresis loop in cyclic loading and unloading, and preconditioning in repeated cycles.

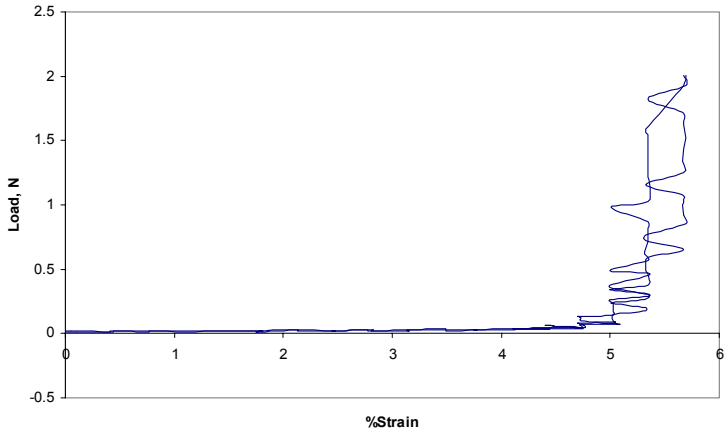
Load, N
%Strain
2.5
2
1.5
1
0.5
0
-0.5
0
1
2
3
4
5
6

(a)

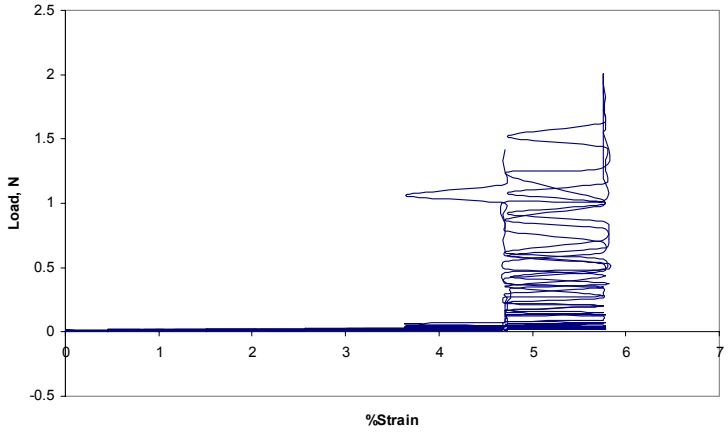
Load, N
%Strain
2.5
2
1.5
1
0.5
0
-0.5
0
1
2
3
4
5
6
7

(b)

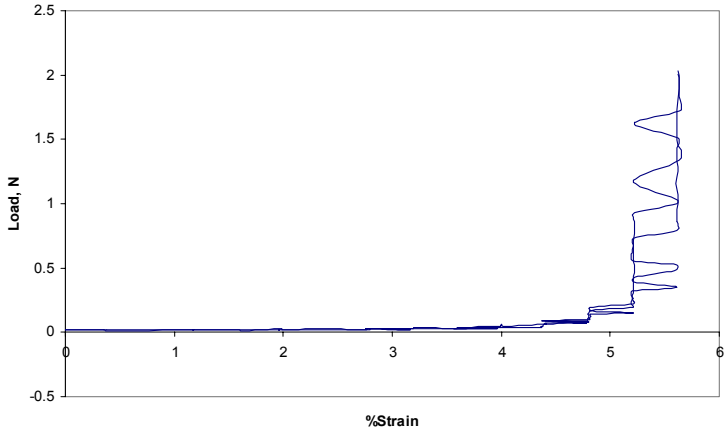
Load, N
%Strain
2.5
2
1.5
1
0.5
0
-0.5
0
1
2
3
4
5
6

(c)

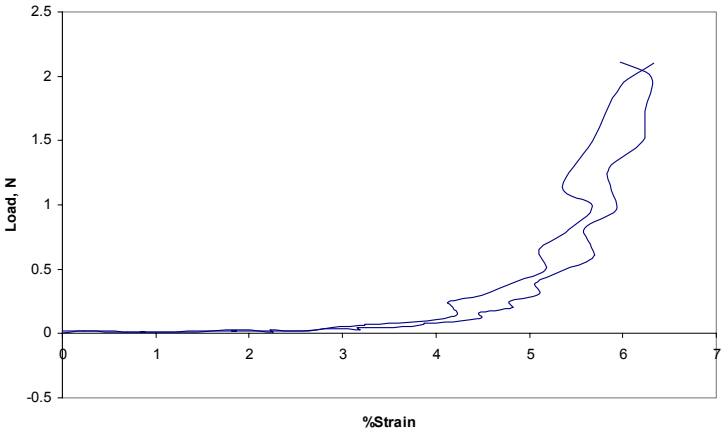
Load, N
%Strain
2.5
2
1.5
1
0.5
0
-0.5
0
1
2
3
4
5
6
7

(d)

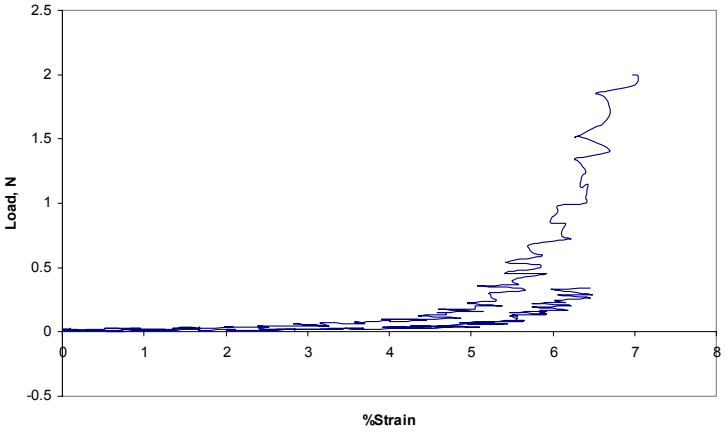
Load, N
%Strain
2.5
2
1.5
1
0.5
0
-0.5
0
1
2
3
4
5
6
7
8

(e)

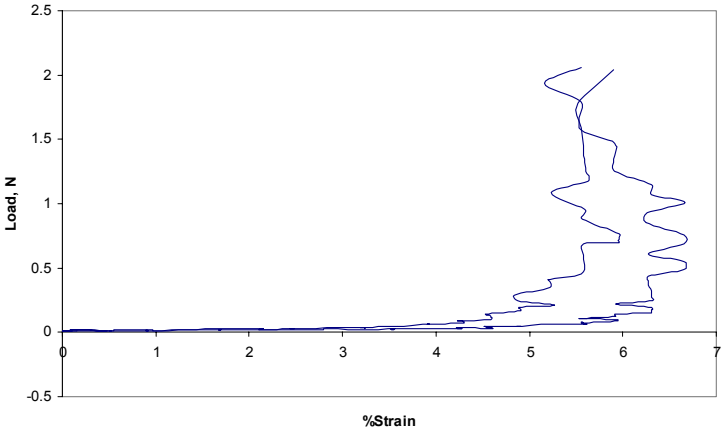
Load, N
%Strain
2.5
2
1.5
1
0.5
0
-0.5
0
1
2
3
4
5
6
7

(f)

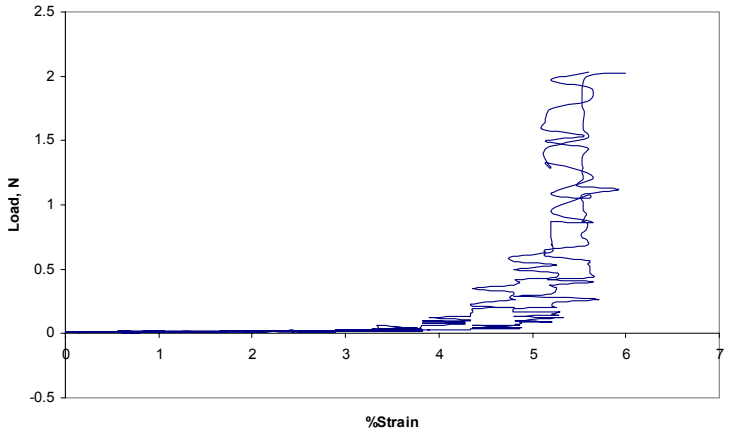
Load, N
%Strain
2.5
2
1.5
1
0.5
0
-0.5
0
1
2
3
4
5
6
7

(g)

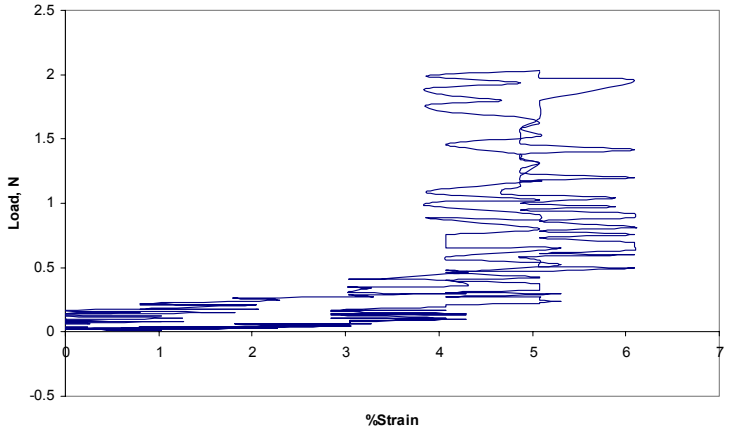
Load, N
%Strain
2.5
2
1.5
1
0.5
0
-0.5
0
1
2
3
4
5
6
7

(h)

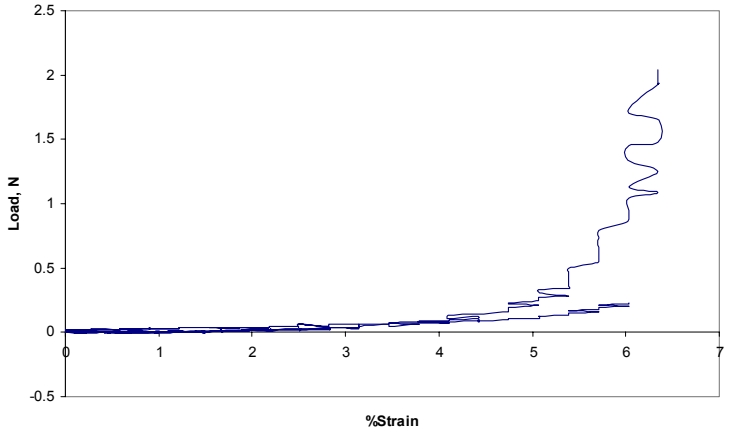
Load, N
%Strain
2.5
2
1.5
1
0.5
0
-0.5
0
1
2
3
4
5
6
7

(i)

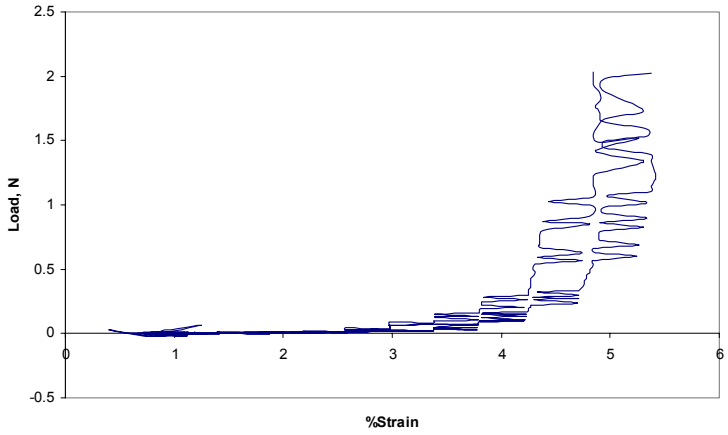

(j)

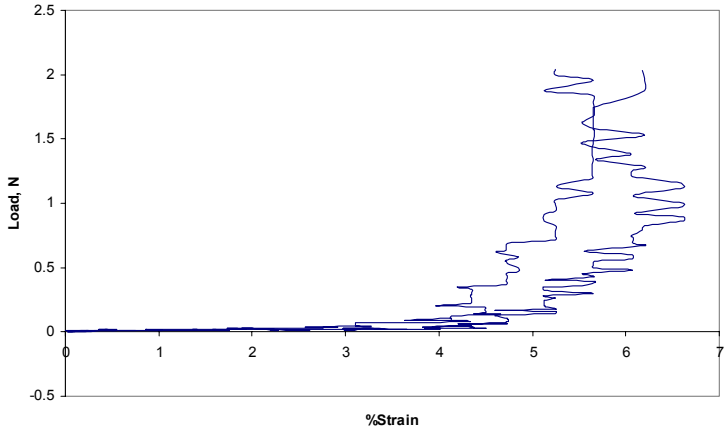

(k)

Figure 5.8: Raw, unfit uniaxial data for the eleven strut chordae. Anterior lateral strut chordae (a, c, e, g, i) and posterior medial strut chordae (b, d, f, h, j, k).

The loading and unloading curves obtained from the uniaxial tests were each fit with separate mixed linear-exponential curve, shown in Figure 5.9. The first portion of the curve can be described with a simple linear fit; however, this portion of the curve was generally in the noise region of the force transducer. The second portion of the curve can be described with an exponential fit. The loading and unloading curve fits for Figure 5.9 were:

Loading curve: $y = 7\ 10^{-5}e^{1.2306x}$ $R^2 = 0.9738$

Unloading curve: $y = 5\ 10^{-5}e^{1.2385}$ $R^2 = 0.9688$.

The "toe" region between A and B, see Figure 5.9, is the physiological range in which the mitral valve chordal tissue normally functions. The section B to C is considered the reserve strength of the chordae. The shift that occurs between the loading and unloading curves during the uniaxial tests describes the amount of hysteresis inherent in the chordae. The hysteresis is dependent on the loading condition and maximum load which was the same for all chordae examined. The amount of hysteresis calculated at mid-load for both the anterior lateral and posterior medial chordae was 9.7% ± 6.6%.

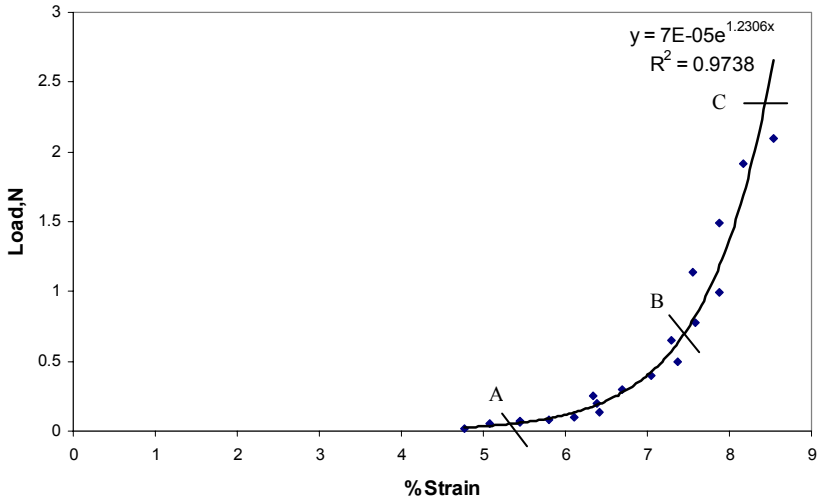

(a)

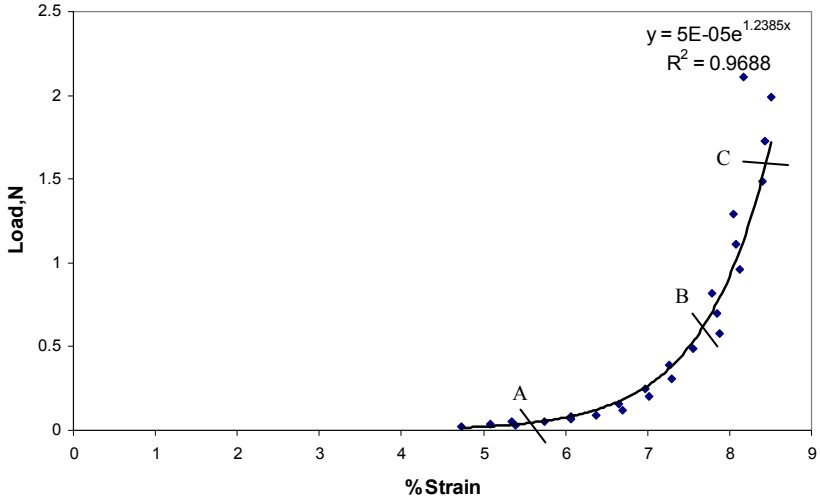

(b)

Figure 5.9: Curve fits of the uniaxial data for (a) unloading curve and (b) loading curve. The "toe" region between A and B is the physiological range in which the mitral valve chordal tissue normally functions. The section B to C is considered the reserve strength of the chordae.

Figure 5.10 below shows the exponential curve fits for the loading and unloading curves for each strut chordae examined. The loading curves had a larger slope than the unloading curves which was expected. The loading curves also began the transition into the "toe" region before the unloading curves which is characteristic of viscoelastic tissues. The r-squared values for the curve fits were above 0.8 for all curves. The transition strain and the slope in the linear region for both the loading and unloading curve were measured. There was no significant difference between the posterior medial and anterior lateral chordae for these three measurements. The transition strain, between A and B, for the posterior medial chordae was 4.95% ± 0.412% strain and for the anterior lateral chordae was 5.41% ± 0.27% strain. The slope of the loading curve for the posterior medial chordae was 3.42 ± 3.08 N / %strain and for the anterior lateral chordae was 3.55 ± 1.27 N / %strain. The slope of the unloading curve for the posterior medial chordae was 2.61 ± 2.25 N / %strain and for the anterior lateral chordae was 2.21 ± 1.00 N / %strain.

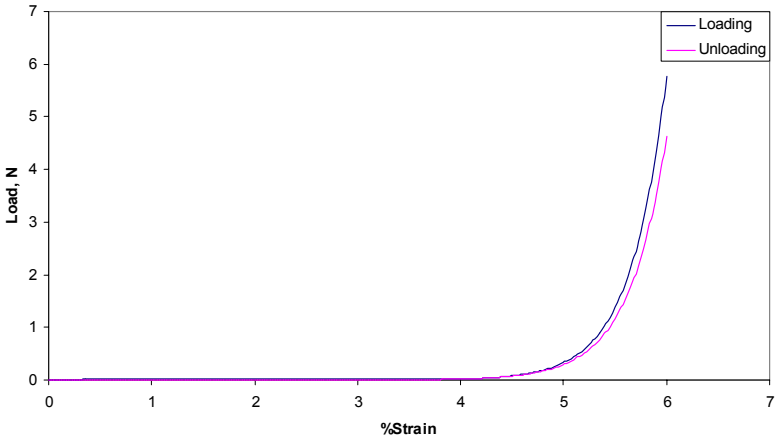

Loading	$y = 1 \cdot 10^{-7} e^{2.8835x}$	$R^2 = 0.8193$
Unloading	$y = 4 \cdot 10^{-7} e^{2.58x}$	$R^2 = 0.8318$

(a)

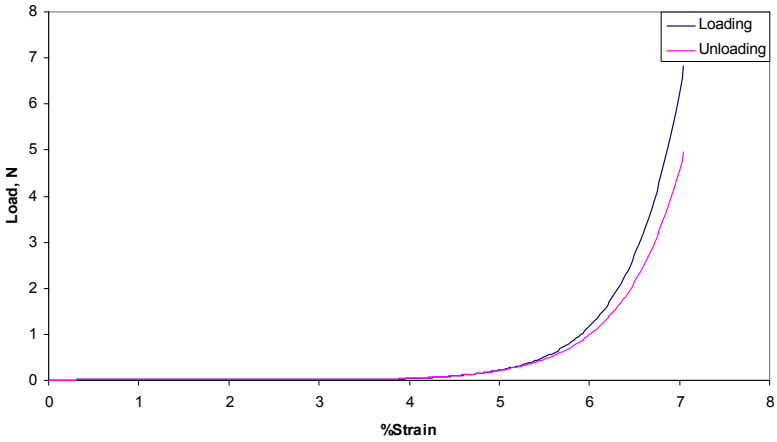

Loading	$y = 7 \cdot 10^{-5} e^{1.6108x}$	$R^2 = 0.7443$
Unloading	$y = 3 \cdot 10^{-4} e^{1.3738x}$	$R^2 = 0.8159$

(b)

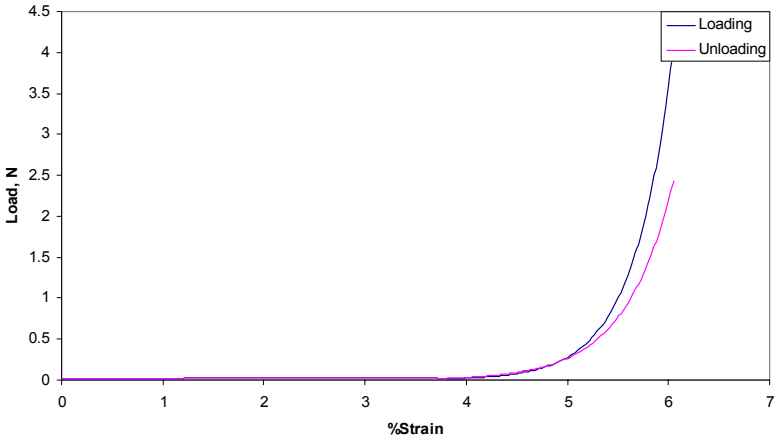

Loading	$y = 7 \cdot 10^{-6}\, e^{2.1086x}$	$R^2 = 0.8201$
Unloading	$y = 8 \cdot 10^{-7}\, e^{2.5514x}$	$R^2 = 0.8747$

(c)

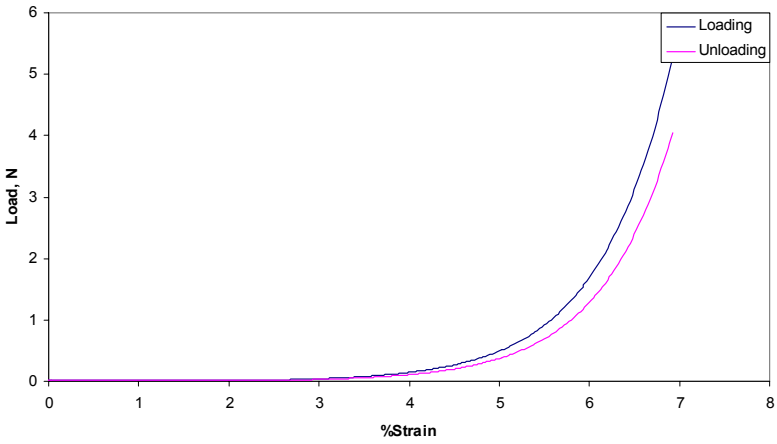

Loading	$y = 7 \cdot 10^{-5}\, e^{1.2306x}$	$R^2 = 0.9738$
Unloading	$y = 5 \cdot 10^{-5}\, e^{1.2385x}$	$R^2 = 0.9688$

(d)

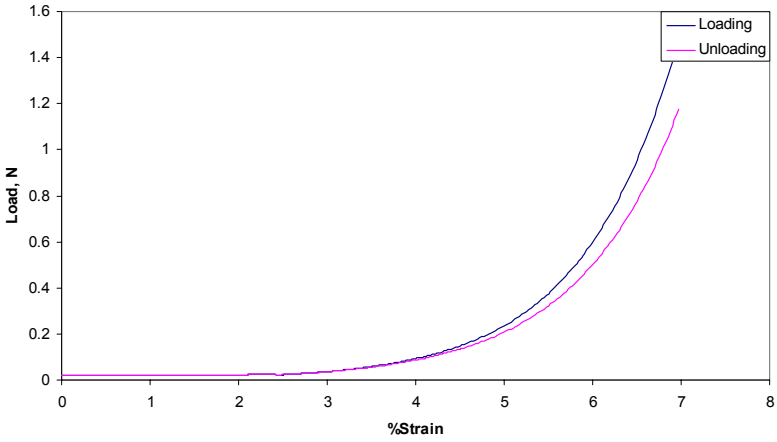

Loading	$y = 2 \cdot 10^{-7} e^{0.932x}$	$R^2 = 0.9277$
Unloading	$y = 4 \cdot 10^{-7} e^{0.8775x}$	$R^2 = 0.9307$

(e)

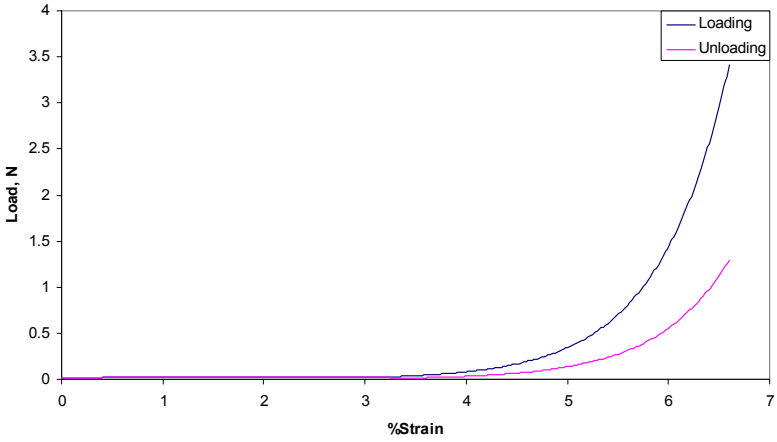

Loading	$y = 4 \cdot 10^{-7} e^{1.4376x}$	$R^2 = 0.8718$
Unloading	$y = 4 \cdot 10^{-6} e^{1.1078x}$	$R^2 = 0.8276$

(f)

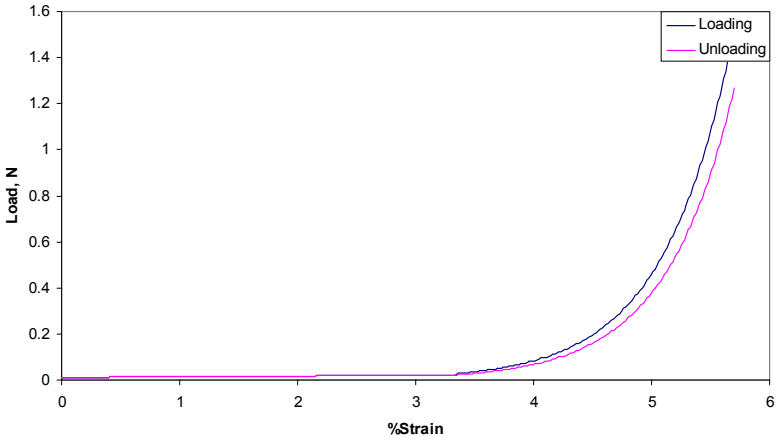

Loading	$y = 1 \cdot 10^{-7}\, e^{1.705x}$	$R^2 = 0.9107$
Unloading	$y = 7 \cdot 10^{-8}\, e^{1.7229x}$	$R^2 = 0.8894$

(g)

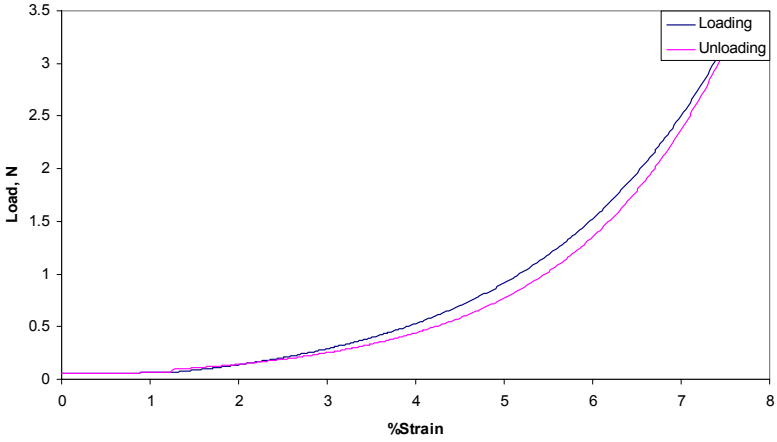

Loading	$y = 0.0988\, e^{0.4681x}$	$R^2 = 0.8131$
Unloading	$y = 0.0468\, e^{0.5608x}$	$R^2 = 0.8774$

(h)

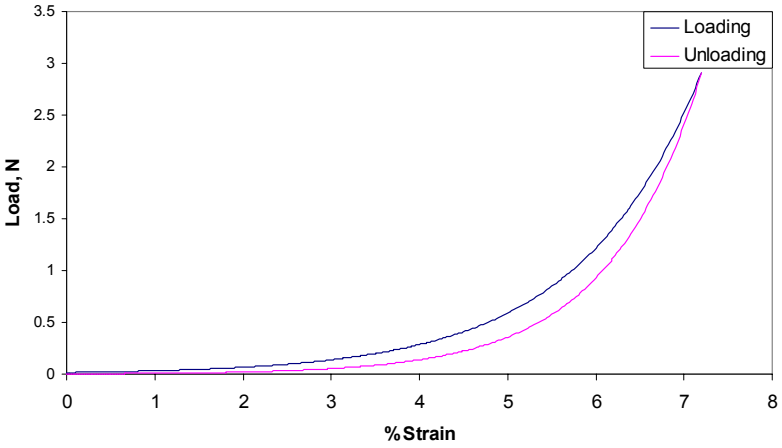

Loading	$y = 1 \cdot 10^{-5}\, e^{0.9531x}$	$R^2 = 0.9652$
Unloading	$y = 2 \cdot 10^{-4}\, e^{0.7262x}$	$R^2 = 0.9225$

(i)

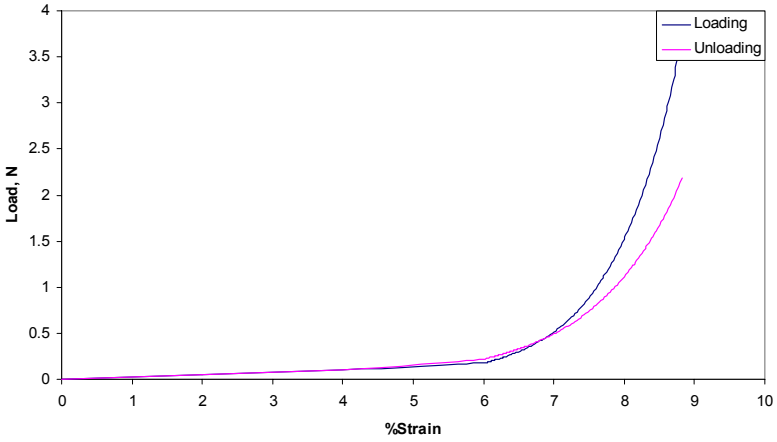

Loading	$y = 0.1747\, e^{1.083x}$	$R^2 = 0.9677$
Unloading	$y = 0.2189\, e^{0.8136x}$	$R^2 = 0.9089$

(j)

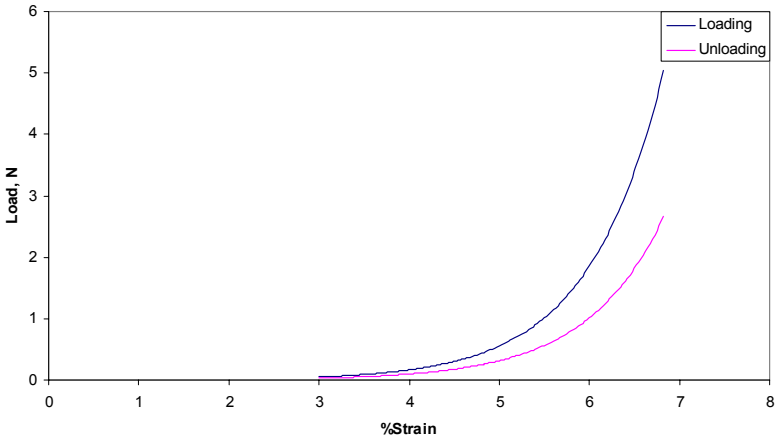

Loading	$y = 0.0491\ e^{1.2105x}$	$R^2 = 0.918$
Unloading	$y = 0.0303\ e^{1.1695x}$	$R^2 = 0.9364$

(k)

Figure 5.10: Exponential curve fits for the uniaxial tests for all eleven strut chordae. Anterior lateral strut chordae (a, c, e, g, i) and posterior medial strut chordae (b, d, f, h, j, k). The loading curves had a larger slope than the unloading curves which was expected. The loading curves also began the transition into the "toe" region before the unloading curves which is characteristic of viscoelastic tissues.

5.5 Histology and Biochemical Composition

5.5.1 DNA Content

A Hoechst fluorescent assay was used to determine the DNA content of the chordae tendineae. The anterior and posterior marginal chordae contained statistically significantly more DNA per mg of tissue than the other chordae ($p<0.01$). The anterior strut chord was found to contain significantly less DNA per mg of tissue (0.63 ± 0.19 µg of DNA per mg of tissue dry weight) than all the other chordae ($p<0.01$). There was no significant difference between the amount of DNA per mg of tissue for the commissural (1.26 ± 0.61 µg of DNA per mg of tissue dry weight), posterior intermediate (1.01 ± 0.40

µg of DNA per mg of tissue dry weight), and basal posterior (1.09 ± 0.38 µg of DNA per mg of tissue dry weight) chordae. There was also no significant difference between the anterior (1.90 ± 1.14 µg of DNA per mg of tissue dry weight) and posterior (2.70 ± 1.24 µg of DNA per mg of tissue dry weight) marginal chordae. The amount of DNA per mg of tissue for each chord is presented in Figure 5.11. The raw data containing values for each chordae can be found in Appendix E.

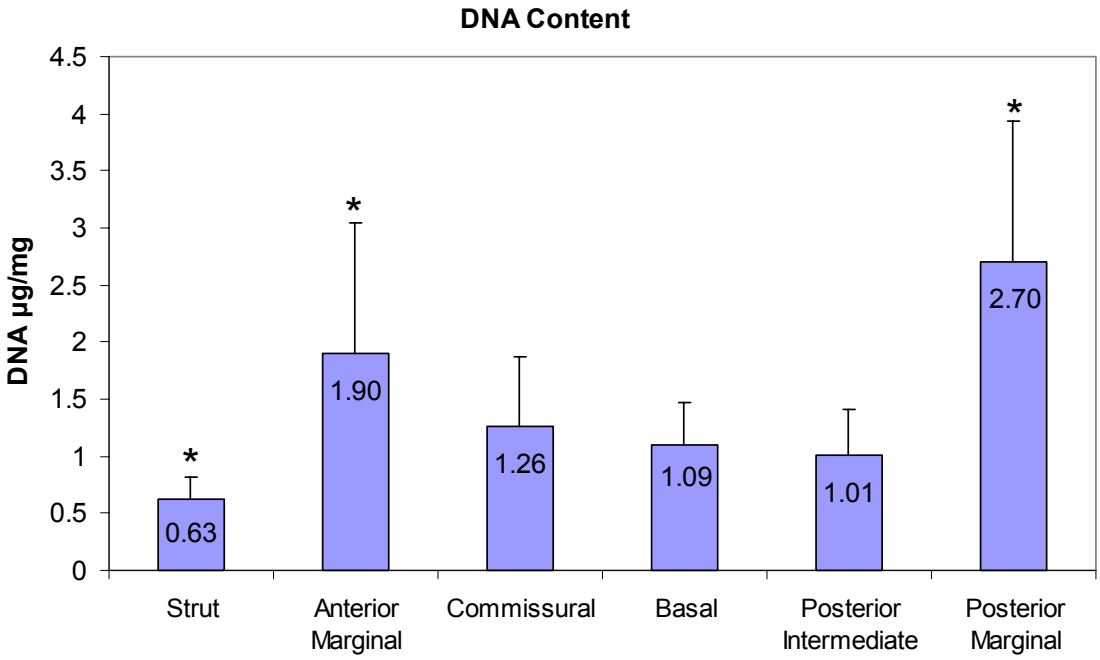

Figure 5.11: Amount of DNA per mg of tissue (* indicates p< 0.05). A Hoechst fluorescent assay was used to determine the DNA content of the chordae tendineae. The anterior and posterior marginal chordae contained statistically significantly more DNA per mg of tissue than the other chordae (p<0.01). The anterior strut chord was found to contain significantly less DNA per mg of tissue than all the other chordae (p<0.01).

5.5.2 Collagen Content

The amount of acid-pepsin soluble collagen was quantified using a sircol red colorimetric assay kit. The amount of collagen per mg of tissue for each chord is presented in Figure 5.12. The results showed that the posterior marginal chord contained significantly more collagen per mg of tissue than the other chordae ($p<0.01$). The posterior marginal chordae contained 14.89 ± 6.83 μg of collagen per mg of tissue dry weight. There was no significant difference between the other chordae. The anterior strut chordae contained 5.49 ± 4.05 μg of collagen per mg of tissue dry weight, the anterior marginal chordae contained 8.94 ± 3.38 μg of collagen per mg of tissue dry weight, the commissural chordae contained 6.24 ± 3.01 μg of collagen per mg of tissue dry weight, the basal chordae contained 6.71 ± 4.21 μg of collagen per mg of tissue dry weight, and the posterior intermediate chordae contained 6.23 ± 3.91 μg of collagen per mg of tissue dry weight. The raw data containing values for each chordae can be found in Appendix E.

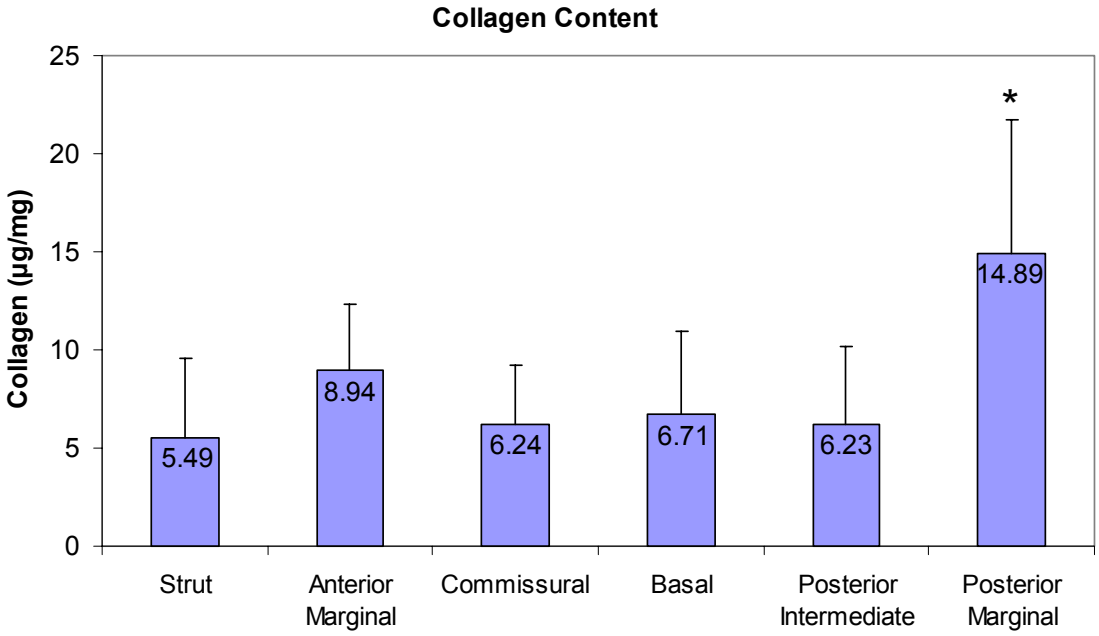

Figure 5.12: Amount of collagen per mg of tissue (* indicates p< 0.05). The amount of acid-pepsin soluble collagen was quantified using a sircol red colorimetric assay kit. The posterior marginal chord contained significantly more collagen per mg of tissue than the other chordae (p<0.01).

5.5.3 Elastin Content

The elastin content for each of the chordae was measured using the Fastin Elastin assay™. The amount of elastin per mg of tissue for each chord is presented in Figure 5.13. The results showed no significant difference in the amount of elastin per mg of tissue between the chordae. The anterior strut chordae contained 16.44 ± 11.03 µg of elastin per mg of tissue dry weight, the anterior marginal chordae contained 34.58 ± 31.02 µg of elastin per mg of tissue dry weight, the commissural chordae contained 48.11 ± 53.58 µg of elastin per mg of tissue dry weight, the basal chordae contained 23.09 ± 14.61 µg of elastin per mg of tissue dry weight, the posterior intermediate chordae contained 19.03 ± 34.77 µg of elastin per mg of tissue dry weight, and the posterior

marginal chordae contained 27.84 ± 62.45 μg of elastin per mg of tissue dry weight. The raw data containing values for each chordae can be found in Appendix E.

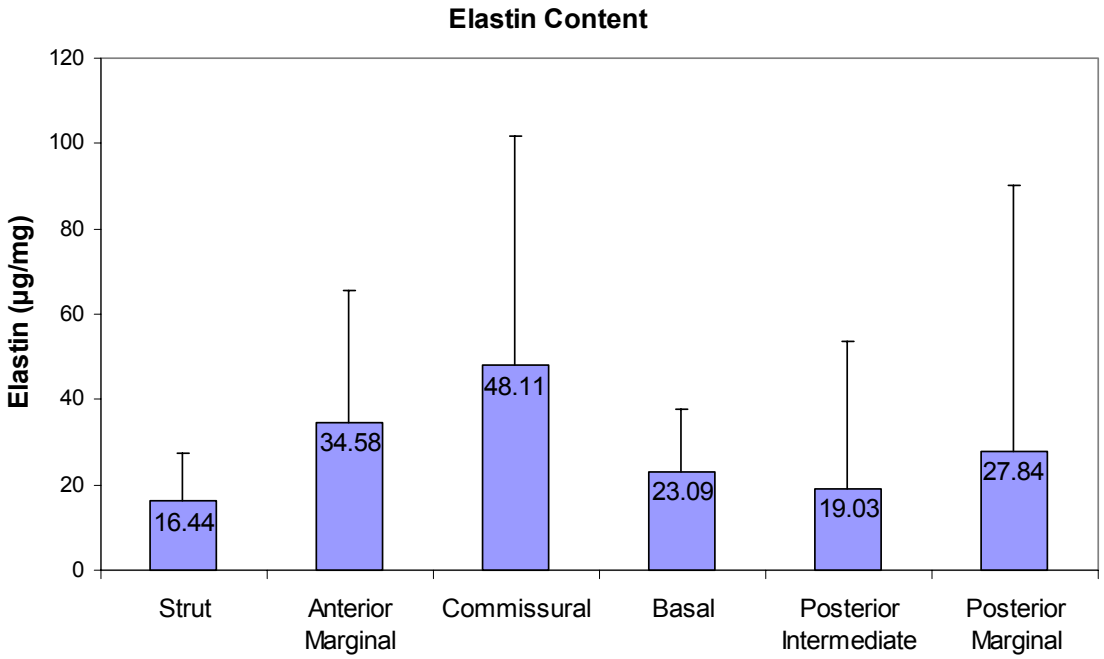

Figure 5.13: Amount of elastin per mg of tissue. The elastin content for each of the chordae was measured using the Fastin Elastin assay™. The results showed no significant difference in the amount of elastin per mg of tissue between the chordae.

5.5.4 Hematoxylin and Eosin Stain

Hematoxylin and Eosin (H & E) stains were performed on each type of chordae to determine cellular distribution. Cell nuclei were stained dark blue, collagen fibers stained dark pink, and elastin fibers stained light pink.

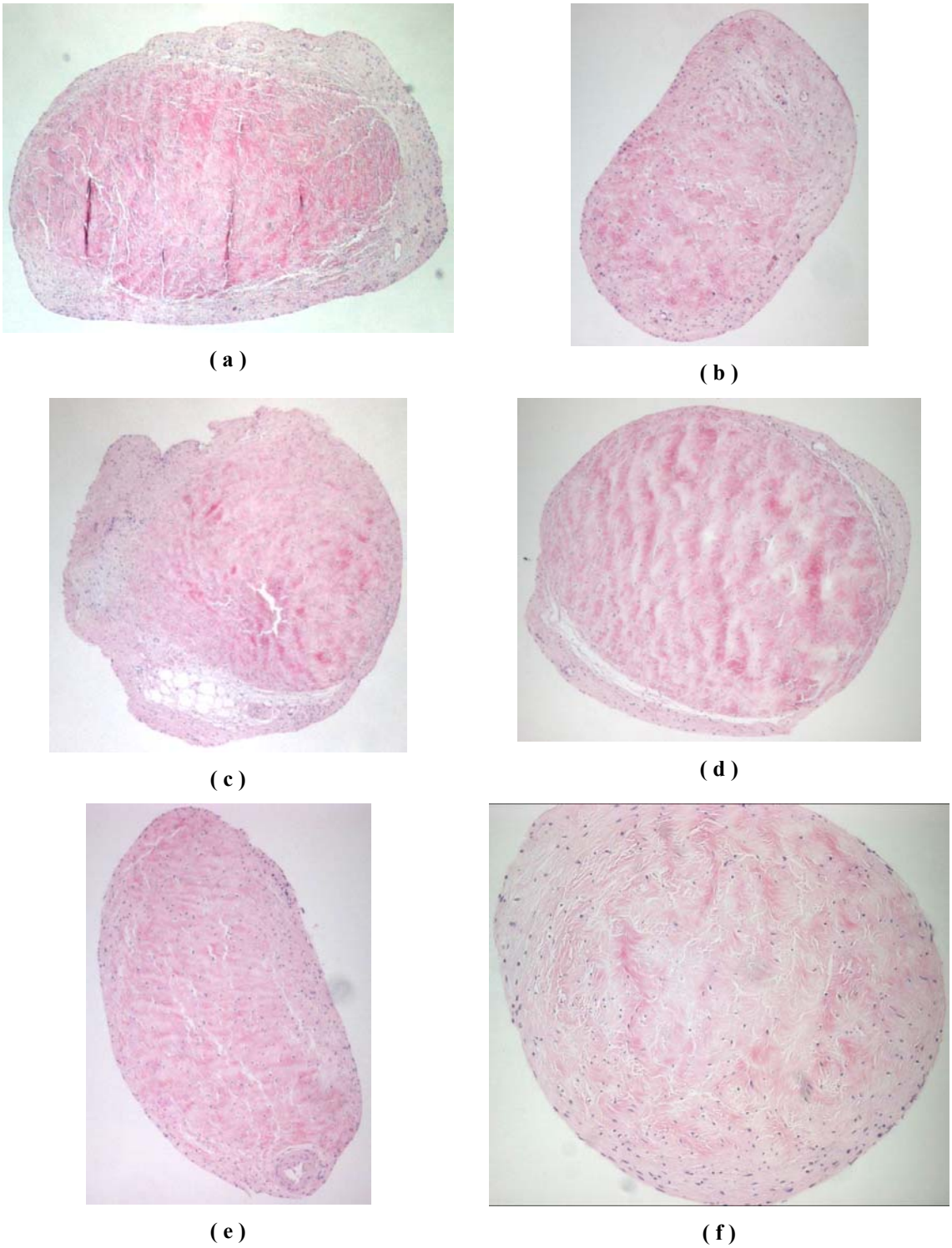

Figure 5.14: H&E stains of all six chordae. (a) strut, radial, 4X; (b) anterior marginal, radial, 10X ; (c) commissural, radial, 4X ; (d) basal, radial, 10X ; (e) posterior intermediate, radial, 10X ; (f) posterior marginal, radial, 20X.

The H & E stained images were viewed using fluorescent microscopy to allow the directional loading crimping to be observed, as shown in Figure 5.15. The collagen fibers aligned in the direction of loading which is characteristic to tissues whose function is mainly to transmit tension[18]. The outer layer of loose collagen fibers did not exhibit the same directional loading as the central core. The fluorescent microscopy also exhibited the natural fluorescence of the elastin fibers. Figure 5.16 shows the elastin fibers in the radial direction and circumferential direction. However, due to the intense staining of the collagen, it was difficult to delineate the elastin fibers from the collagen; therefore, a Verhoeff counterstained with a light green stain was used to distinguish the elastin fibers.

Figure 5.15: H&E stain of a strut chord observed under fluorescent microscopy to observe directional crimping. The collagen fibers aligned in the direction of loading which is characteristic to tissues whose function is mainly to transmit tension[18]. The outer layer of loose collagen fibers did not exhibit the same directional loading as the central core.

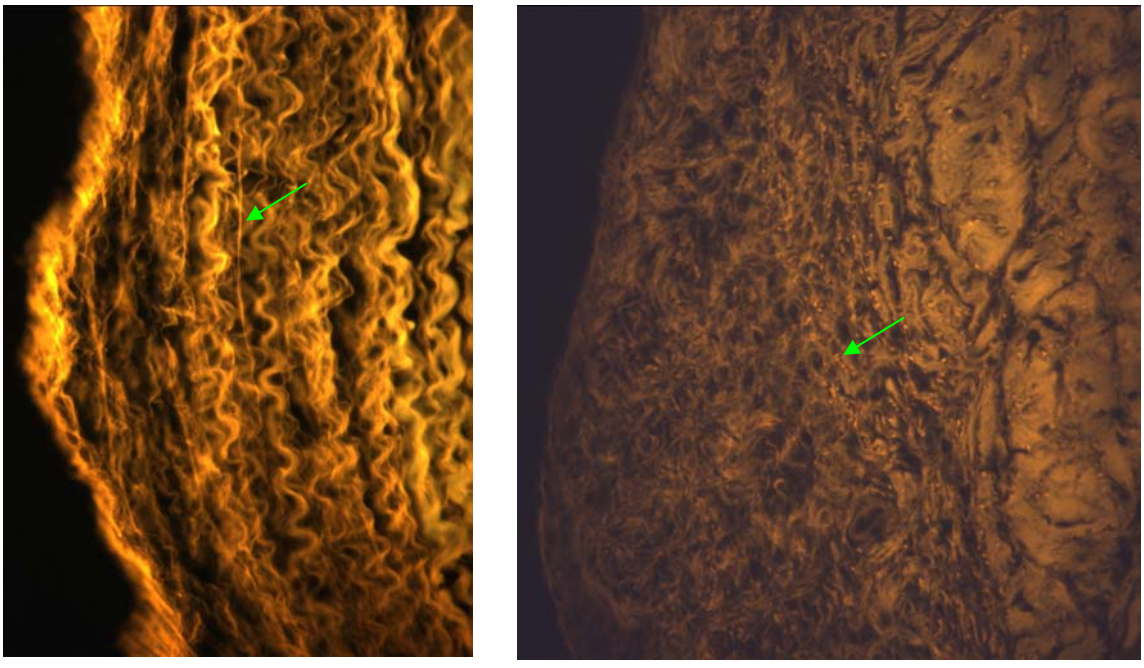

(a) **(b)**

Figure 5.16: H&E stain of strut chordae observed under fluorescent microscopy to distinguish elastin fibers in the (a) longitudinal and (b) radial directions. The elastin fibers ran in the longitudinal direction in both the inner collagen core, and the middle layer of loose collagen.

5.5.5 Verhoeff & Light Green Stain

A Verhoeff stain, counterstained with a light green, stained the elastin fibers and cell nuclei black and the remaining tissue light green. Elastin fibers were observed in both the inner collagen core and the outer loose layer of collagen. The elastin was found to exist as single fibers and not arranged in fibrils as normally found in soft tissues. Figure 5.17 shows elastin fibers interwoven with the collagen fibers in the central collage core.

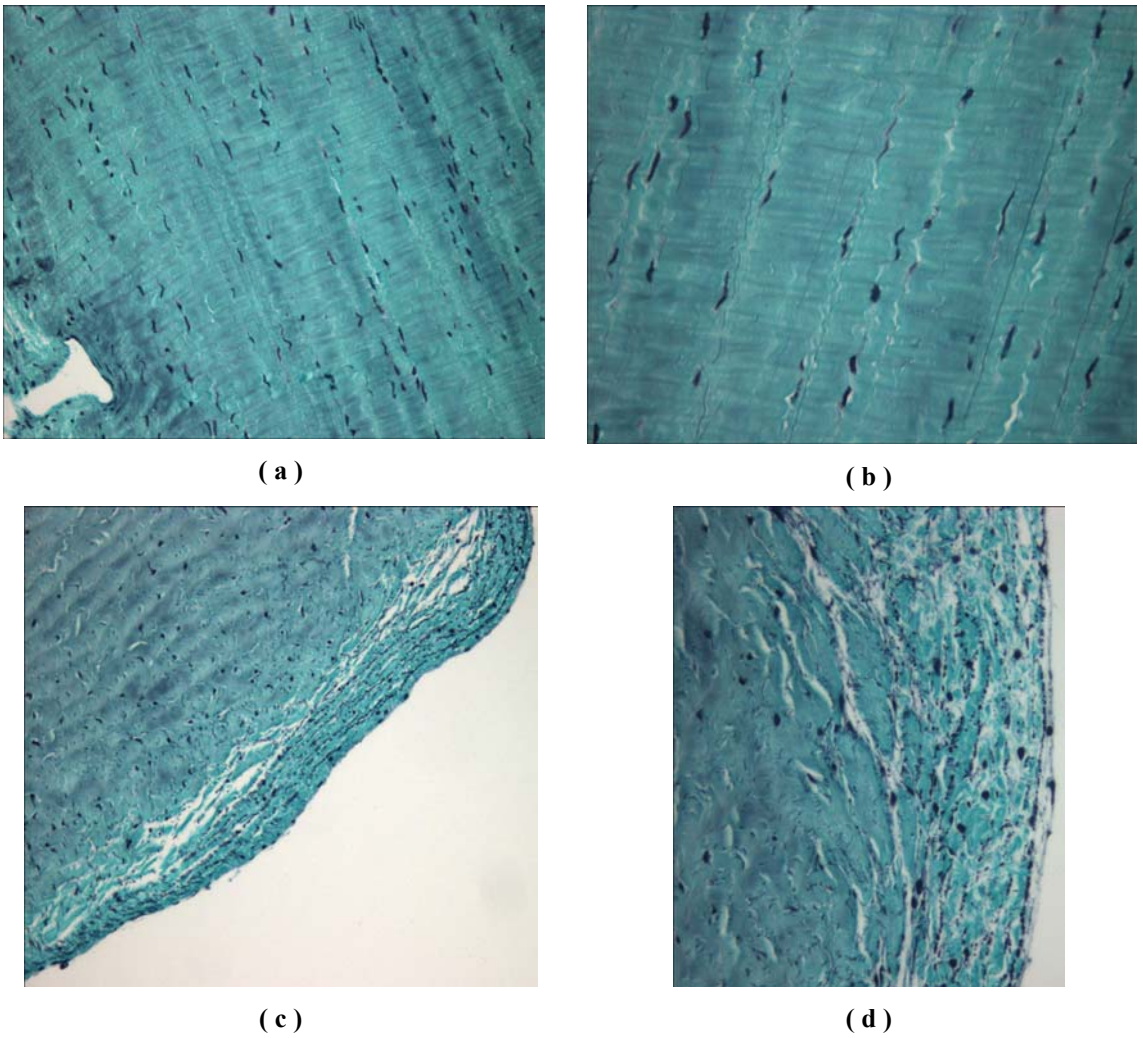

(a) **(b)**

(c) **(d)**

Figure 5.17: Anterior strut chordae stained with Verhoeff counterstained with light green. The cell nuclei and elastin fibers stain black and the surrounding tissue stains green. Sections are 5 microns thick in both the radial and longitudinal directions. (a) strut, longitudinal, 20X; (b) strut, longitudinal, 40X; (c) strut, radial, 20X; (d) strut, radial, 40X. The elastin was found to exist as single fibers and not arranged in fibrils as normally found in soft tissues.

5.5.6 Verhoeff & van Gieson Stain

A Verhoeff stain, counterstained with a van Gieson stain, was performed to distinguish between the collagen, elastin, cellular nuclei, and the surrounding tissue. The collagen was stained red, the elastin black, the cellular nuclei black and surrounding tissue yellow. As shown in Figure 5.18, the outer layer of the chordae stained red for collagen. This is in contrast to previous findings stating that the outer layer is composed entirely of elastin[6]. There were a few single elastin fibers that were seen in the Verhoeff/light green stain. Areas in the outer layer of the chordae stained yellow, indicating tissue that was not composed of collagen or elastin. These structures were vessels; this was verified with immunohistochemistry. The vessels were found to run in the longitudinal direction. This indicates that the vessels did not run directly up the chordae, but circle the chordae as they proceed from the papillary muscles to the leaflet. Staining was performed on six samples of each chordae. Figure 5.18 below shows a representative sample of each chordae stained with the Verhoeff/van Gieson stain in the radial direction. Figure 5.19 shows the vascular distribution between the six chordae. Each chordae contained vessels; however, it was found that the anterior strut chordae contain significantly more vessels than the other chordae. The anterior strut chordae contained 4.73±3.13 vessels, the anterior marginal chordae contained 1.50±2.07 vessels, the commissural chordae contained 1.50±1.35 vessels, the basal posterior chordae contained 1.27±1.74 vessels, the posterior intermediate chordae contained 1.43±1.13 vessels, and the posterior marginal chordae contained 1.00±1.53 vessels.

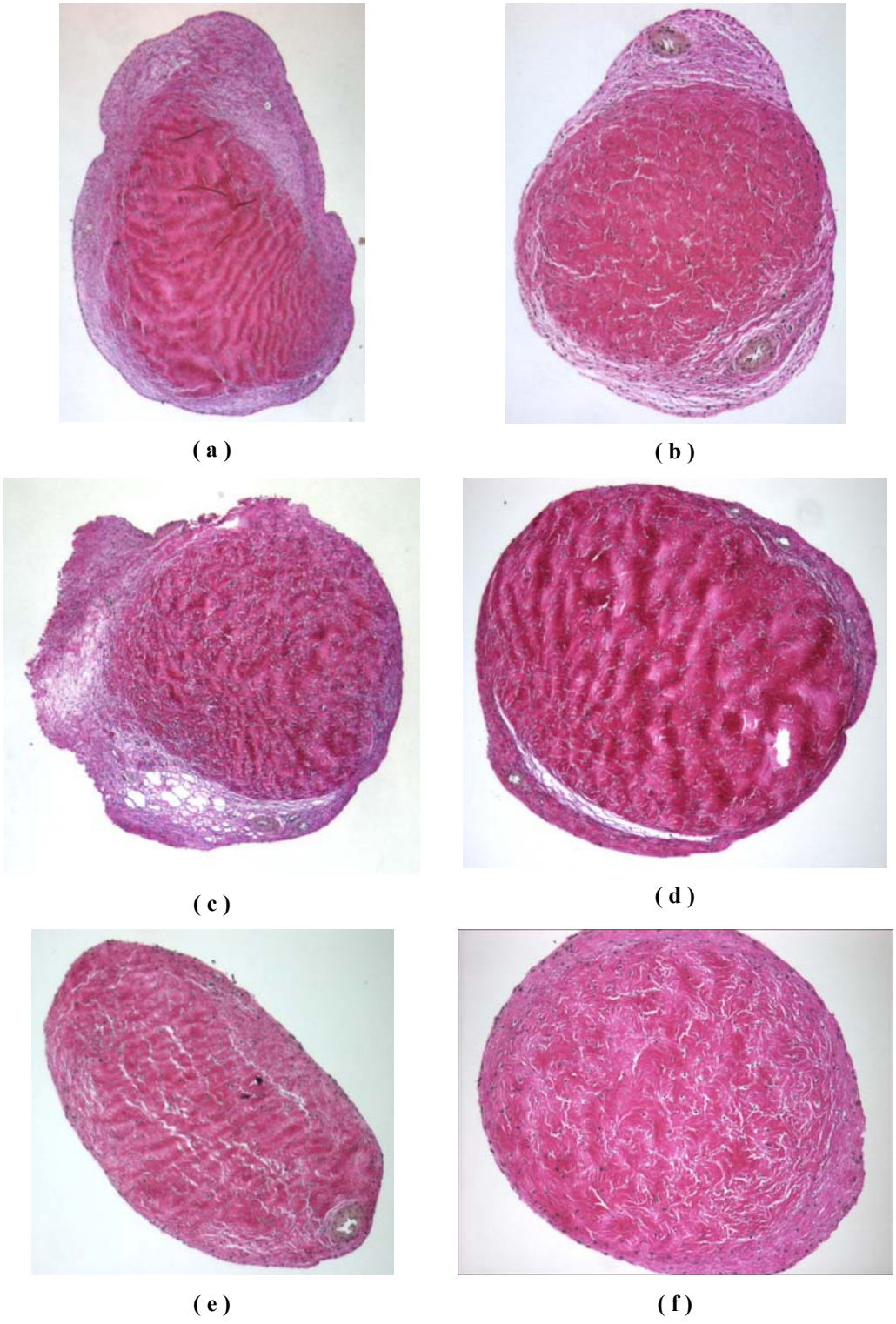

Figure 5.18: Verhoeff and van Gieson stain of all six chordae. The collagen stains red, the elastin and cell bodies stain black, and the remaining tissue stains yellow. (a) strut, radial, 4X; (b) anterior marginal, radial, 10X; (c) commissural, radial, 4X; (d) basal, radial, 10X; (e) posterior intermediate, radial, 10X; (f) posterior marginal, radial, 20X. This stain allows the vessel structure to be differentiated from the surrounding tissue. The vessels were found to run in the longitudinal direction

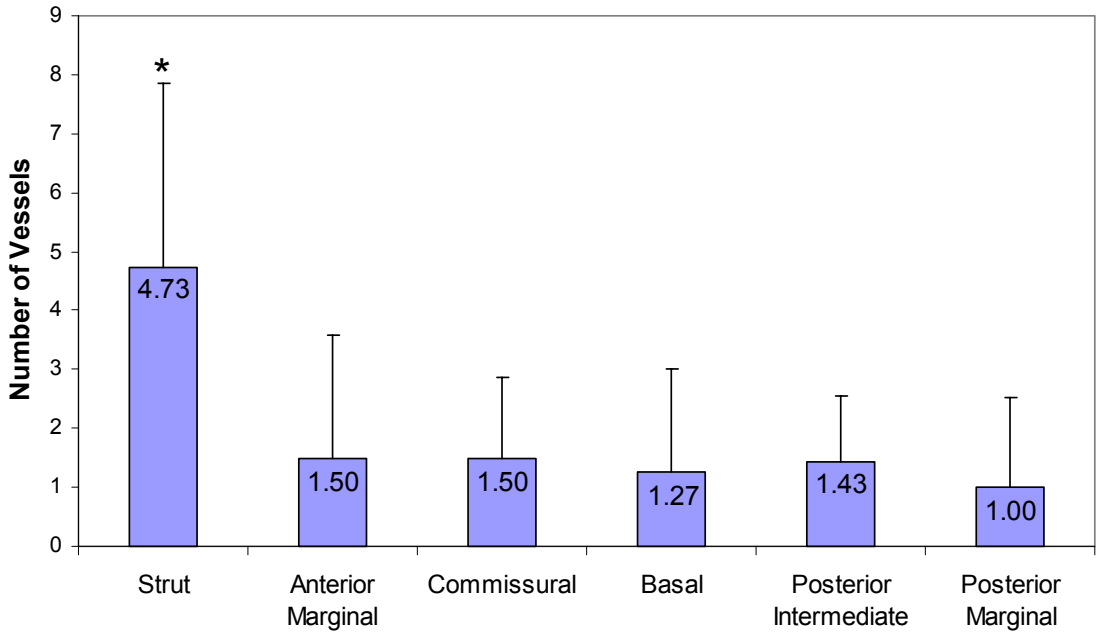

Figure 5.19: Number of vessels in all six chordae. The strut chordae contain significantly more vessels than the other chordae (* indicates p< 0.05).

Table 5.3 below contains the number of vessels contained in each of the six types of chordae. The p-values between each chord are listed in Table 5.4. The number of vessels for each type of chord was compared with the other 5 types of chordae using a t test for paired comparison. A p-value less than 0.05 was considered significant. Statistical analysis was computed using Minitab (version 14) software.

Table 5.3: Number of vessels per chordae. The strut chordae contain significantly more vessels than the other chordae.

Specimen	Strut	Anterior Marginal	Commissural	Basal	Posterior Intermediate	Posterior Marginal
1	4	0	1	3	3	0
2	4	2	4	5	2	2
3	4	2	2	0	2	0
4	9	6	2	0	2	1
5	5	0	2	0	0	0
6	4	0	1	0	0	0
7	1	0	0	1	1	4
8	12	2	3	0		
9	4		0	0		
10	3		0	2		
11	2			3		
Average	4.73	1.50	1.50	1.27	1.43	1.00
St. Dev	3.13	2.07	1.35	1.74	1.13	1.53

Table 5.4: The number of vessels for each type of chord was compared with the other 5 types of chordae using a t test for paired comparison. p-values are listed below. A p-value less than 0.05 was considered significant. The strut chord was significantly different than the other five chordae.

	Strut	Anterior Marginal	Commissural	Basal	Posterior Intermediate	Posterior Marginal
Strut	-	0.022	0.007	0.005	0.017	0.01
Anterior Marginal	0.022	-	1	0.798	0.937	0.608
Commissural	0.007	1	-	0.744	0.911	0.488
Basal	0.005	0.798	0.744	-	0.837	0.739
Posterior Intermediate	0.017	0.937	0.911	0.837	-	0.562
Posterior Marginal	0.01	0.608	0.488	0.739	0.562	-

5.5.7 Immunohistochemistry

Immunohistochemistry was performed with von Willebrand factor to stain for porcine endothelial cells. The endothelial cells were stained dark brown, the surrounding tissue a light gray and non-endothelial cell nuclei blue. This stain was performed to verify the finding of vasculature in the chordae. In addition to the vascular endothelium, a single layer of endothelial cells surrounding the chordae was detected. Figure 5.20 shows an example of the IHC in the radial direction.

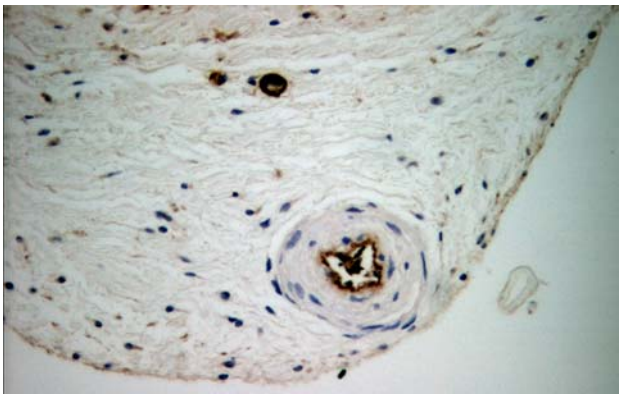

(a)

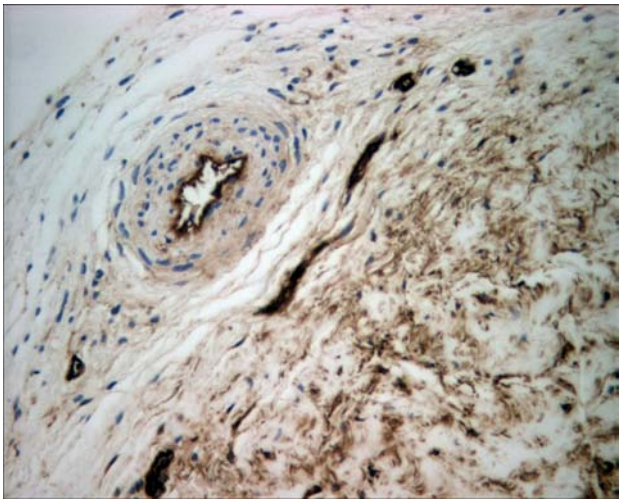

(b)

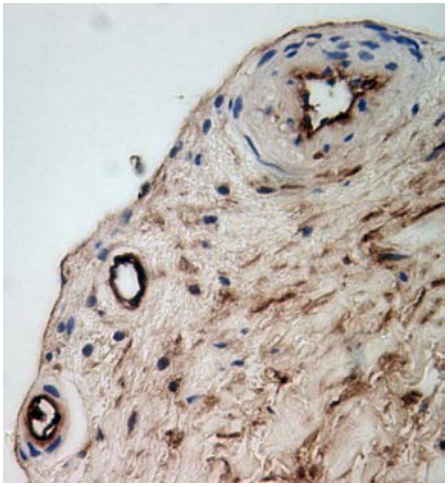

(c)

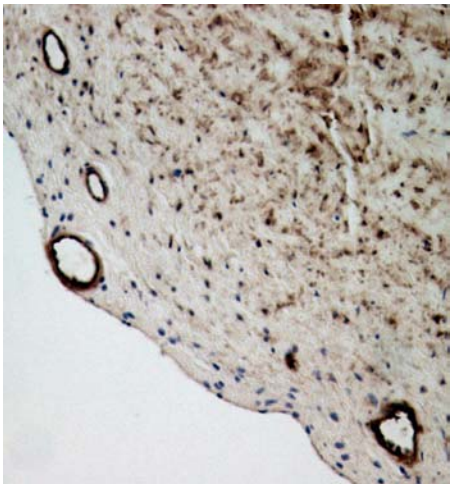

(d)

Figure 5.20: IHC of the chordae in the radial direction. The endothelial cells are stained brown, other cell nuclei are stained blue, and the surrounding light gray. Sections are 5 microns in the radial direction. (a) anterior marginal, radial, 40X; (b) anterior marginal, radial, 40X; (c) strut, radial, 40X; and (d) strut, radial, 20X.

CHAPTER 6

DISCUSSION

In this study, dual camera stereo photogrammetry was used to measure *in vitro* strains experienced by the chordae tendineae of the mitral valve under physiologic conditions. This technique has been used in previous studies to measure strains on the surface of the anterior leaflet of the mitral valve[5], but has never been utilized to measure strains on the chordae tendineae.

This is the first study to measure dynamic strains on the mitral valve chordae *in vitro* under normal physiologic conditions. This study further helps to understand the material properties, specifically the load and strain characteristics, of the chordae tendineae of the porcine mitral valve.

The *in vitro* flow loop experiments show that there is no significant difference in the strain rate during the loading and unloading phases. The small but insignificant difference in strain rates between the loading and unloading rates are consistent with the loading and unloading seen during the uniaxial tests. It shows the inherent hysteresis in the chordae which is found in most soft tissues (Figure 4.3.4). These differences in the loading and unloading phases are in contrast to the differences in strains rates on the surface of the anterior leaflet found by Sacks et al.[5]. The anterior leaflet had slightly higher strain rates during the unloading phase (opening) than the loading phase (closing). The difference in strain rate response during the loading and unloading phases between the chordae and the anterior leaflet is due to their function during the cycle. During the closing phase, the chordae must ensure the leaflets form a line of coaptation preventing

regurgitation. The closing phase happens in response to an increase in pressure causing the valve to close. The chordae are put under high strain rates as they straighten to ensure coaptation. During the opening phase, the leaflets are subjected to a higher negative transmitral pressure differential causing the leaflets to open. This pressure forces the leaflets to open and allows blood to fill the ventricle hence creating a higher strain rate on the leaflets during opening as blood surges through the valve. Therefore, the chordae withstand a higher loading rate during the closing phase while they prevent leaflet prolapse, and the anterior leaflet withstands a higher loading rate during the opening phase in response to the decrease in pressure in the ventricle. The mitral valve apparatus is a complex system containing many components that work together in synchronization to ensure functioning of the mitral valve.

The loading and unloading strain rates for the strut chordae which originate from either the posterior medial or the anterior lateral papillary muscles were also compared (see Figures 4.1.1 and 4.2.4). The strut chord which originates from the posterior medial papillary muscle is significantly longer from the insertion point in the anterior leaflet to the origin point in the papillary muscle and thicker in diameter than the strut chord which originates from the anterior lateral papillary muscle. The anterior lateral papillary muscle is located closer to the annulus than the posterior medial papillary muscle, and hence has a shorter strut chord. It was found that although there is a statistically significant difference in the diameter and length of these two strut chordae, there is not a statistically significant difference between the loading and unloading rates. The strut chord which inserted into the posterior medial papillary muscle did not have a significant difference between loading and unloading rates than the strut chord which originated from the

anterior lateral papillary muscle. When placed in the normal papillary muscle position, there was no significant difference in the maximum strain attained during valve closure between the two strut chordae. Even though the two strut chordae differ significantly in anatomical measurements, there is no significant difference in their mechanical properties which is supported by the uniaxial test results. There was no significant difference between the loading and unloading curves of the uniaxial tests between the two strut chordae. Also, if the forces on the anterior leaflet generated by the strut chordae differ on either side of the leaflet, then the shape of the annulus may not be conserved leading to a redistribution of forces among the other chordae tendineae. This redistribution of forces could lead to premature chordal dysfunction, if the force is greater than the chord can withstand, or malcoaptation between the anterior and posterior leaflets. The tension during valve closure and the angle of insertion into the anterior leaflet is similar between the two strut chordae[19]. Therefore, in order to maintain valve integrity, the strut chordae must have differences in their points of origin in the papillary muscles, insertion angle or location, so that the two strut chordae exert the same mechanical force on the anterior leaflet.

As found on the surface of the anterior leaflet[5], there is a plateau of nearly constant strain in the chordae during valve closure. This constant plateau indicates that there is minimal creep during valve closure. Although this plateau does not extend over the entire closure period as that seen in the anterior leaflet, it still suggests that there is minimal creep. The highly crosslinked collagen within the chordae contain the mechanisms to prevent creep due to the low amount of proteoglycans. The tissue in the chordae must act more as an elastic tissue, which would have minimal creep

characteristics such that there is no regurgitation. If the chordae experienced creep seen in many visco-elastic tissues, the chordae would become elongated during valve closure and malcoaptation would occur leading to regurgitation. It is known that collagen types I and III has a significant amount of stress relaxation. Stress relaxation studies conducted on collagen substrates show that when collagen is held at a constant strain (2%), there is a 30% decrease in stress at 50 seconds due to stress relaxation[20]. The collagen/GAG structure found in the chordae help to prevent the stress relaxation that could occur during the cycle[37]. The amount of fibrillar interactions affects the amount of relaxation in the chordae. The chordae which contain more fibrillar interactions, such as the anterior and posterior marginal chordae, would have less slippage of the collagen bonds and have less relaxation[37]. This is important in maintaining the function of the marginal chordae during the closure period. Without the integrity of the marginal chordae, the tips of the valve could cause miscoaptation leading to regurgitation.

The strain plateau experienced during valve closure had strain values between 3.75-4.29%, which is in the "toe" region of the uniaxial test, indicating that the strain incurred on the chordae during valve closure occurs in the range of normal physiologic function for the chordae. This is similar to the findings of Sacks et al.[5] when measuring surface strains on the anterior leaflet. It was found that the strain plateau on the anterior leaflet during valve closure was within the "toe" region of the stress-strain curve. In the "toe" region, the collagen fibers have been stretched until they are straight. After the "toe" region, the collagen fibers lock and there is a nonlinear stress-strain response. The stretching in the region immediately following the locking of the collagen fibers involves the straining of the bonds and bond angles within the fibrils[11]. The tissue becomes stiff

to the point where further deformations of the tissue are prevented even when the transmitral pressure increases. If the chordae functioned outside of the "toe" region, further deformation of the tissue, such as plastic deformation of the collagen, could occur during this strain plateau. Histological studies are being conducted to evaluate if the collagen fibers lock subsequent to the "toe" region of the stress-strain curve.

During the time period of the strain plateau, the collagen fibers lock and a force greater than the initial force, the force needed to cause the valve to close, is needed to strain the tissue. A study conducted by Lim et al.[9] showed that the elastin fibers cannot contribute to the initial segment of the stress-strain curve (Figure 5.9), and the transition into the "toe" region is due to the locking of the collagen fibers. Once the collagen fibers have straightened, the elastin fibers begin to stretch along with the collagen fibers. In order to keep the collagen fibers from stretching to a point of plastic deformation during the strain plateau, the elastin fibers must have an inherent property to prevent stress relaxation. After the collagen fibers have locked, the elastin begins to stretch and withstand the effects of constant strain preventing the collagen fibers from stretching further. The amount of stretch the chordae can withstand due to the decrease in crimp period, decreases with age. As a person ages, Lim et al.[11] showed that the waviness, the amount of crimp, of the collagen decreases by 7%. This decrease in waviness in the collagen could be due to the stress relaxation of the collagen since the chordae have a significantly more amount of collagen per dry weight than elastin. Due to the increase in the amount of collagen later in life[11], the elastin fibers can no longer provide the elasticity needed to bring the chordae back to the initial state before loading. The amount of crimp in the collagen fibers will then decrease. The decrease in crimp causes a shift in the stress-

strain curve, and the collagen fibers will lock earlier causing the "toe" region to occur with less strain. The strut chordae will still have a maximum strain of approximately 5.5%; however, the functioning range of the chordae will occur under less strain due to the shift of the "toe" region. Hence, the chordae withstand a larger strain, relative to their functioning range, during the later years of life causing more stress relaxation in the chordae. The elastin fibers may not prevent stress relaxation due to the increase in the amount of collagen and the chordae could become longer causing the mitral valve to prolapse and hence induce regurgitation.

During valve opening, there is a sharp increase in strain at approximately 488 msec (see Figure 5.4). This sharp increase in strain stretches the strut chordae to a taut position while the leaflet is farthest from the line of coaptation. It is thought that the strut chordae help to keep the leaflet from opening too far towards the septum during diastole. When the strut chordae are cut, the inflow tract for blood goes from a funnel shape with a transversely curved anterior leaflet whose concavity is toward the mitral orifice, to a flat shape in which the central and lateral portions of the anterior leaflet move homogeneously[21]. This funnel shaped curvature should direct the blood flow towards the apex of the heart and facilitate ejection. Figure 6.1 shows the curvature of the anterior leaflet during the opening phase of the mitral valve from both the atrial and ventricular sides. The red line drawn shows the transversely curved anterior leaflet whose concavity is toward the mitral orifice. This creates a funnel shape seen in (b) which directs the blood flow towards the apex of the heart and facilitates ejection. In (b), the anterior and posterior leaflets create a funnel shape which is seen by the curvature of the red lines.

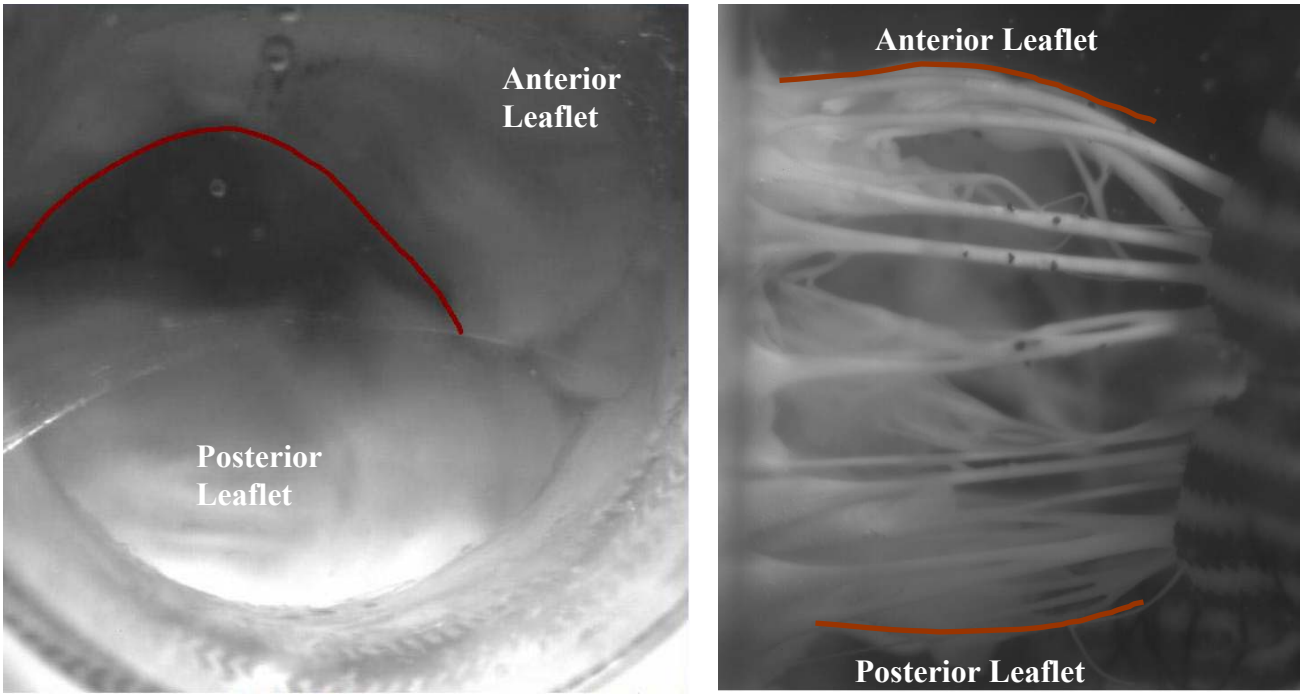

Figure 6.1: (a) Picture of the mitral valve from the atrial side during the open phase. The red line drawn shows the transversely curved anterior leaflet whose concavity is toward the mitral orifice. This creates a funnel shape seen in (b) which directs the blood flow towards the apex of the heart and facilitate ejection. (b) Picture of the mitral valve from the ventricle side during the open phase. The anterior and posterior leaflets create a funnel shape which is seen by the curvature of the red lines.

Figure 6.2 is a diagram representation of the change in curvature of the leaflet surface after sectioning of the strut chordae. In (a), the lateral portions of the anterior leaflet are held by the strut chordae. After sectioning of the chordae as in (b), the lateral and central region of the anterior leaflet form a flat shape allowing the two areas of the leaflet surface to move homogeneously during closure.

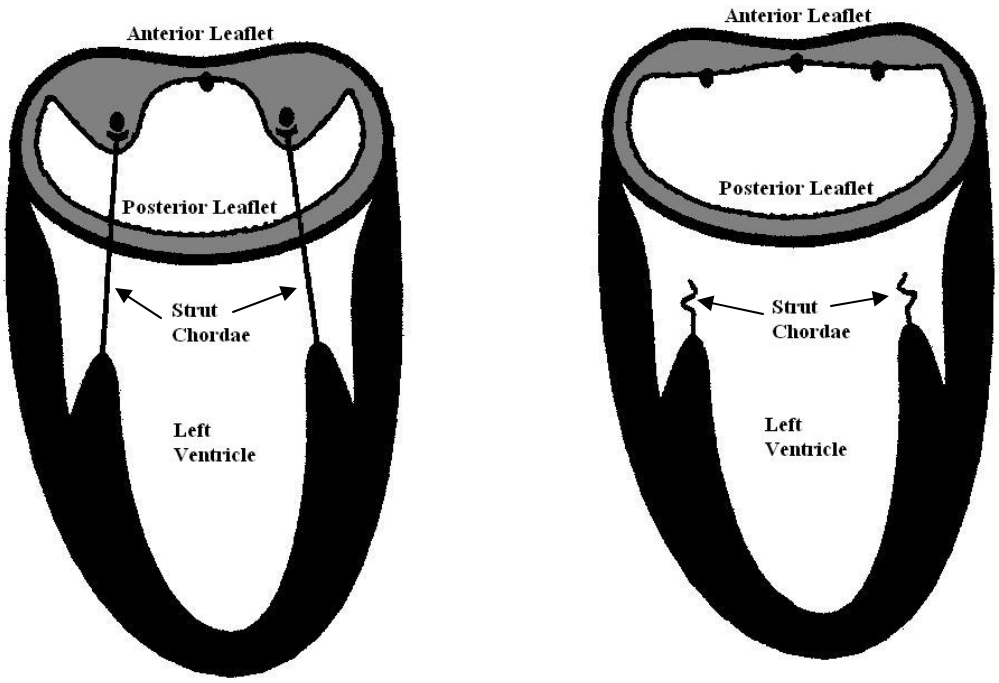

Figure 6.2: Diagram of the mitral valve (a) before sectioning of the strut chordae and (b) after sectioning of the strut chordae. In (a), the lateral portions of the anterior leaflet are held by the strut chordae. After sectioning of the chordae, the lateral and central region of the anterior leaflet form a flat shape allowing the two areas of the leaflet surface to move homogeneously during closure. Picture adapted from Goetz et al.[21].

Studies conducted by Messas et al.[22] showed that cutting of the strut chordae for surgical treatment of functional ischemic mitral regurgitation abolished the tethering of the body of the anterior leaflet, which increased leaflet coaptation. However, this surgical repair technique is for patients in whom the papillary muscles have relocated towards the apex of the heart. Since the lengths of the chordae remain constant during the relocation, the amount of anterior and posterior leaflet surface used for coaptation will decrease. By cutting the strut chordae, the motion of the central region of the anterior leaflet was flat with the central and lateral portions of the anterior leaflet moving homogeneously. Although this increased the amount of anterior leaflet surface used for coaptation, the anterior leaflet did not generate a funnel shape and could potentially interfere with the

aortic valve outflow tract. Figure 6.3 below describes the mitral valve in the open state with (a) both the strut chordae intact and (b) the strut chordae cut. In (a), the strut chordae prevent the leaflet from obstructing the aortic outflow tract and also generate a funnel shaped curvature to direct the blood flow towards the apex of the heart. With the strut chordae cut as shown in (b), the anterior leaflet protrudes into the aortic outflow tract. The blood is not directed towards the apex of the heart which could influence blood recirculation inside the left ventricle and inefficient systolic ejection.

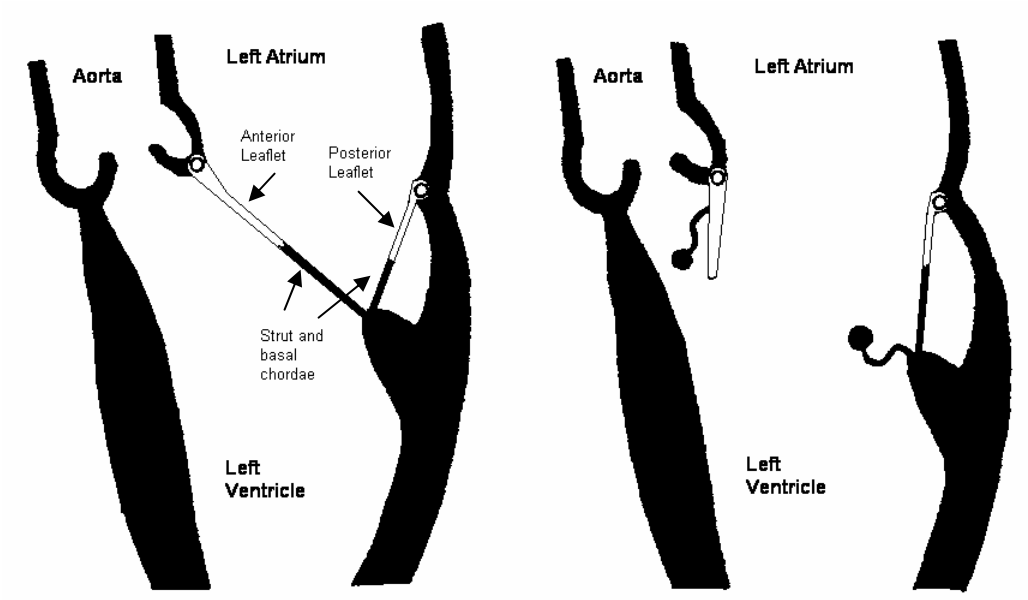

Figure 6.3: Models of the mitral valve in the open position with (a) the strut chordae intact and (b) the strut chordae cut. In (a) the leaflets form a funnel shape to direct blood flow to the apex of the heart. In (b) the anterior leaflet protrudes into the aortic outflow tract. Picture adapted from Messas et al.[22].

Small oscillations in the chordae occur when the valve is open and the fluid flows from the atrial chamber through the mitral valve and into the left ventricle chamber. During these oscillations, the strain on the chordae can reach a negative value as seen in Figures 5.2 and 5.4. The negative values could be a result of the reference frame in which the

chordae are not in a relaxed, no strain situation, but rather a situation in which a constant strain is seen on the chordae. No *in vivo* data has been collected to determine if the chordae are under a small strain during the entire cardiac cycle. This negative strain value could also be the result of out of plane motion. The strain definition used to determine the amount of strain seen in the chordae only accounts for the in plane strain. However, due to the dynamic nature of the chordae, there could be out of plane strain that needs to be taken into account. Since the in plane motion was 77.5%±7.7%, the amount of strain attributed to the out of plane motion was neglected.

The uniaxial tests of the chordae show the viscoelastic properties that are characteristic to most soft tissues[18]. Three features can be observed from the uniaxial tests: a non-linear load-strain relationship; a hysteresis loop in cyclic loading and unloading; and preconditioning in repeated cycles. Several other investigators have performed uniaxial tests on the chordae tendineae of the mitral valve; however, their testing procedures involve the strain to be computed using the cross-head displacement technique[8,9,11,12]. It can be seen that there is a significant difference in the amount of strain incurred when comparing the cross-head displacement and the displacement between graphite markers located on the central region of the chordae. The failure properties of the chordae will be correct since these do not depend on the strain measurement; however, the extensibility measurements will be biased. There are many methods available to complete load-strain tests on soft tissue specimens: direct elongations from the testing machine (cross-head displacements), extensometer-based measurements, and strains based on non-contact optical methods[23]. All three methods have inherent limitations. In direct strain measurements from the testing machine, extra strain energy is lost due to end effects.

This also occurs when the clamps are placed directly on the specimen, causing a significant stress concentration around the clamping mechanism. Therefore, when testing tendons many protocols include leaving the tendon attached to the bone and muscle, and place the bone and muscle between the clamping mechanism and not the tendon tissue. The other two methods of testing, extensometers and non-contact optical methods contain their own inherent problems. When using non-contact optical methods, measurements are taken over a specific region of the tissue specimen. Due to variabilities in tissue microstructure over a specimen's length, the measurements over the specific region imaged may not exhibit a true representation of the entire specimen. However, histological studies have shown that the chordae exhibit the same biological make up throughout the entire length of the specimen. The relative concentrations of collagen, elastin, and extracellular matrix components were found to be consistent throughout the length of the chordae[24]. Therefore, the use of non-contacting optical methods to measure strains during uniaxial testing of the chordae tendineae will provide unbiased results as compared to direct elongations from the testing machine. Also, since the *in vitro* experiments were limited to a specific region of the chordae, the uniaxial test should use optical methods to measure the strain in the same region of the chordae such that the strains measured during the two separate tests can be compared.

There are many similarities between the chordae tendineae and other tendons. Tendons are composed of collagen fibrils arranged parallel to the direction of loading[18]. A similar microstructure was found in the chordae tendineae. Along with the microstructure, the mechanical properties of the chordae tendineae and tendons are also similar in the functioning range. It is known that tendons have a "toe" region between 2-

5% which represents their normal physiologic functioning range[18]. The "toe" region of the chordae was between 3.5-4.5% which lies within the functioning range of the human calcaneal tendon[25]. However, the failure strain and failure load of the human calcaneal tendon are significantly less and significantly higher than the mitral valve chordae, respectively. The failure strain of the mitral valve chordae varies according to chordal type: posterior marginal 24.9% strain; basal 33.1% strain; anterior marginal 30.3% strain; and strut 43.9% strain[8]. The human calcaneal tendon had failure strains for the tendon substance of 8.8% strain[25]. The human calcaneal tendon has a greater failure load than the chordae. The failure load of the chordae varies according to chordal type: posterior marginal 4.20 N, basal 12.93 N, anterior marginal 7.30 N; and strut 22.70 N[8]. The failure load of the human calcaneal tendon is 1189 N[25]. Although the chordae and tendon exhibit different failure properties, the mechanical properties are similar in the extensibility region ("toe" region).

Surgeons are currently using ePTFE sutures to replace diseased, damaged, or torn mitral valve chordae tendineae. These sutures need to have the same mechanical properties as the native chordae in the functioning range. When sutured to tissue, testing has shown that the ePTFE suture, the most commonly used suture material for chordae replacement, has a knot strength of approximately 10 N[26], which is above the maximum load attained for the chordae during valve closure[13, 17]. A study conducted by Cochran et al.[27] found that the elastic modulus of ePTFE sutures was significantly higher than that of the native porcine mitral valve chordae tendineae; however, the ePTFE suture did exhibit some viscoelastic characteristics, hysteresis and creep, that begin to approach native chordae properties. The suture materials can support a higher load during failure like the tendon,

but they do not exhibit the same properties in the functional range[28]. The intermediate results from patients who underwent replacement of diseased, damaged, or torn chordae tendineae with ePTFE sutures show a patient freedom from reoperation at 86% to 94% at 10 years[29]. However, of the patients needing reoperation, 69% have had rupture of other native chordae[30, 31, 32]. This failure of other native chordae could be attributable to force redistribution on the native chordae after chordal replacement. Tissue engineering constructs developed out of smooth muscle cells and composed of collagen have been developed[33]. The tissue engineered constructs developed have a significantly decreased failure stress and extensibility than native chordae[33]. The strain studies presented here show that the constructs do not necessarily need to a have a significant strength reserve, but they must be able to support maximum strains of approximately 4%. The tensile strength and fatigue resistant characteristics of the native chordae has yet to be imitated with synthetic materials. Presently, ePTFE sutures appear to be the best synthetic alternative for chordal replacement due to its viscoelastic characteristics and its ability to allow tissue ingrowth[27]. There is still a need to develop a better synthetic or tissue replacement for the chordae tendineae that more nearly approximates the mechanical behavior of mitral valve chordae tendineae. Therefore, surgeons could potentially use tendons to replace torn, damaged, or diseased chordae since the tendons exhibit the same properties in the functioning range but can support a higher load during failure.

Previous morphology studies of the chordae showed an inner collagen core surrounded by a middle layer of elastic fibers, and an outer layer of endothelial cells[6]. Histological examinations conducted during this study show that there are three distinct layers as previously reported; however, the middle layer is not completely composed of elastic

fibers. A three dimensional model, representing all six types of chordae, is shown in Figure 6.4 illustrating the three distinct layers.

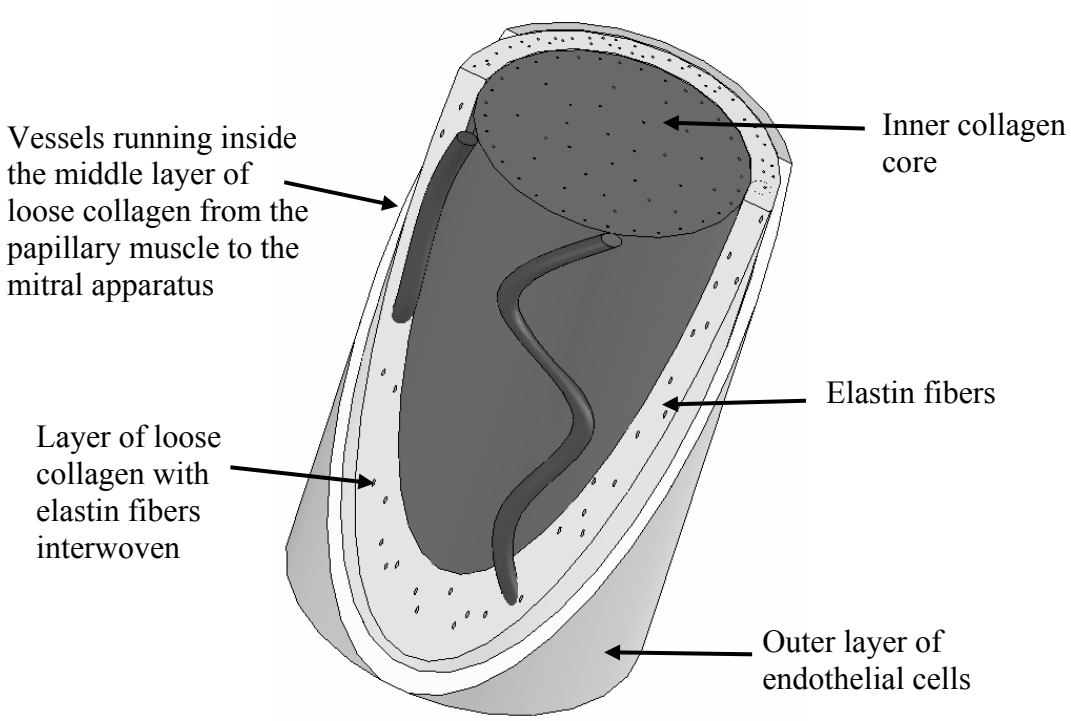

Figure 6.4: Three dimensional model of the mitral valve chordae tendineae describing the histological composition. There are three distinct layers: an inner collagen core, a middle layer of loose collagen with elastin fibers interwoven, and an outer layer of endothelial cells. Vessels were observed running in the middle layer up the length of the chordae in a twisting motion.

The inner layer is composed mainly of densely packed, highly cross-linked collagen fibrils with few elastic fibers. The collagen fibers provide the mechanical strength and integrity for the chordae. The middle layer (Figure 6.4) was found to be composed of a loosely connected layer of collagen with elastic fibers interspersed within the collagen fibrils. In a loose configuration, the collagen fibrils do not exhibit the high degree of strength found in the densely packed collagen fibers in the inner layer. The elastin fibers found in this middle layer provide the elasticity seen in the chordae at lower stress levels when the collagen fibers are uncrimping. Histological examination showed that during a

relaxed state, the collagen in the chordae had a crimped configuration and the elastic fibers were straight, hence giving the chordae mechanical properties that are similar to those exhibited by a composite material. The initial segment of the nonlinear stress-strain curve is due to the uncrimping of the collagen and the final slope of the curve is attributed to the response of the elastin and the inner collagen core[9]. The highly crosslinked collagen seen in the inner layer of the chordae function to prevent creep and ultimately chordal elongation during valve closure. Without the highly crosslinked collagen fibers, the chordae would lengthen during valve closure and allow the leaflets to prolapse and induce regurgitation. A single layer of endothelial cells surrounds the entire chord.

Using biochemical assays to study the compositional makeup of the six types of chordae (strut, anterior marginal, commissural, basal posterior, posterior intermediate, and posterior marginal), it was found that the anterior marginal and posterior marginal chordae contain significantly more DNA per milligram of tissue than the other chordae. The anterior marginal and posterior marginal chordae function to secure the anterior and posterior leaflets, respectively, during valve closure ensuring a line of coaptation. The larger chordae, such as the strut and basal chordae, function to prevent the leaflets from prolapsing during valve closure and withstand the highest mechanical load during the cardiac cycle. The thinner chordae, anterior and posterior marginal chordae, function to transmit the contractions of the papillary muscles to the mitral leaflets to ensure proper coaptation configuration. The collagen structure in the chordae provides the tensile strength needed to perform these functions. In order to ensure that the collagen structure does not degrade, fibroblasts must be present to repair and remodel the collagen matrix

by producing extracellular proteins under mechanical loading conditions[34]. In order to elucidate the need for fibroblasts to maintain collagen structure, a study was conducted on rabbit patellar tendon in which the collagen producing cells were extracted from the patellar tendon. It was found that stress enhancement can affect the extracellular matrix of the patellar tendon without living cells[35] . This infers that intrinsic fibroblasts inhibit the mechanical deterioration and repair micro-damage of the extracellular matrix induced by the stress enhancement. Further studies investigated the response of fibroblasts to mechanical loading to conclude if mechanical loading was needed to stimulate these cells to produce and maintain the collagen matrix. Sutker et al.[36] and Yang et al.[34] report that cyclic uniaxial mechanical stretching stimulates the collagen synthesis and proliferation of fibroblasts *in vitro* which further supports the findings of Tohyama et al.[35]. The increase in collagen synthesis and proliferation of fibroblasts which occurs during mechanical loading conditions, such as the loading on the chordae during the cardiac cycle, is important to the long term functionality of the chordae tendineae. The higher concentration of DNA in the anterior and posterior marginal chordae suggests that these chordae have higher rates of cellular turnover and collagen production than the other chordae, in order to maintain the microstructure of the chordae and prevent mechanical deterioration. These marginal chordae are essential for the correct coaptation of the leaflets; and therefore, they would contain more fibroblasts to maintain the collagen matrix in order to ensure mechanical function.

All six types of chordae (strut, anterior marginal, commissural, posterior intermediate, basal posterior, and posterior marginal) contain the same amount of elastin per milligram of tissue. The commissural chordae showed higher values of elastin which could be in

response to the amount of constant strain they withstand throughout the cycle. The commissural chordae are taut throughout the cardiac cycle during both valve opening and closing. This would infer that they are under a constant strain throughout the cycle causing the commissural chordae to be susceptible to higher stress relaxation conditions. Elastin has been shown to have lower stress relaxation properties than collagen[18]; therefore, a tissue containing more elastin would withstand the effects of stress relaxation more than a tissue with lower amounts of elastin. The commissural chordae contain more elastin fibers than the other types of chordae in order to prevent stress relaxation during the cycle.

The posterior marginal chordae contain more collagen per milligram of tissue than the other chordae. This is in agreement with the DNA results which showed significantly more DNA per milligram of tissue. The chordae which contain more DNA, contain more fibroblasts (connective tissue cells) which secrete an extracellular matrix rich in collagen and other macromolecules which influence the rate of collagen production and turnover. The more collagen the chord contains, the stiffer the chord under elevated stress levels. This finding is in agreement with Liao et al.[8] who found that the thicker strut chordae were more extensible and less stiff than the thinner marginal chordae. The stiffness of the posterior marginal chordae is important during valve closure. During valve closure, the anterior and posterior leaflets move homogeneously until the marginal chordae are extended. The free margin of the anterior leaflet continues to move toward the posterior leaflet until the line of coaptation is formed. The posterior marginal chordae is responsible for maintaining the position of the posterior leaflet during valve closure, while the free margin of the anterior leaflet continues to move. After the posterior leaflet

has commenced movement and the anterior leaflet continues to move, the posterior marginal chordae needs a high degree of strength to prevent the posterior leaflet from prolapsing into the atrium during closure.

The histological and biochemical examinations of the chordae describe the differences between the types of chordae based on function and insertion site on the mitral valve leaflets. These differences must be considered during chordal translocation procedures as they may be essential to the long term outcome of the procedure.

It was previously believed that the chordae tendineae of the mitral valve were simple collagenous structures which provided a means of communication between the papillary muscles and the mitral valve apparatus during the cardiac cycle[6]. However, vessels have been located in the chordae tendineae of the mitral valve and support the conclusion that the chordae are more than simple collagenous structures, but living tissues that act to support and feed the mitral apparatus. The observed blood vessels, approximately 200μm in diameter, were found in the middle layer of the chordae running in a longitudinal manner from the papillary muscle to the mitral apparatus. The vessels tended to twist around the chordae while ascending. The vessels appear to feed the mitral apparatus and not the chordae. This is supported by that observation that the major vessels running along the length of the chordae did not branch until they inserted into the leaflets. Like other tendons, the chordae are thought to be fed through diffusion. The nutrients from the blood first diffuse into the tissue fluid that surrounds the cells and then into the cells through four methods: gases and lipid-soluble substances (fatty acids, dissolved gases) cross through the lipid layer of the cell membrane; water crosses by osmosis; ions cross by facilitated diffusion; and glucose and animo acids cross by active transport. It is not

known whether the chordae receive nutrients from the diffusion of the nutrients from the blood circulating in the heart, or from the diffusion of the nutrients from the blood contained within the vessels traveling in the chordae. Further investigation of these diffusion processes is necessary to have a definite answer as to how the chordae obtain nutrients from blood.

Previous studies have shown that the mitral leaflets do contain vessels which bring a rich blood supply containing nutrients to the leaflet tissue[36]. These vessels were thought to have originated in the annulus of the mitral valve; however, the study presented here shows that some blood vessels which do insert into the mitral leaflets extend from the papillary muscles through the chordae and into the leaflets. Further investigations, such as dye injection studies, are necessary to determine the origin of the vessels in the mitral leaflets.

The strut chordae, which insert into the rough zone of the anterior leaflet, were found to have significantly more vessels than the other chordae. The marginal chordae, which insert into the edges of the anterior and posterior leaflets, may be too small in diameter to support many vessels. The size of the posterior leaflet as compared to the anterior leaflet may provide the reasoning behind the lack of vessels in the basal posterior and posterior intermediate chordae as compared to the strut chordae, even though they are similar in diameter. Since the posterior leaflet is smaller in height from the valve annulus to the free margin than the anterior leaflet, it can obtain more blood from the annulus. Therefore, the need for a blood supply through the chordae is not necessary. The blood vessels through the strut chordae lead to the thinner regions of the anterior leaflet which are farther from the annulus. This may imply that the leaflets which are smaller in height

from the valve annulus to the free margin, commissural and posterior leaflets, obtain more blood from the annulus itself; whereas, the anterior leaflet receives blood from both the annulus and the chordae.

Mitral valve repair is becoming a more attractive option instead of replacement. Currently silk, nylon, ePTFE, and Gortex sutures are used for chordal replacement. If these synthetic materials are used to replace the native chordae, then the leaflet tissue where the native chordae insert may become necrotic due to a lack of blood and nutrient supply.

CHAPTER 7

CONCLUSIONS

This study demonstrates the first *in vitro* examination of the strain experienced by the chordae tendineae of the mitral valve. Dual camera stereo photogrammetry was used to measure *in vitro* strains experienced by the chordae tendineae of the mitral valve under physiologic function. This non-invasive technique allows measurements of other sections of the mitral apparatus during physiologic and pathologic loading conditions.

Geometrical measurements showed that although there was a significant difference in the length and diameter of the two strut chordae, there was an insignificant difference in the mechanical properties. This alludes to the conclusion that the anatomical positions of the strut chordae are related to the point of insertion in the papillary muscle so that the chordae exert the same mechanical forces on either side of the anterior leaflet.

It was found that the chordae experience different strain rates in the loading (75.3% ± 48.6%) and unloading (-54.8% ± -56.6%) phases as the valve closes and opens. This is similar to the properties of the anterior leaflet of the mitral valve[5]. There is a strain plateau of 4.43% ± 3.43% reached during valve closure that supports the hypothesis that there is minimal creep experienced by the chordae during valve closure. During valve opening, the strut chordae hold the central region of the anterior leaflet in a funnel like shape to facilitate efficient filling of the ventricle during diastole. Three features can be observed from the uniaxial tests: a non-linear

load-strain relationship; a hysteresis loop in cyclic loading and unloading; and preconditioning in repeated cycles which all are typical responses of biological soft tissues. This suggests that the chordae exhibit similar material properties to the human calcaneal tendon in the normal functioning range.

Histological examination indicated that previous studies have not adequately described the histological composition of the mitral valve chordae tendineae. Contrary to earlier belief, blood vessels were found in the chordae running from the papillary muscle to the insertion sites of the chordae on the mitral leaflets. These vessels do not provide blood to the chordae, but rather act as a supply source to other parts of the mitral apparatus. The presence of vessels characterize the chordae tendineae as complex living components that must work in coordination with the papillary muscles and valve leaflets to ensure proper mitral valve physiologic function. Therefore, chordal translocation and cutting procedures must consider the presence of these biological structures as they will be essential to the long term outcome of these procedures.

Chordae tendineae of the mitral valve have different microstructures according to chordal type. Biochemical examination showed that the chordae contain different amounts of collagen, elastin, and DNA depending on chordal type. It was concluded that the amounts of these different components is related to the function and location of the chordae. The chordae which hold the largest load during the cardiac cycle, strut chordae, contained more collagen; all six types of chordae have similar elastin content to prevent stress relaxation during constant strain, and the chordae, anterior and posterior marginal, which function to ensure coaptation of the anterior and

posterior leaflets contain more DNA. During chordal translocation procedures, surgeons must consider the biochemical composition of each chordae as it is specific to its location and function in the mitral apparatus.

The findings in this study confirm that the mitral apparatus is composed of many components which work together in a complex, dynamic environment to ensure proper function. Further understanding of the mitral apparatus, including the chordae tendineae, will help better define surgical techniques aimed at repairing the mitral valve to its normal functioning state.

CHAPTER 8

LIMITATIONS AND RECOMMENDATIONS

8.1 Chordae Tendineae Marker Technique

The *in vitro* study was used to define a technique that could measure strains experienced on the chordae tendineae of the mitral valve using a physiologic *in vitro* flow model. However, this study was limited to only measure strains on the anterior strut chordae. The amount of movement, i.e. the wide range of motion, of the anterior marginal chordae compared with the small amount of strain experienced during the cardiac cycle made spatial resolution a major factor with this technique. The markers could not be clearly defined during the entire cardiac cycle. A better calibration technique needs to be established to correct this limitation in spatial resolution.

This study also focused only on normal physiologic conditions. The study could be extended to include the pathological conditions in which the papillary muscles are moved in the apical, septal-lateral, and lateral directions. The working fluid analog used was 0.9% saline which does not have the same properties as blood. The viscosity of saline is lower than that of blood; however, to use a blood analog with the same viscosity such as glycerin/water, the tissue properties would be compromised.

Only strain information could be obtained using the developed method which is not sufficient to understanding chordal function. However, forces on chordae have been measured in previous studies[17] and compliment this study.

8.2 Uniaxial Tests

Uniaxial tests should be completed in which the sampling rate is 500 frames per second which is the limitation set by the camera system. This would ensure less noise and fluctuations in the load/strain curves. The uniaxial tests could also be used to measure differences in loading behavior between the six different chordae tendineae; however, previous studies have demonstrated the differences between the chordae during uniaxial tests[8,9,11,12]. The viscoelastic effect was not quantified to determine the error in load measurement and high speed loading control.

8.3 Histology

The histological studies need to be conducted on human chordae tendineae. The vascularization of the tissue may be inherent only to porcine tissue. The exact function of the vessels in the tissue has not been determined. Using a micro-CT, dye can be injected into the tissue and the vessel morphology can be determined. Also, a dye angiography can be used on living animals to also determine the role of the vessels during normal heart function.

It has been postulated that the chordae tendineae of the mitral valve do not contain nerve fibers; however, it was also postulated that they do not contain vessels. Therefore, a nerve stain should also be completed to determine the innervation of the chordae. Preliminary experiments have been conducted on this; however, the controls for both methods revealed flaws in the experimental procedure and definite conclusions could not be made. The tissue should be injected with acetylcholinesterase immediately after harvest and then snap frozen. The tissue could then be sectioned and stored as in standard histological staining.

APPENDIX A

VALVE PREPARATION AND HARVESTING PROTOCOL

Valve Preparation and Harvesting (Estimated time: 4 hours)

A. Harvesting and mounting – Obtain fresh, small, porcine hearts from the abattoir (available Mondays and Wednesdays only; call a day ahead 770-786-2086). Measure the size of the annulus while intact inside the heart using the Edwards measurement system (use valve no larger than 34). Dissect out the mitral valve, preserving chordae tendineae and papillary muscles (PM). Suture the papillary muscles and annulus to their holders.

1. Dissection/harvesting
    a. Identify left and right atria. Remove left atrium to expose mitral valve. Remove right atrium and ventricle.
    b. Identify the aorta. Cut the aorta lengthwise and into the ventricular septum. Cut through the septum to open the left ventricle.
    c. Cut around the papillary muscles and around the annulus.
    d. Inspect the valve for damage before proceeding. Using the curved scissors, trim around the annulus, leaving 3-5mm for suture. Trim the papillary muscles as small as possible leaving insertion points intact.
    e. Refrigerate in saline.
2. Suturing
    a. Papillary muscles – Cut a piece of Dacron cloth to fit around the papillary muscles. Using 3-0 sutures (braided silk, Ethicon, NJ), suture the fabric to the muscle (side, middle, side). Sew the fabric between the chordae. Try not to deform the muscle or the chordae.
    b. Annulus – Suture the valve to the saddle-shaped annulus – Position the valve such that the anterior side is facing the flat side of the annulus

holder. Tack down four corners with knots (anterior, posterior, commissures). From the last corner, begin suturing around the posterior half using the cross-stitch technique. Sew the anterior half using 2 threads. Cross-stitch out from the center of the anterior leaflet. Finish all threads with at least three knots.

APPENDIX B

ENGINEERING DRAWINGS OF THE IN VITRO FLOW LOOP

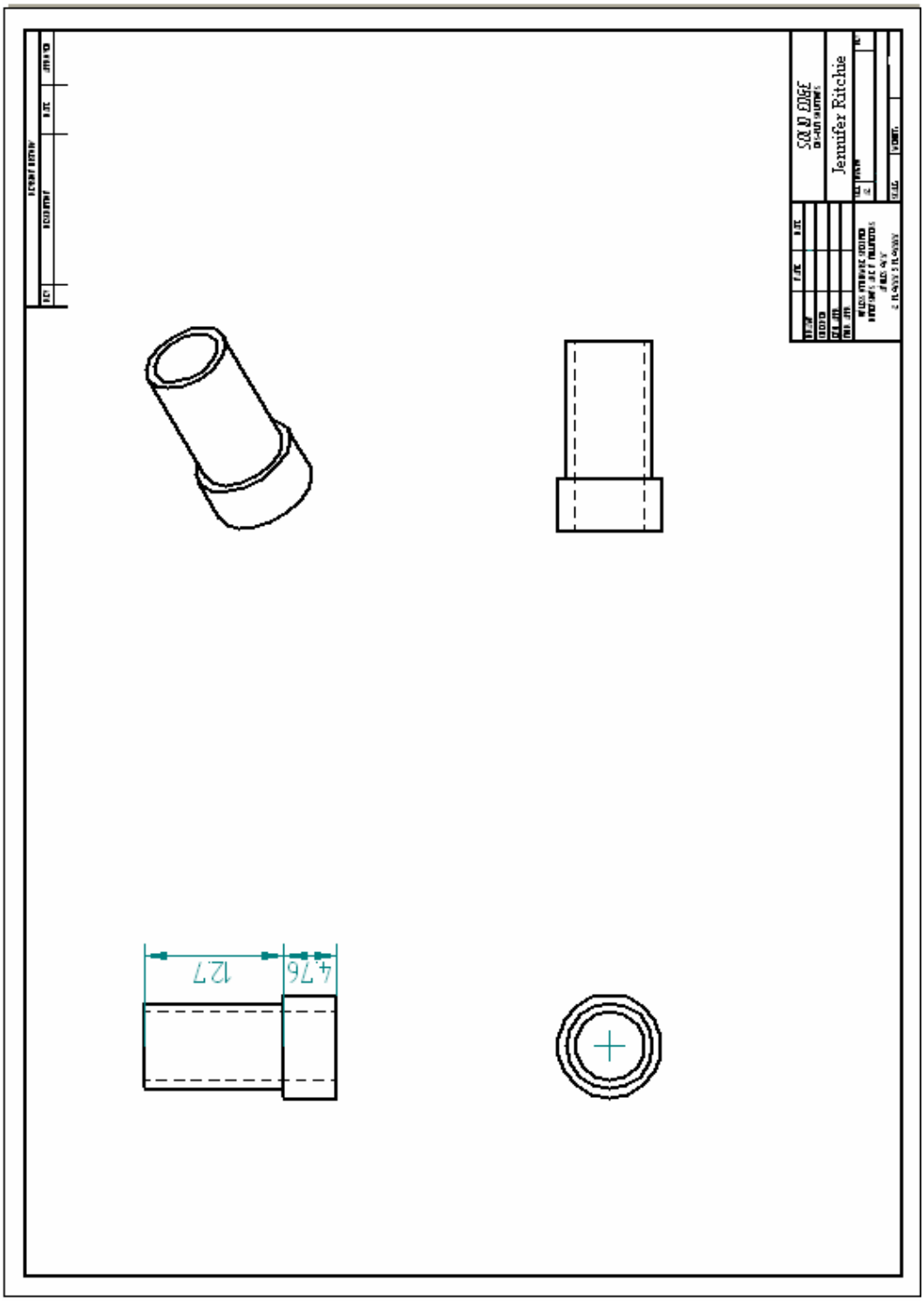

Figure B.1: Plastic spacer placed at the end of the force rod.

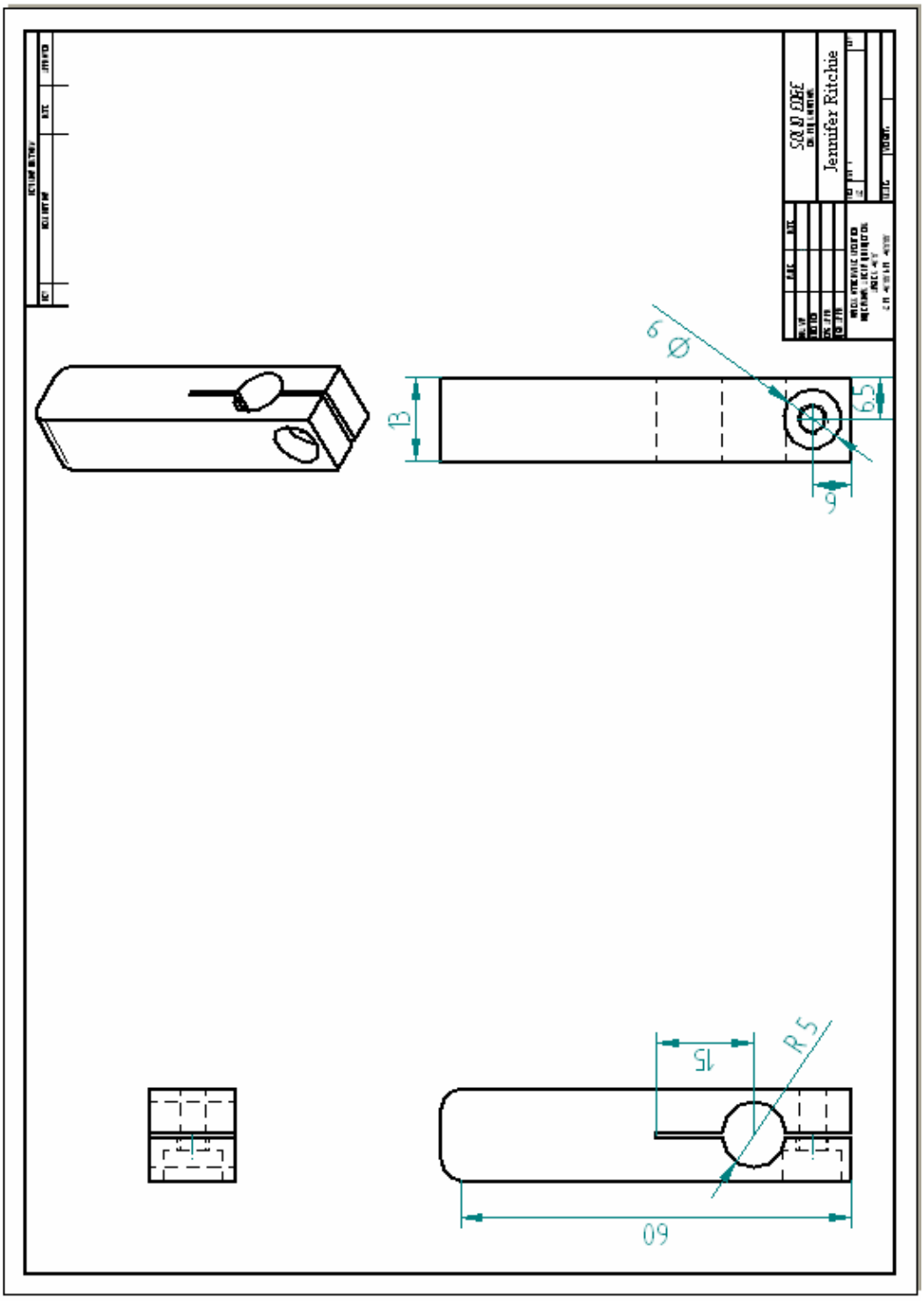

Figure B.2: Metal turn rod placed at the end of the force rod to enable turning of the force rod.

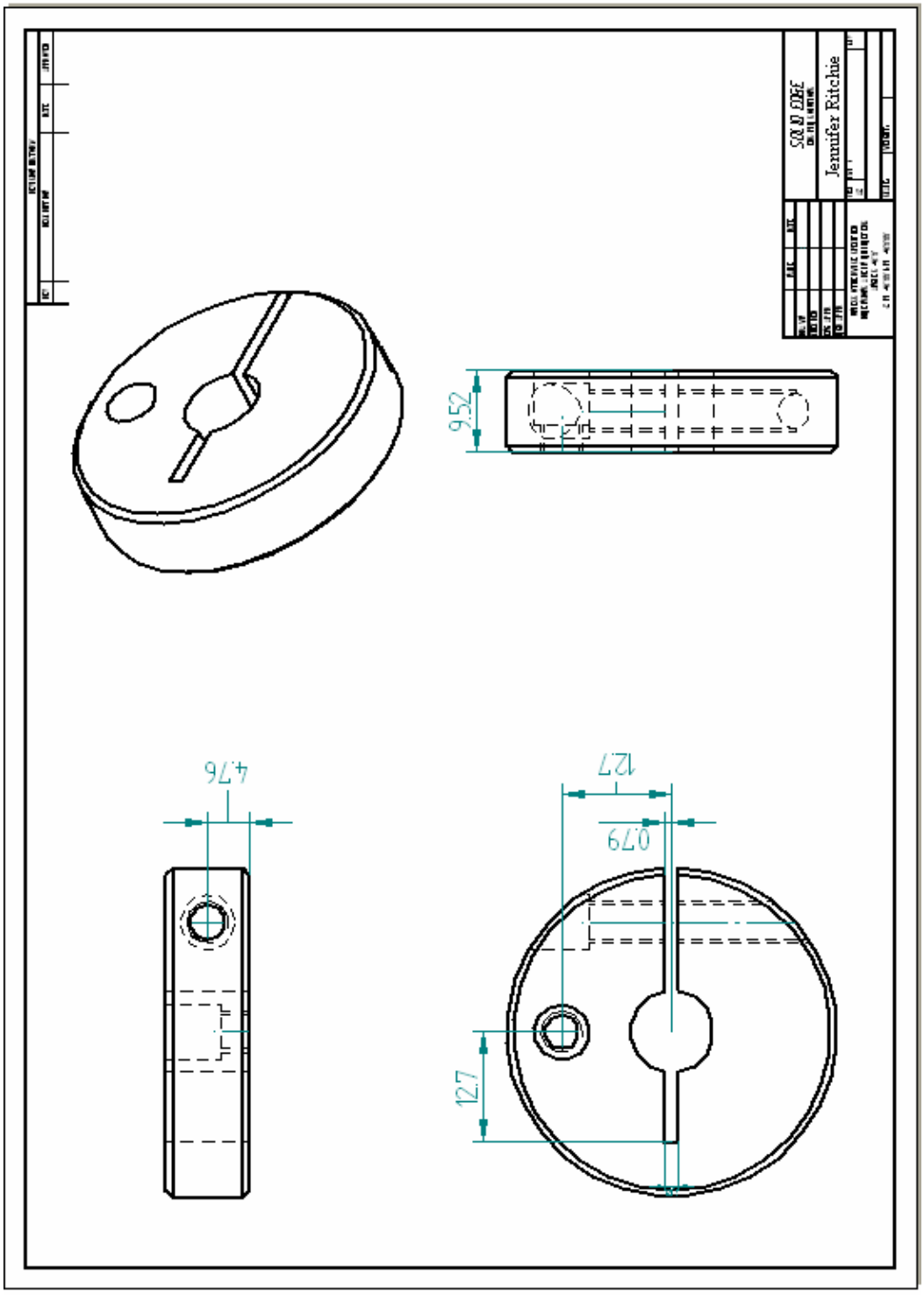

Figure B.3: Metal cylinder placed on the force rod on the outer side of the ventricle chamber. This connects to the inner metal cylinder to ensure no leakage through the hole in the back of the chamber in which the force rod travels through.

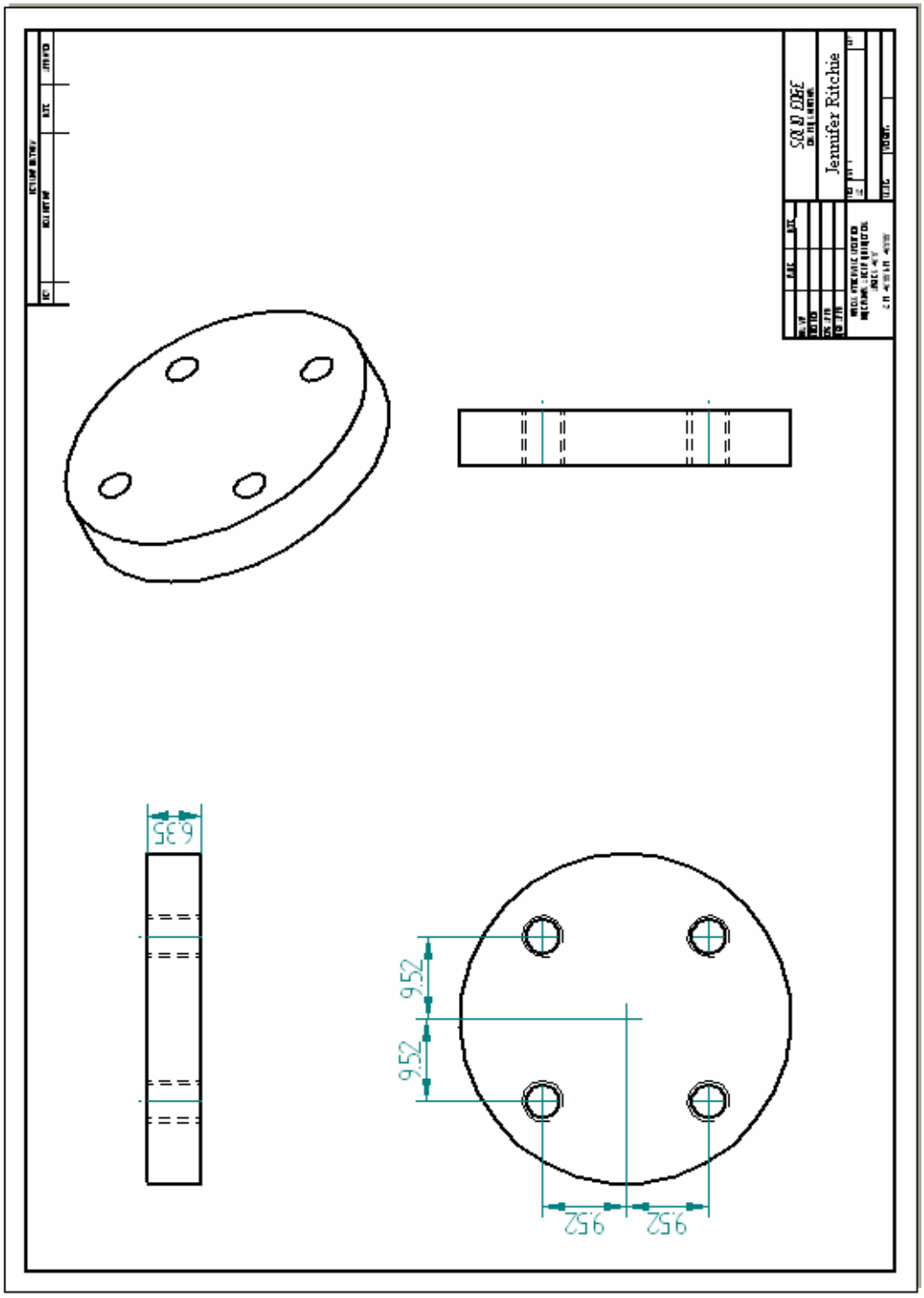

Figure B.4: Metal cylinder placed on the force rod on the inner side of the ventricle chamber. This connects to the other inner metal cylinder to ensure no leakage through the hole in the back of the chamber in which the force rod travels through.

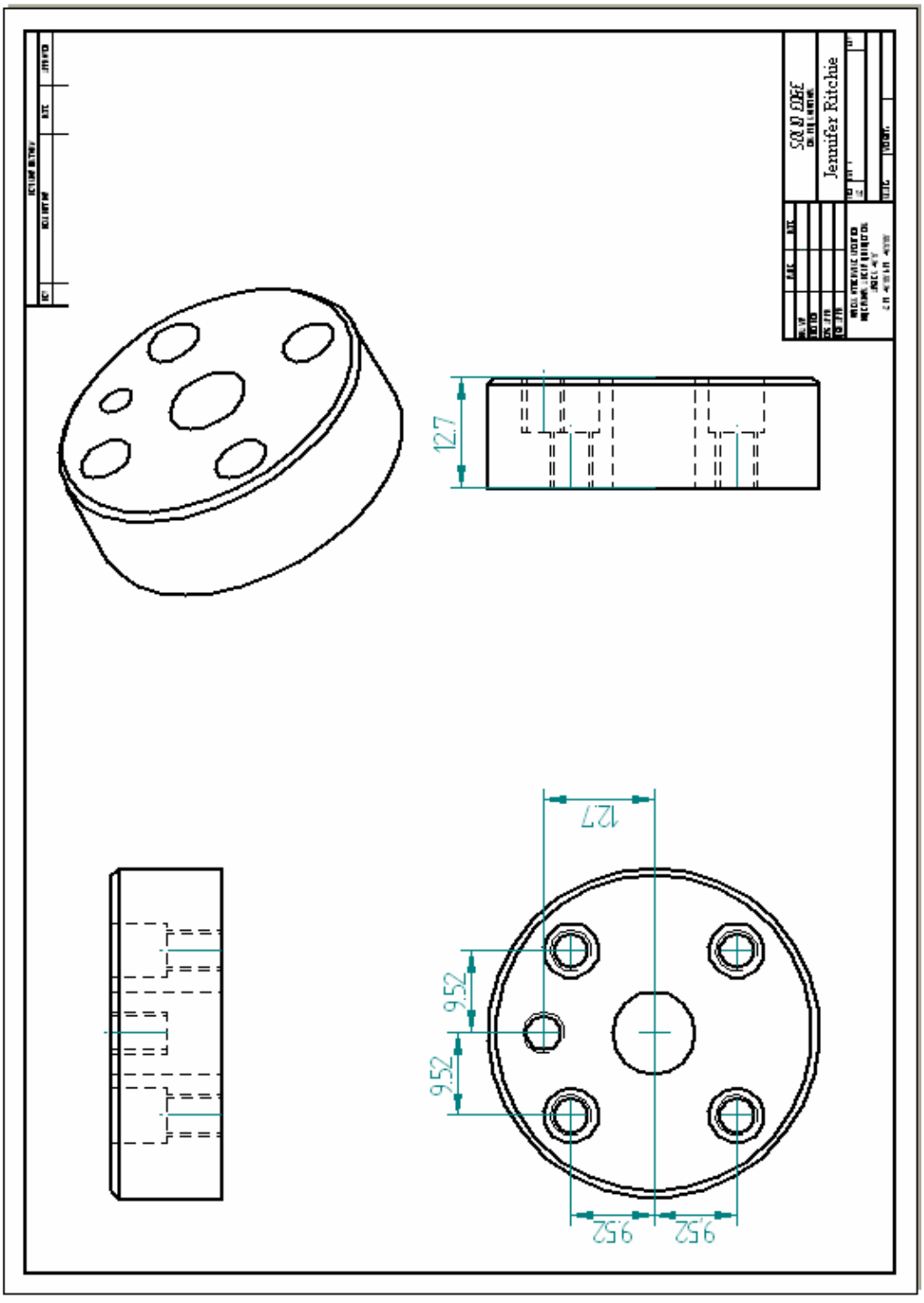

Figure B.5: Metal cylinder placed on the force rod on the inner side of the ventricle chamber. This connects to the outer metal cylinder to ensure no leakage through the hole in the back of the chamber in which the force rod travels through.

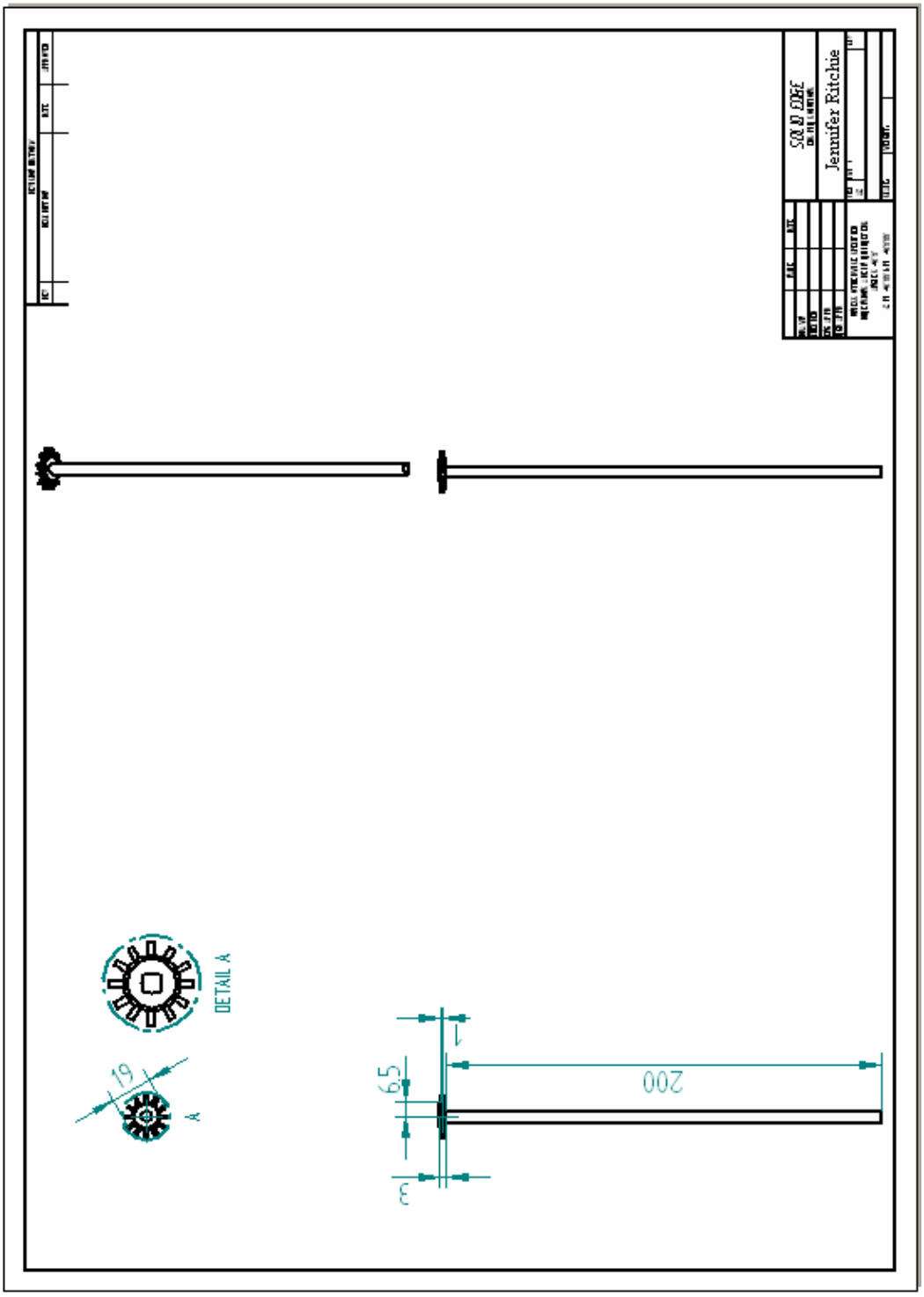

Figure B.6: The inner rod which extends out the back of the ventricle model. The gears allowing turning of the force rod screw from outside the ventricle chamber. Therefore, the ventricle chamber does not need to be opened to change papillary muscle position.

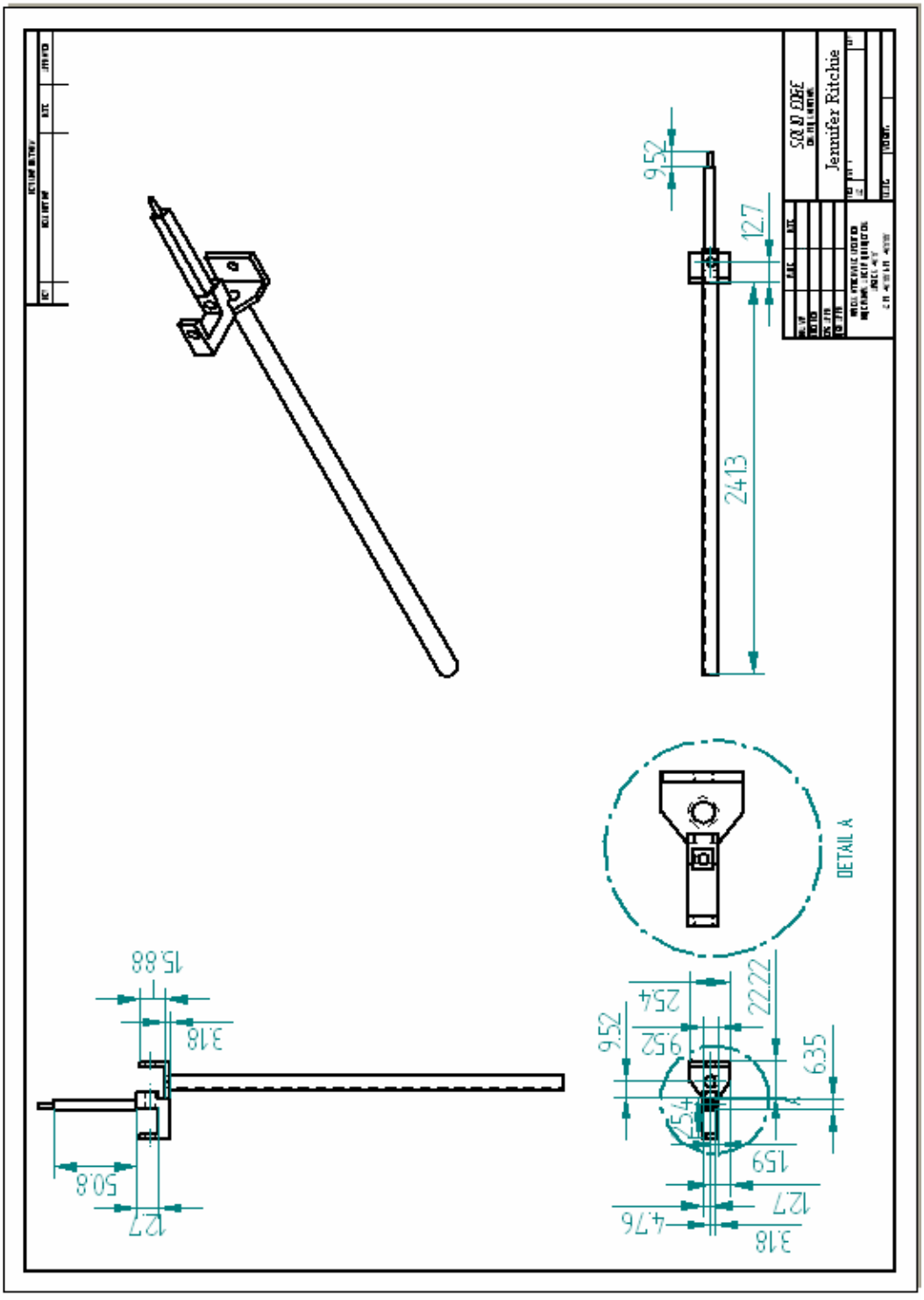

Figure B.7: Outer sheath of the force rod. The inner rod travels through this to the outside of the ventricle chamber. The papillary muscle holding disks connect directly to the end of the rod.

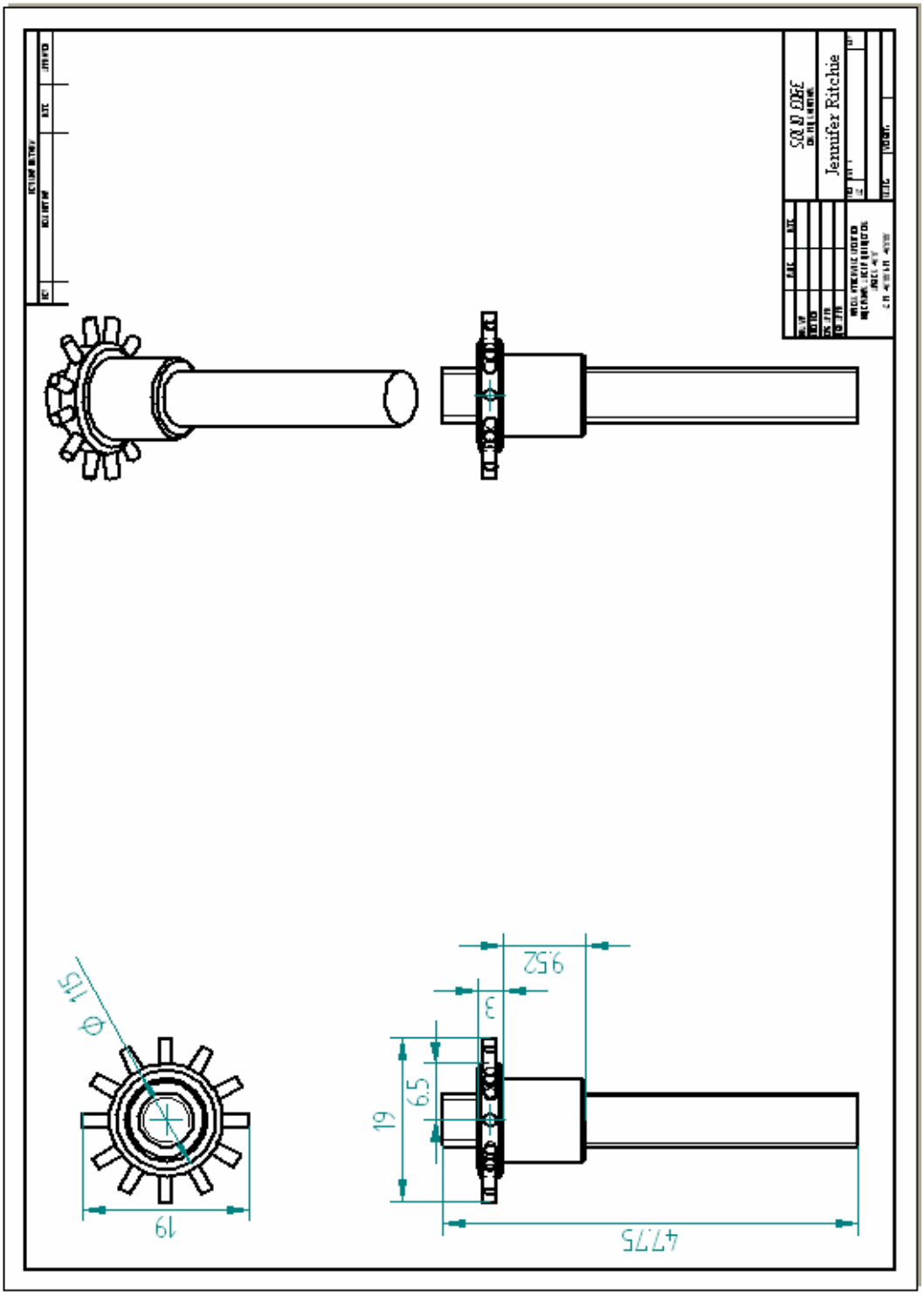

Figure B.8: Force rod screw. The gears connect to the gears on the inner force rod to allow movement of the papillary muscles from outside the ventricle chamber.

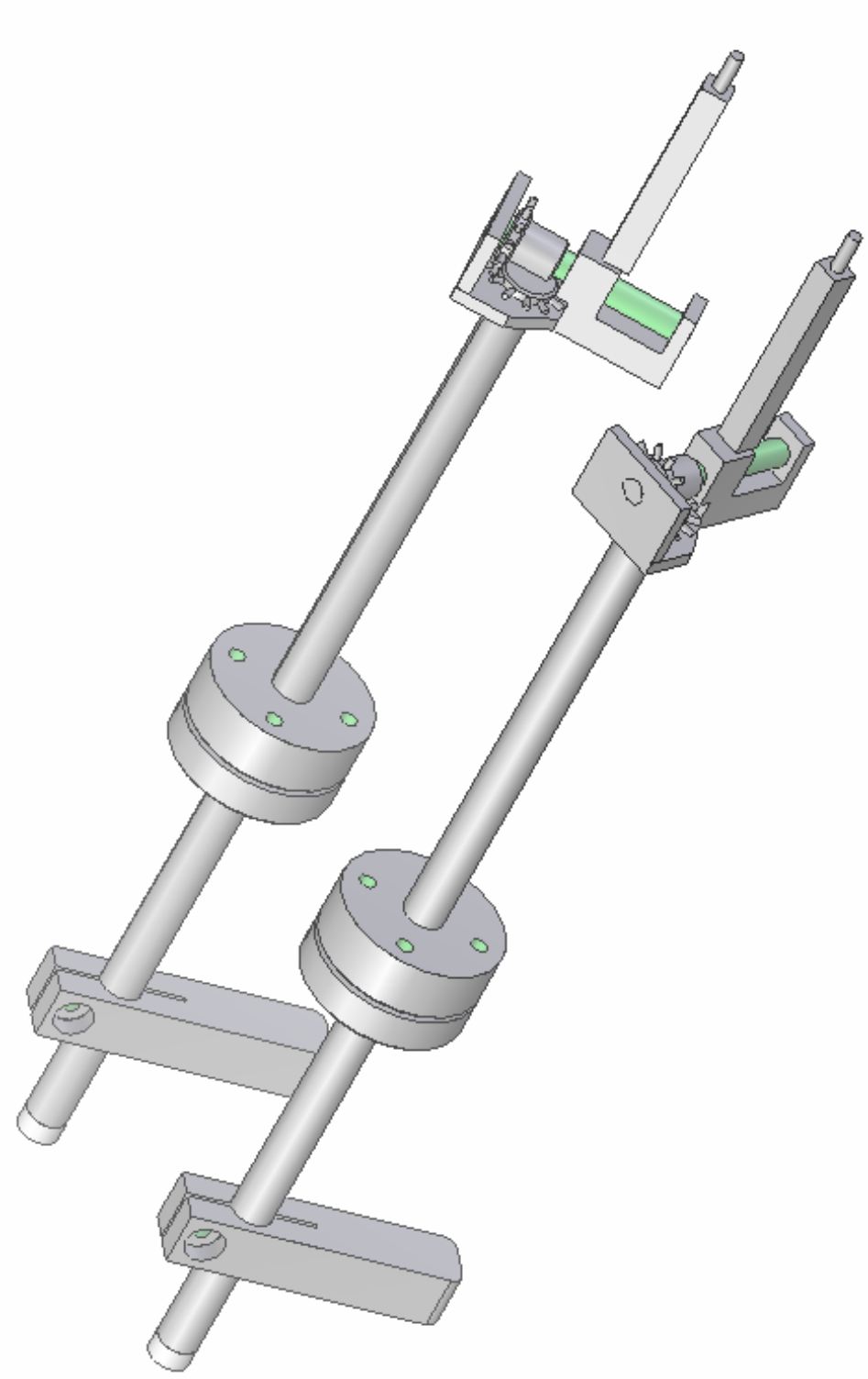

Figure B.9: Assembly drawing of the papillary muscle holding system.

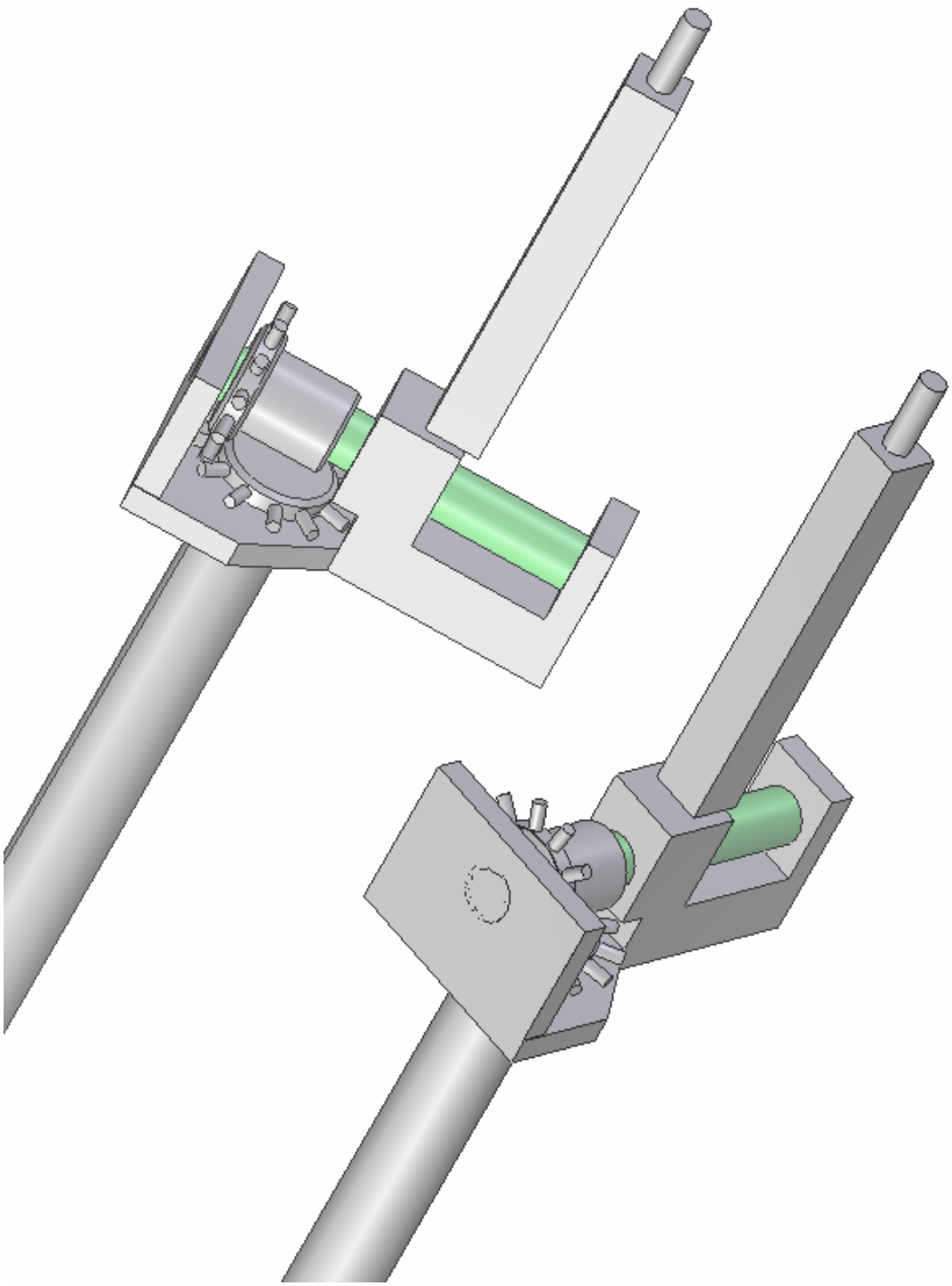

Figure B.10: Expanded view of the gear assembly.

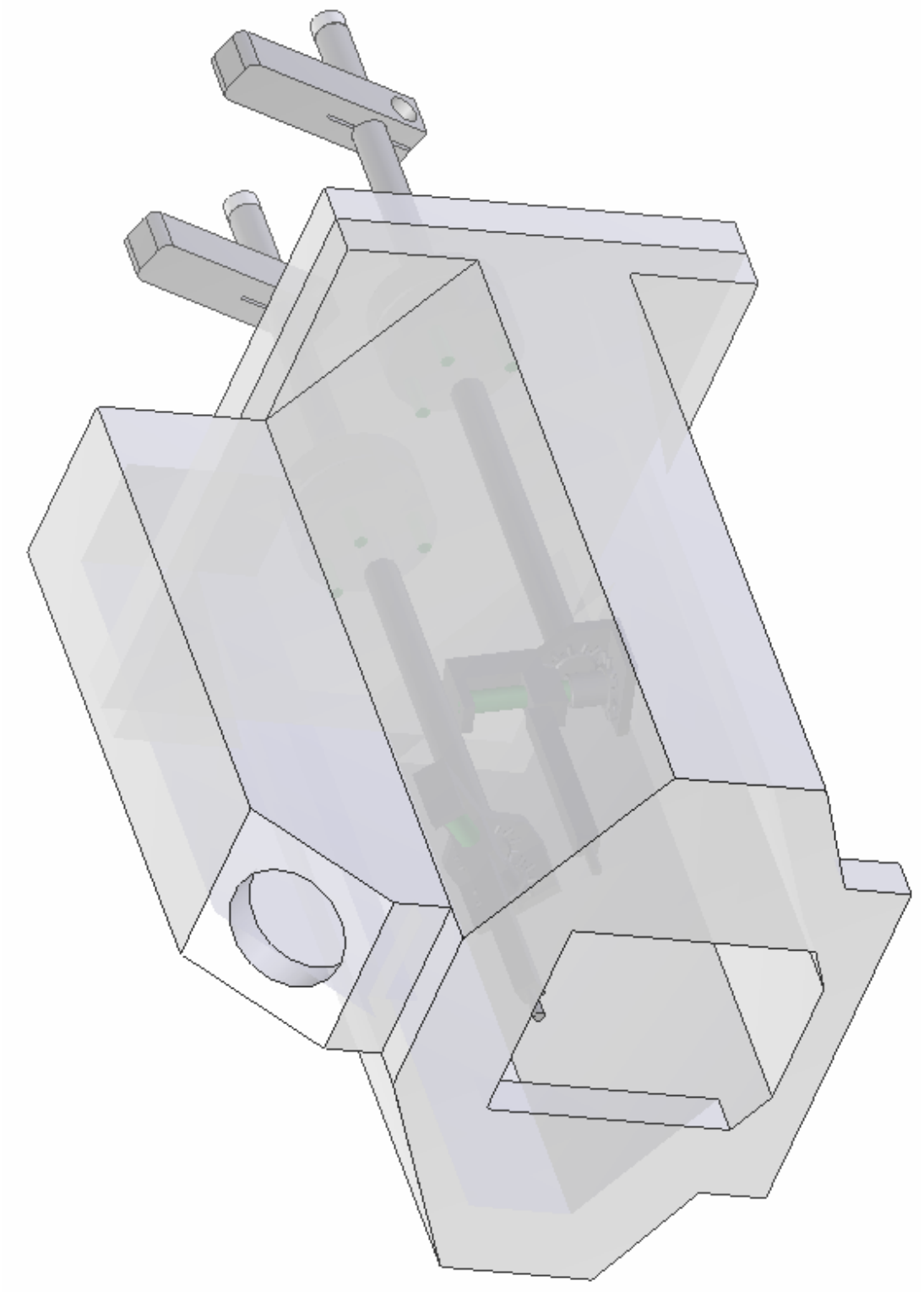

Figure B.11: Assembly view of the left ventricle model with the papillary muscle holding system attached.

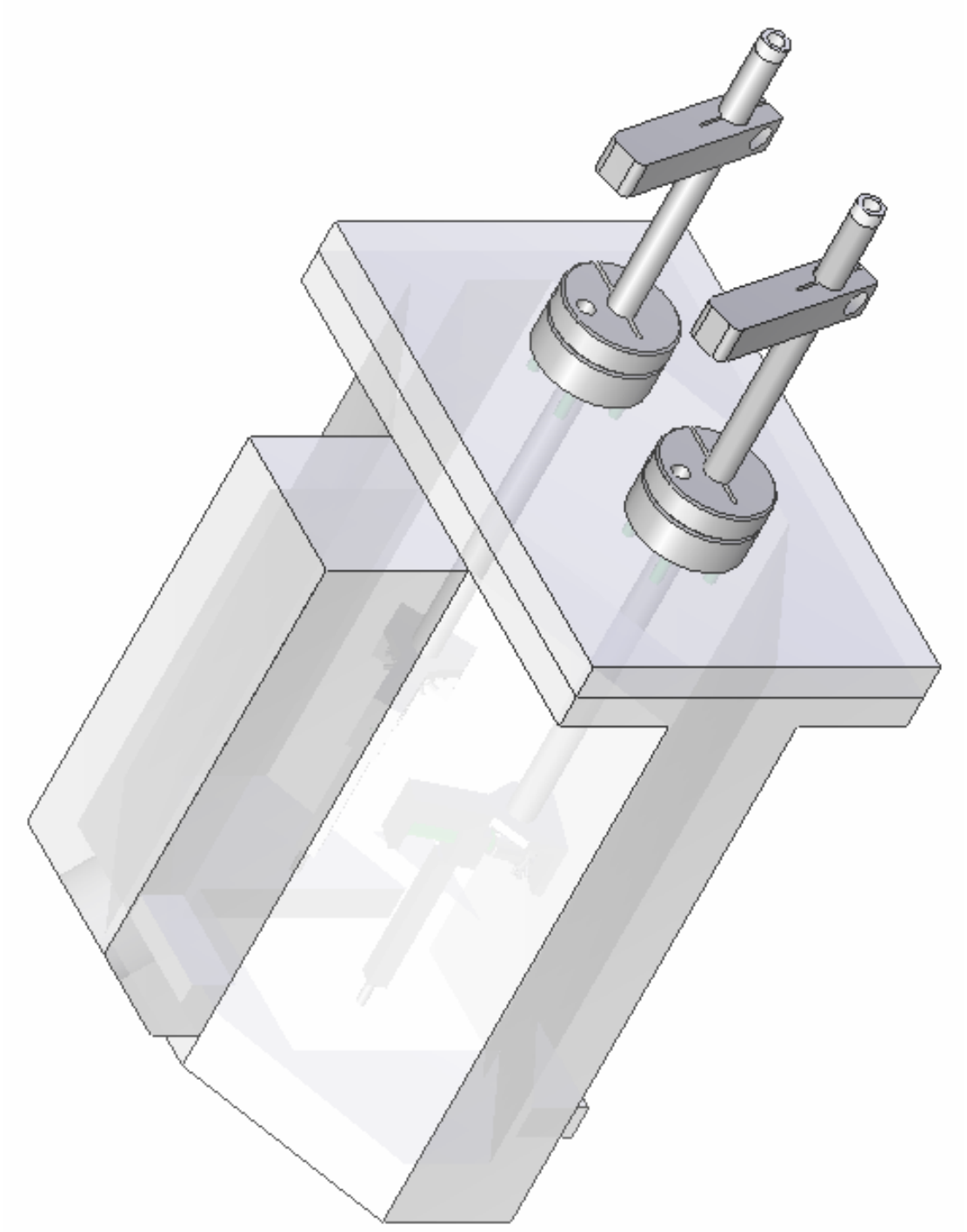

Figure B.12: Assembly view of the left ventricle model from the back with the papillary muscle holding system attached.

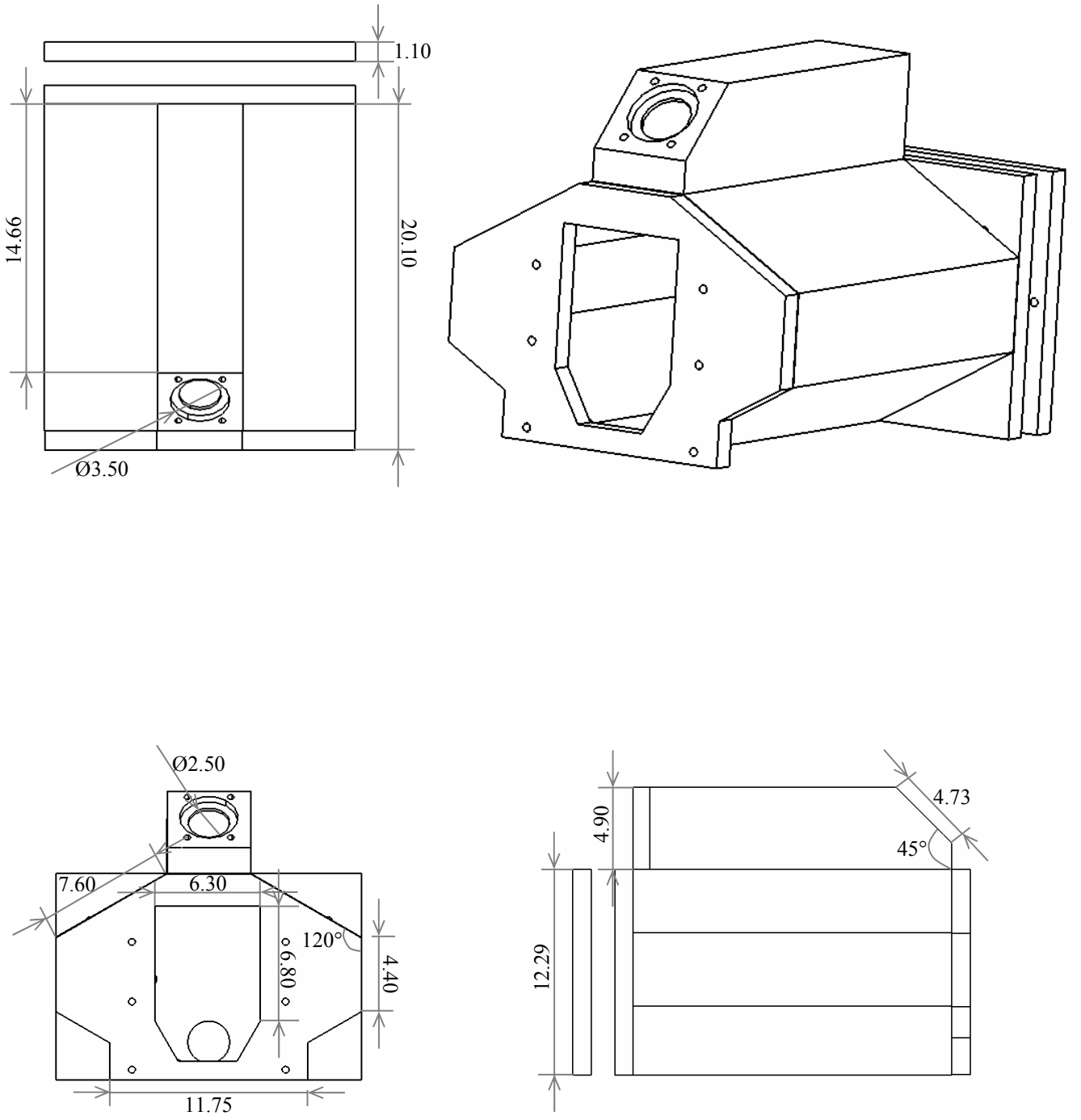

Figure B.13: Left ventricle model. The octagonal shape allows viewing of all the chordae with the two cameras.

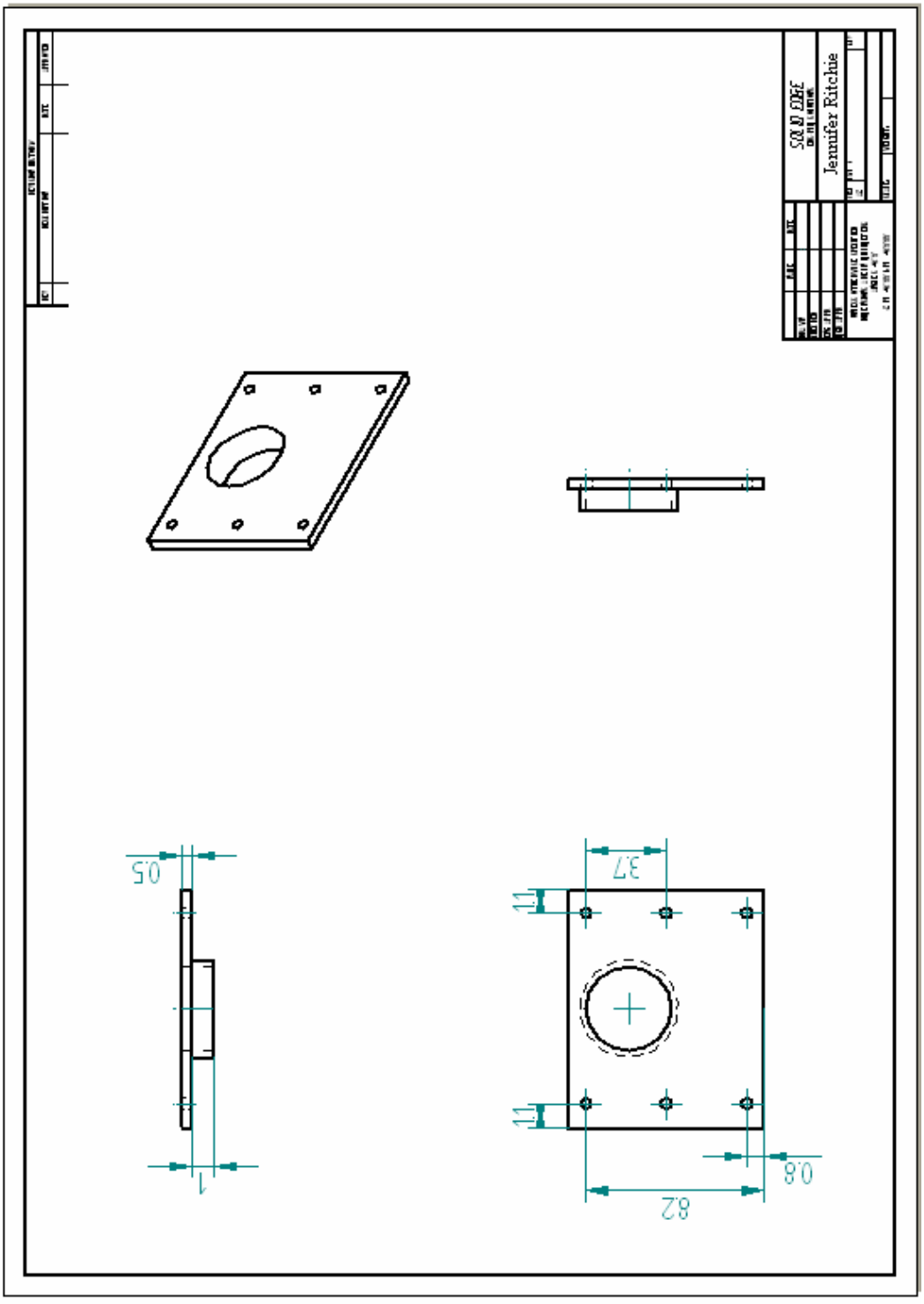

Figure B.14: Annular board which the mitral valve is sutured to after extraction from the heart.

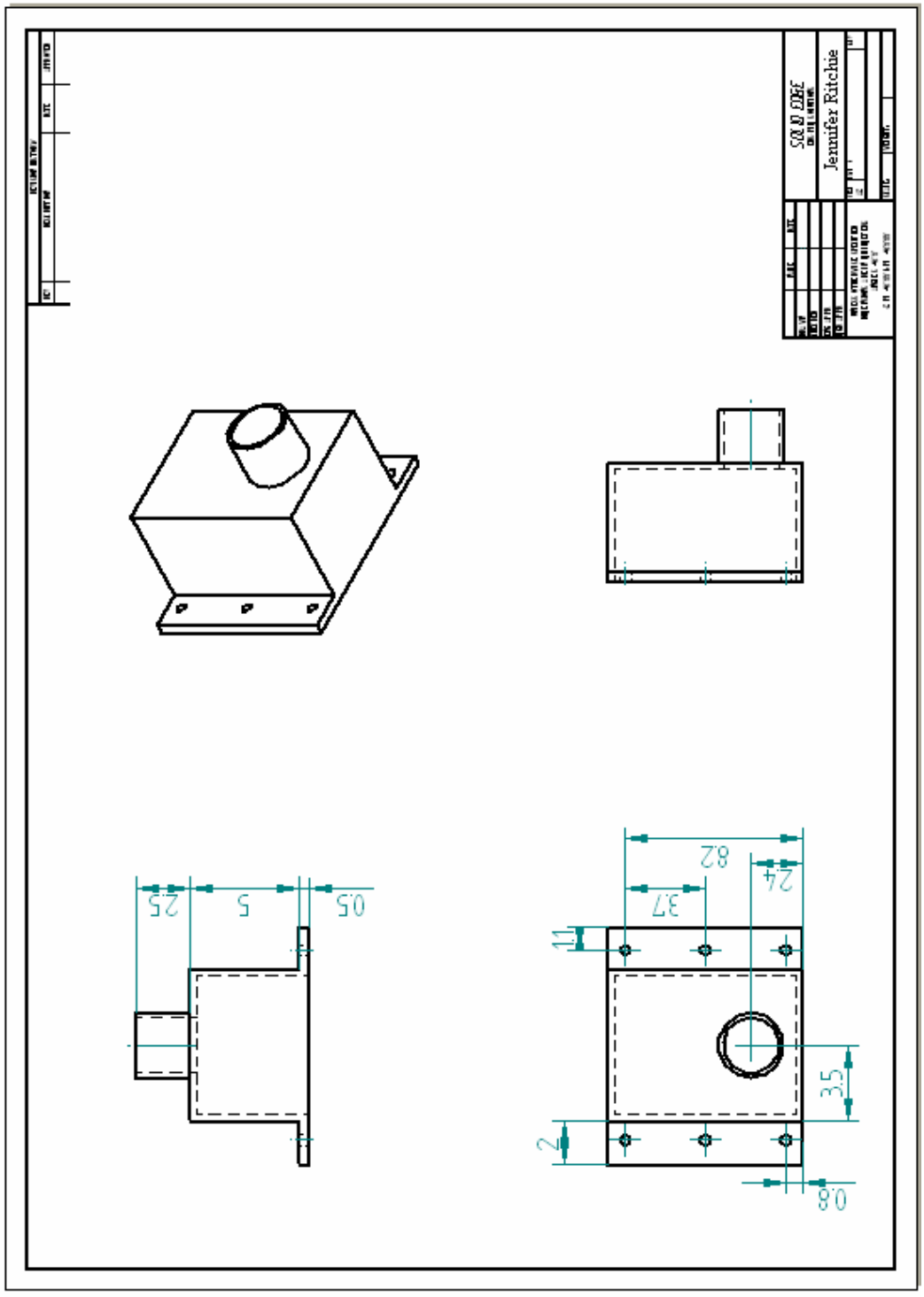

Figure B.15: Atrial chamber drawing view. The atrial chamber is attached to the ventricle chamber after the valve is in place.

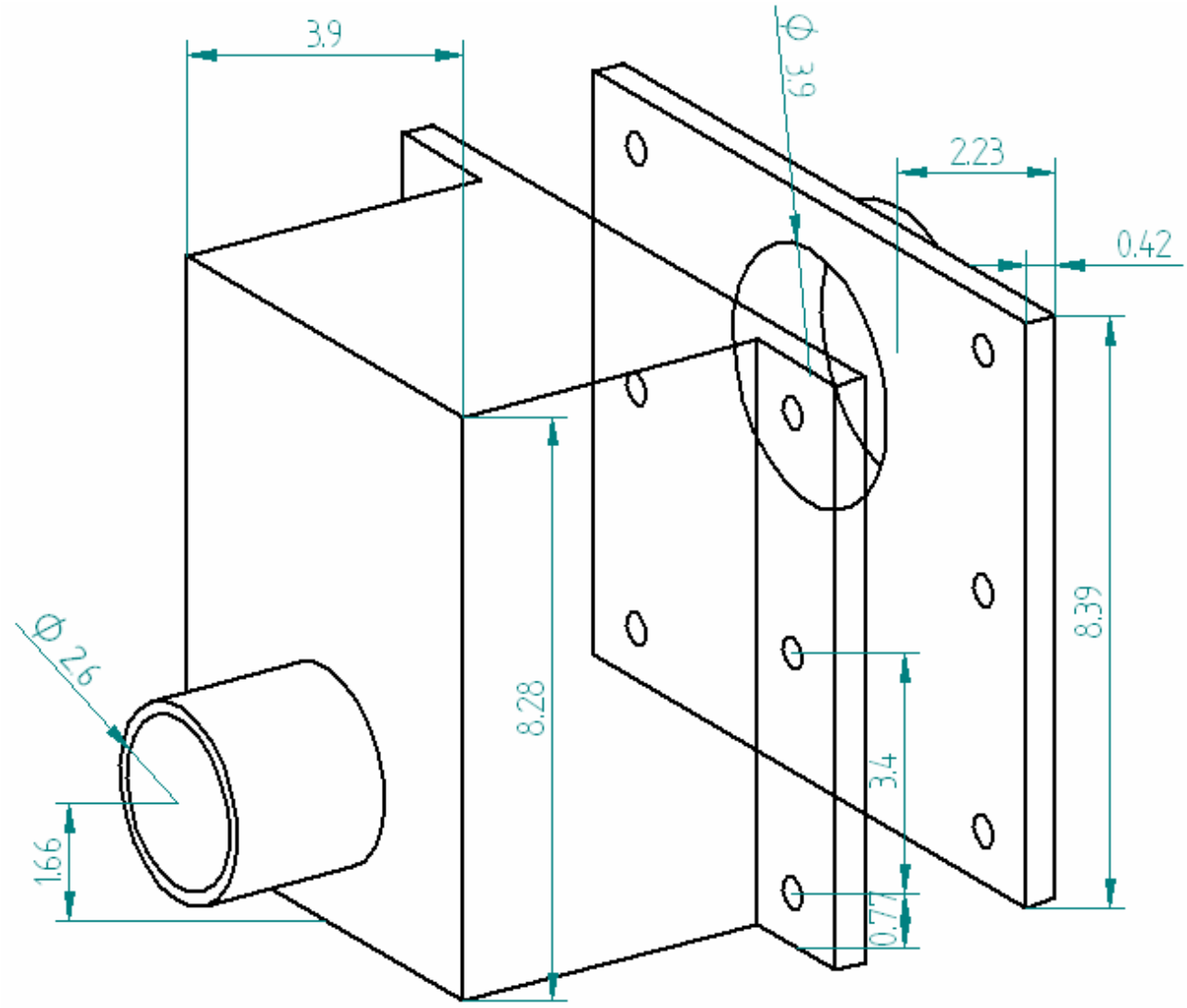

Figure B.16: Assembly view of the atrial chamber and annular board.

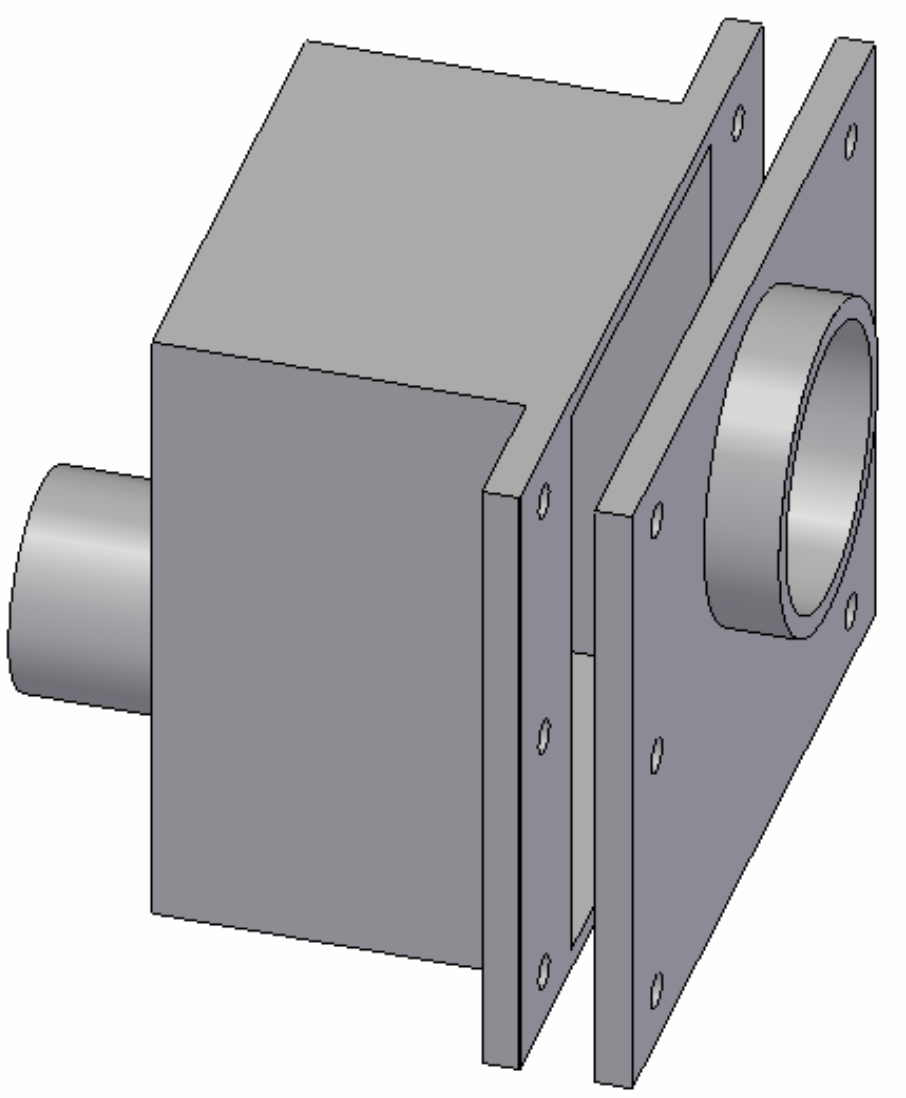

Figure B.17: Assembly view of the atrial chamber and annular board.

APPENDIX C

DATA ANALYSIS ALGORITHMS

C.1 Autotracking Algorithm

C.1.1 Documentation for Autotracking1.m and marker_check1.m

1. Copy all picture files to the folder containing the autotracking software
2. Open Matlab and set the directory to the folder containing the autotracking software
3. At the command prompt, type “autotracking(‘filename’,first frame, last frame, number of markers)”. For example, if you are tracking camera 1, frames 0 to 500, and 3 markers, you would type “autotracking(‘a’,0,500,3)”.
4. On the picture that appears, select the region of interest around each marker to be tracked. Put the cursor in the upper, left corner of the marker and drag to create a box around the marker. When you release the cursor, the program will record the coordinates of the search box and show the picture again for the user to select the next marker. Complete this for all markers.
5. After the last marker is selected, the algorithm will proceed through all the pictures. At the end of tracking, the program will display “You have successfully tracked the markers. Test the coordinates with "marker_check.m"”.
6. At the command prompt, type “marker_check(‘filename’,first frame, last frame)”.
7. The first frame will appear with a black dot on the centroid of the marker. Hit the enter key to move through all the pictures and check the location of the centroid.
8. After checking the pictures, the program will respond “You have checked the marker_array. Would you like to create the export file? y/n:”.
9. If you answer no, the program will exit.
10. If you answer yes, the program will respond with “You just checked the series starting with frame 0 and ending with frame 500”. It will then ask for a name for the export text file.
11. After typing the name of the text file, enter the first frame number in the series you want to export and the last frame number in the series you want to export.
12. Note, you can start and end the text file at any frame number you desire. You can also start the autotracking program at any frame number you desire.
13. Caution, if you restart the atutoracking program, the markerarray will be erased; therefore, if you want to keep any data, you must run the marker_check algorithm and export a text file.

C.1.2 Autotracking1.m

```
%_____________________PROGRAM AUTOTRACKING1.M_____________________
% Deveoped by Dennis D. Soerensen on 6/11/2003
% This software was developed to track markers placed on the leaflet and chordae of the
% mitral valve during the cardiac cycle.
% This autotracking uses the minima approach in cropped subimages.
% This program takes four input arguments: the name of the picture files, the number of
% the first picture, the number of the last picture, and the total number of marker you
% wish to track.
```

```
function autotracking(tif_image , num_of_first , num_of_last , num_of_markers)

% If function is not passed 4 arguments, the error message will be shown
if nargin ~= 4
    error('Wrong number of input arguments. Use the following format: autotracking( first
    part of image.tif name , number of first image , number of last image , number of
    markers)')
end

disp(sprintf('\n\nThis autotracking uses the lower 10% intensity to threshold\n\n'))


% Renaming of the picture files such that Matlab can read each one consecutively.
first_frame = num_of_first;
num_of_frames = num_of_last - num_of_first + 1;
numofbins = 255;
ThreeByThree = ones(3)/9;
% Difference between conv and corr: matrix filter rotated 180 degrees. Using a
% symmetric filter matrix means that there is no diff
j=1;

if num_of_first < 10
        image = imread(sprintf('%s00%d.tif', tif_image , num_of_first ));
elseif num_of_first < 100
        image = imread(sprintf('%s0%d.tif', tif_image , num_of_first ));
elseif num_of_first >= 100
        image = imread(sprintf('%s%d.tif', tif_image , num_of_first ));
end

image = double(image)/255;

%%%%%%%  Defining the search boxes locations and sizes    %%%%%%%

for i = 1:num_of_markers
   [ x , y , I , rect ] = imcrop(image);
   filtered_cropped_image = imfilter( I , ThreeByThree , 'replicate' , 'same');
   [counts,bin] = imhist(filtered_cropped_image , numofbins);
   nonzeros_in_counts = find(counts);
   BandA = nonzeros_in_counts(size(nonzeros_in_counts));
        % BandA equals stop and start indeces, respectively, of the nonzeros in counts in
        % a (2,1) matrix
   b = BandA(1);
   a = BandA(2);
   intensity_span = b-a;
   threshold = a + round( intensity_span/10 );
```

```
   BW = im2bw(filtered_cropped_image,threshold/255);
   regionalminima = ones(size(BW))-BW;
   [labeled,numObjects] = bwlabel(regionalminima , 4);
         % Finds connected sets. If more than one connected set, the right set have to be
         % chosen.
            if numObjects > 1
                  % Highly unlikely that the user would choose a marker crop region
                  % containing more than one marker minima. But in the case it should
                  % happen, the user gets another chance to define which off the minima is
                  % interesting
               labeled = imclearborder(labeled,8);
               [labeled,numObjects] = bwlabel(labeled , 8);

               if numObjects ~= 1
                  [labeled,numObjects] = bwlabel(regionalminima , 8);
                              % Label components.

                  STATS = regionprops(labeled,'Area');

                  for position = 1:numObjects
                     area = STATS(position).Area;
                     area_vector(1,position) = area;
                  end

                  [max_value,max_location] = max(area_vector);
                  [r,c] = find(labeled==max_location);
                  labeled = bwselect(regionalminima,c,r,4);

                  labeled = bwlabel(labeled,8);
                  area_vector = 0;
               end
            end

   centroid = regionprops(labeled,'Centroid');
         % the first element of Centroid is the horizontal coordinate (or x-coordinate) of
         % the center of mass, and the second element is the vertical coordinate (or y-
         % coordinate).
   center_pixel_coordinates_in_cropped_image = round(centroid.Centroid);
         %To get the values in the structure centroid , could probably have used
         % Centroid{1,2}
   rect_rounded = round(rect);
   center_pixel_coordinates_of_marker = rect_rounded([1,2]) +
center_pixel_coordinates_in_cropped_image([1,2]);

   center_pixel_coordinates_in_array(1,1,i,j) = center_pixel_coordinates_of_marker(1,1);
   % i = marker munber
```

```
   center_pixel_coordinates_in_array(1,2,i,j) = center_pixel_coordinates_of_marker(1,2);
   % j = frame number
end

disp('First frame tracked.')

% All the marker coordinates are now found for the first frame. Now the next two frames
% are tracked

if num_of_frames > 1
          num_of_first = num_of_first + 1;
          for n = num_of_first : num_of_first+1
% Need to run 2 loops to have enough for prediction, which needs 3 frames

   if n < 10
          image = imread(sprintf('%s00%d.tif', tif_image , n ));
   elseif n >= 100
          image = imread(sprintf('%s%d.tif', tif_image , n ));
   else
           image = imread(sprintf('%s0%d.tif', tif_image , n ));
   end

   image = double(image)/255;

          for p = 1:num_of_markers
             rect_adjust(1,1,p,j+1) = center_pixel_coordinates_in_array(1,1,p,j) -
ceil(rect_rounded(1,3)/2);              % New x_upper_right_corner
             rect_adjust(1,2,p,j+1) = center_pixel_coordinates_in_array(1,2,p,j) -
ceil(rect_rounded(1,4)/2);              % New y_upper_right_corner
             x_rect = rect_adjust(1,1,p,j+1);
             y_rect = rect_adjust(1,2,p,j+1);

             rect_adjusted = [x_rect , y_rect , rect_rounded(1,3) , rect_rounded(1,4)];
             cropped_image = imcrop( image , rect_adjusted);
% cropping rect w/ center of crop on previous marker center
             filtered_cropped_image = imfilter( cropped_image , ThreeByThree , 'replicate' ,
'same');
             [counts,bin] = imhist(filtered_cropped_image , numofbins);
             nonzeros_in_counts = find(counts);
             BandA = nonzeros_in_counts(size(nonzeros_in_counts));
          % BandA equals stop and start indeces, respectively, of the nonzeros in counts in
          % a (2,1) matrix
             b = BandA(1);
             a = BandA(2);
             intensity_span = b-a;
             threshold = a + round( intensity_span/10 );
```

```
            BW = im2bw(filtered_cropped_image,threshold/255);
            regionalminima = ones(size(BW))-BW;
            [labeled,numObjects] = bwlabel(regionalminima , 4);     % Label components.

            if numObjects > 1
          % Highly unlikely that the user would choose a marker crop region containing
          % more than one marker minima. But in the case it should happen, the user gets
          % another chance to define which off the minima is interesting
                labeled = imclearborder(labeled,8);
                [labeled,numObjects] = bwlabel(labeled , 8);

                if numObjects ~= 1
                   [labeled,numObjects] = bwlabel(regionalminima , 8);
                            % Label components.
                   STATS = regionprops(labeled,'Area');

                   for position = 1:numObjects
                      area = STATS(position).Area;
                      area_vector(1,position) = area;
                   end

                   [max_value,max_location] = max(area_vector);
                   [r,c] = find(labeled==max_location);
                   labeled = bwselect(regionalminima,c,r,4);
                   labeled = bwlabel(labeled,8);
                   area_vector = 0;
                end
             end

            centroid = regionprops(labeled,'centroid');  % the first element of Centroid is
the horizontal coordinate (or x-coordinate) of the center of mass, and the second element
is the vertical coordinate (or y-coordinate).
            center_pixel_coordinates_in_cropped_image = round(centroid.Centroid); %To
get the values in the structure centroid , could probably have used Centroid{1,2}

            center_pixel_coordinates_of_marker(1,1,p,j+1) = rect_adjusted(1,1) +
center_pixel_coordinates_in_cropped_image(1,1);
            center_pixel_coordinates_of_marker(1,2,p,j+1) = rect_adjusted(1,2) +
center_pixel_coordinates_in_cropped_image(1,2);

            center_pixel_coordinates_in_array(1,1,p,j+1) =
center_pixel_coordinates_of_marker(1,1,p,j+1);       % p = marker munber
            center_pixel_coordinates_in_array(1,2,p,j+1) =
center_pixel_coordinates_of_marker(1,2,p,j+1);       % j = frame number
        end
```

```
        disp(sprintf('Frame %d tracked.', n ))
        j = j+1;
end
    j = j+1;
end

%%%%%%%%%%%%% % 4th frame and forward   %%%%%%%%%%%%%%%

if num_of_frames > 3

for n = num_of_first+2 : 1 : num_of_last    % Now there is enough frames for prediction
in the last. This loop will start with the 4th frame

   if n < 10
        image = imread(sprintf('%s00%d.tif', tif_image , n ));
   elseif n >= 100
        image = imread(sprintf('%s%d.tif', tif_image , n ));
   else
        image = imread(sprintf('%s0%d.tif', tif_image , n ));
   end

   image = double(image)/255;

   for p = 1:num_of_markers

      % Motion estimation

      rx0 = center_pixel_coordinates_in_array(1,1,p,j-1);
      ry0 = center_pixel_coordinates_in_array(1,2,p,j-1);

      vx = (center_pixel_coordinates_in_array(1,1,p,j-1) -
center_pixel_coordinates_in_array(1,1,p,j-2));
      vy = (center_pixel_coordinates_in_array(1,2,p,j-1) -
center_pixel_coordinates_in_array(1,2,p,j-2));

      vx0 = (center_pixel_coordinates_in_array(1,1,p,j-2) -
center_pixel_coordinates_in_array(1,1,p,j-3));
      vy0 = (center_pixel_coordinates_in_array(1,2,p,j-2) -
center_pixel_coordinates_in_array(1,2,p,j-3));

      avx = vx - vx0;
      avy = vy - vy0;

      x_estimate = round(rx0 + vx + 0.5*avx);
      y_estimate = round(ry0 + vy + 0.5*avy);
```

```
      % The estimated coordinates are inserted into the rect_adjust

      rect_adjust(1,1,p,j) = x_estimate - ceil(rect_rounded(1,3)/2);
           % New x_upper_right_corner
      rect_adjust(1,2,p,j) = y_estimate - ceil(rect_rounded(1,4)/2);
         % New y_upper_right_corner
      x_rect = rect_adjust(1,1,p,j);
      y_rect = rect_adjust(1,2,p,j);

      rect_adjusted = [x_rect , y_rect , rect_rounded(1,3) , rect_rounded(1,4)];
      cropped_image = imcrop( image , rect_adjusted);
         % cropping rect w/ center of crop on previous marker center
      filtered_cropped_image = imfilter( cropped_image , ThreeByThree , 'replicate' ,
'same');

      [counts,bin] = imhist(filtered_cropped_image , numofbins);
      nonzeros_in_counts = find(counts);
      BandA = nonzeros_in_counts(size(nonzeros_in_counts));
        % BandA equals stop and start indeces, respectively, of the nonzeros in counts in
       % a (2,1) matrix
      b = BandA(1);
      a = BandA(2);
      intensity_span = b-a;
      threshold = a + round( intensity_span/10 );
      BW = im2bw(filtered_cropped_image,threshold/255);
      regionalminima = ones(size(BW))-BW;
      [labeled,numObjects] = bwlabel(regionalminima , 8);     % Label components.

      if numObjects > 1                          % Worst case scenario is numObjects = 5
         labeled = imclearborder(labeled,8);
         [labeled,numObjects] = bwlabel(labeled , 8);
      end

            if numObjects > 1
         % Highly unlikely that the user would choose a marker crop region containing
         % more than one marker minima. But in the case it should happen, the user gets
         % another chance to define which off the minima is interesting
               labeled = imclearborder(labeled,8);
               [labeled,numObjects] = bwlabel(labeled , 8);

               if numObjects ~= 1
                  [labeled,numObjects] = bwlabel(regionalminima , 8);
                           % Label components.
                  STATS = regionprops(labeled,'Area');

                  for position = 1:numObjects
```

```
                    area = STATS(position).Area;
                    area_vector(1,position) = area;
                end

                [max_value,max_location] = max(area_vector);
                [r,c] = find(labeled==max_location);
                labeled = bwselect(regionalminima,c,r,4);
                labeled = bwlabel(labeled,8);
                area_vector = 0;
            end
        end

    centroid = regionprops(labeled,'centroid');  % the first element of Centroid is the
horizontal coordinate (or x-coordinate) of the center of mass, and the second element is
the vertical coordinate (or y-coordinate).

    center_pixel_coordinates_in_cropped_image = round(centroid.Centroid); %To get the
values in the structure centroid , could probably have used Centroid{1,2}

    center_pixel_coordinates_of_marker(1,1,p,j) = rect_adjusted(1,1) +
center_pixel_coordinates_in_cropped_image(1,1);
    center_pixel_coordinates_of_marker(1,2,p,j) = rect_adjusted(1,2) +
center_pixel_coordinates_in_cropped_image(1,2);

    center_pixel_coordinates_in_array(1,1,p,j) =
center_pixel_coordinates_of_marker(1,1,p,j);       % p = marker munber
    center_pixel_coordinates_in_array(1,2,p,j) =
center_pixel_coordinates_of_marker(1,2,p,j);       % j = frame number

   end

      image = 0;    % image set to zero, to reduce the size of 'markerarray.mat' by ~10 MB
      save markerarray;
      disp(sprintf('Frame %d tracked.', n ))

  j = j+1;
end
end
  image = 0;       % image set to zero, to reduce the size of 'markerarray.mat' by ~10 MB
  save markerarray;

disp('You have successfully tracked the markers. Test the coordinates with
"marker_check.m"')
```

C.1.3 Marker_check1.m

```
%_____________________PROGRAM MARKER_CHECK1.M_____________________
%Developed by Dennis D. Soerensen on 6/11/2003
%This software was developed to check the tracking function of
%autotracking1.m
%This program generates a text file with the 2D pixel coordinates of each
%marker placement determined by autotracking1.m.
%This program takes three input arguments: the name of the picture files,
%the number of the first picture, and the number of the last picture.

function marker_check(string_part , num_first , num_last )

if nargin ~= 3
 %If function is not passed 3 arguments, the error message will be shown
    error('Wrong number of input arguments. Use the following format: autotracking(
string part of image.tif , number of first image to check , number of last image to check )')
end

load markerarray
% center_pixel_coordinates_in_array and num_of_first  and other variables are loaded


% The following is done to make it possible for the user to choose certain frames to
check so the user wont have to go through the entire marker_array

for n = num_first:1:num_last

   if n < 10
         image = imread(sprintf('%s00%d.tif', string_part , n ));
   elseif n >= 100
          image = imread(sprintf('%s%d.tif', string_part , n ));
   else
          image = imread(sprintf('%s0%d.tif', string_part , n ));
   end

   X_pos = center_pixel_coordinates_in_array(1,1,:,n-first_frame+1);
   Y_pos = center_pixel_coordinates_in_array(1,2,:,n-first_frame+1);

   figure(n+1)
   imshow(image);
   hold on;

   for p = 1:num_of_markers
        figure(n+1);
      fill([X_pos(1,1,p) X_pos(1,1,p) X_pos(1,1,p) X_pos(1,1,p)],[Y_pos(1,1,p)-4
Y_pos(1,1,p)-4 Y_pos(1,1,p)+4 Y_pos(1,1,p)+4] ,'b')
```

```
      fill([X_pos(1,1,p)-4 X_pos(1,1,p)+4 X_pos(1,1,p)+4 X_pos(1,1,p)-4],[Y_pos(1,1,p)
Y_pos(1,1,p) Y_pos(1,1,p) Y_pos(1,1,p)] ,'b')
      % fill([X_pos-2 X_pos+2 X_pos+2 X_pos-2],[Y_pos-2 Y_pos-2 Y_pos+2
Y_pos+2] ,'r')
      hold on;
   end

   [P1 P2]=ginput(1);
    hold off
    close
end
clc
reply = input('\nYou have checked the marker_array. \nWould you like to create the
export file? y/n: ','s');

if isempty(reply)
   reply = 'y';
end

if reply == 'n'
  disp('OK. You are done.')

elseif reply == 'y'

   disp(sprintf('\n\nYou just checked the series starting with frame %d and ending with
frame %d.', num_first , num_last))
   disp(sprintf('\nMarkerarray starts with frame %d and ends with frame %d.', first_frame
, num_of_last))
   text_file_name = input('\nType the name for the export text file (only the part
BEFORE .txt !):','s');
   string_first = input('\nPlease enter FIRST frame number in the series you want to
export:','s');
   chosen_num_of_first = str2num(string_first);

   string_last = input('\nPlease enter LAST frame number in the series you want to
export:','s');
   chosen_num_of_last = str2num(string_last);

   fid=fopen(sprintf('%s.txt',text_file_name),'w');
   fprintf(fid,'%d\t',chosen_num_of_first);
   fprintf(fid,'%d\n',chosen_num_of_last);

   y_origin = 1023; %image(1,1)

      for n1 = chosen_num_of_first : 1 : chosen_num_of_last,
```

```
        for n2 = 1 : num_of_markers,

        x_coordinate = center_pixel_coordinates_in_array(1,1,n2,n1-first_frame+1);
        fprintf(fid,'%d\t',x_coordinate-2);                % minus 2 to reduce offset error

        y_coordinate = center_pixel_coordinates_in_array(1,2,n2,n1-first_frame+1);
        fprintf(fid,'%d\r',y_origin-y_coordinate+2);       % 3D software has y=0 at
bottom of image, MATLAB at top of image

        end
      end

   fclose(fid);

   disp(sprintf('You are done.\nFrame number %d to frame number %d have been
converted and saved in "%s.txt"\nYou can import the file in the 3D software',
chosen_num_of_first , chosen_num_of_last , text_file_name))

end
```

C.2 3D Transformation Algorithm

C.2.1 Documentation of MATLAB 3D coordinate calculation (README1.doc)

This documentation describes the programs sw3d6.m, revised by S. Wanant from the v6.m demo sent by B. Sugimoto from the University of Pittsburgh. All original code has been left in, but commented out where necessary. Extensive additional comments have been added for clarification. Please refer to the code itself for programming details. This documentation is meant only to define variables and functions for the user.

MATLAB 3-dimensional reconstruction program (sw3d6.m)
This program computes 3D coordinates (X,Y,Z) from 2D coordinates (U,V) by Direct Linear Transform (DLT).
The program utilizes the functions dltfu.m and reconfu.m originally written by Christoph Reinschmidt from the University of Calgary.

There are 4 phases: Loading the 2D data sets, Calibrating camera coordinates, Computing 3D coordinates, and Writing the output file.

Loading 2D data sets – The program will ask for 2 file names. These are where the 2D coordinates are stored for each camera (e.g. acoord.txt and bcoord.txt). Press ENTER for these defaults. These should be .txt files in the format:

	Column 1	Column 2
Row 1	First frame number	Last frame number
Row 2	U_1	V_1
…	…	…
Row n+1	U_n	V_n

The first row holds the frame number limits, which are used to synchronize the cameras with each other and with the pressure-flow data. The limits are read and stored and is cropped off the matrix. The matrices from the 2 cameras are then compared and cropped so that they are the same size and are synchronized with respect to frame numbers. (The matrices will not be the same size if one of the cameras cannot see all of the markers in a certain frame number. Those frames will be discarded.) The new matrices are combined and stored in matrix D in the form:

	Column 1	Column 2	Column 3	Column 4
Row 1	U_{A1}	V_{A1}	U_{B1}	V_{B1}
Row 2	U_{A2}	V_{A2}	U_{B2}	V_{B2}
…	…	…	…	…
Row n	U_{An}	V_{An}	U_{Bn}	V_{Bn}

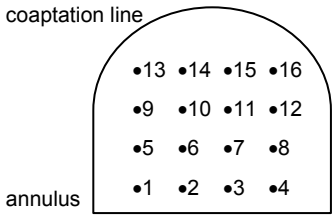

Markers may be digitized in any order as long as it is consistent. For example, a 4×4 array may be numbered as shown at right (all images are handled as they appear in the acquired images, i.e. upside-down in reality; however, it should be noted that the orientation of the cameras does not matter.):

Calibrating camera coordinates – The program will ask for 3 files. These are where the calibration files (2D coordinates of cube corners) and reference file (known 3D coordinates of cube) are stored (e.g. acal.txt, bcal.txt, reference.txt). Calibration files should be .txt files in the format:

	Column 1	Column 2
Row 1	U_1	V_1
Row 2	U_2	V_2
…	…	…
Row 7	U_7	V_7

The reference file should also be a .txt and should be similar to:

```
0          0          0
0          0          9.525
0          9.525      9.525
0          9.525      0
9.525      0          0
9.525      0          9.525
9.525      9.525      9.525
```

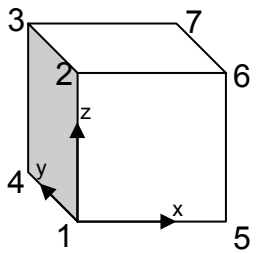

These columns correspond to (X,Y,Z) coordinates for a 0.375in (9.525mm) cube with the origin located at point 1 as shown on

previous page. The reference file can be modified to accommodate any numbering scheme; however, the calibration data should be digitized using a consistent numbering scheme.

Each calibration matrix is sent with the reference matrix to the function dltfu.m. Dltfu.m returns a column vector containing 11 DLT coefficients (L_1-L_{11}). (See notes on DLT method or www.kwon3d.com/theory/dlt/dlt.html.) The column vectors from each camera are combined into matrix A:

	Column 1	Column 2
Row 1	L_{A1}	L_{B1}
Row 2	L_{A2}	L_{B2}
…	…	…
Row 11	L_{A11}	L_{B11}

Computing 3D coordinates

Function reconfu.m receives matrices A (DLT coefficients) and D (2D coordinates) and returns matrix H (See notes on DLT or www.kwon3d.com/theory/dlt/dlt.html.):

	Column 1	Column 2	Column 3	Column 4	Column 5
Row 1	X_1	Y_1	Z_1	residual error	cameras used
Row 2	X_2	Y_2	Z_2	residual error	cameras used
…	…	…	…	…	…
Row n	X_n	Y_n	Z_n	residual error	cameras used

'Residual error' refers to the residual from using the least squares regression method. 'Cameras used' will be 12; this means cameras 'one two', not 'twelve'.

Writing the output file – The program will ask for a filename for the output (e.g. markers3d.txt). The program will also ask for 2 pressure files (ventricular and transmitral) (e.g. LVpq.txt and TMpq.txt, respectively).

The output will be written in the following format:

	Column 1	Column 2	Column 3	Column 4
Row 1	# of frames	# of markers		
Row 2	<blank>			
Row 3	Frame #	Time	LV pressure	TM pressure
Row 4	X_1	Y_1	Z_1	
…	…	…	…	
Row 19	X_{16}	Y_{16}	Z_{16}	
…	<blank>			
for each frame…	Frame #	Time	LV pressure	TM pressure
…	X_1	Y_1	Z_1	

C.2.2 SW3D6.m

```
%_____PROGRAM SW3D6_____
%This program computes 3D coordinates (X,Y,Z) from 2D coordinates (U,V) by Direct
%Linear Transform (DLT).  The program utilizes the functions dltfu.m and reconfu.m
%originally written by Christoph Reinschmidt from the University of Calgary.
%
%There are 4 phases: Loading the 2D data sets, Calibrating camera coordinates,
%Computing 3D coordinates, and Writing output file.
%
%(1)Loading 2D data sets- The program will ask for 2 filenames.  These are where
%the 2D coordinates are stored for each camera.  Press ENTER for defaults (acoord
%& bcoord).
%
%(2)Calibrating camera coordinates- The program will ask for 3 filenames.  These
%are where the 2D coordinates of cube corners (acal & bcal) and known 3D
%coordinates of cube (reference) are stored.
%
%(3)Computing 3D coordinates- X,Y,Z coordinates will be calculated using the
%least squares method.
%
%(4)Writing output file- The program will ask for a filename for the output
%(markers3d).  The program will also ask for 2 pressure files (ventricular and
%transmitral).  The output will be in the following format:
%               Row 1: #frames, #markers
%               Row n: frame#, time, LVpressure, TMpressure
%               Row n+1: X,Y,Z

%_____END HELP TEXT_____
```

```
% 3D location calc using part of KineMat demo
% with addition of writing text file
% May 27, 2001
%This revision allows the operator to input filenames to be used.
%This revision allows the 2D marker data to be read from separate files.
%This revision adds frame number data to input and output marker files.
%This revision sets default file names.
%This revision reformats the output file.  7/5/01

clc
disp(' ')
disp('3D RECONSTRUCTION')
disp('This program executes the 3d reconstruction routine.')
disp('camera coefficients will be calculated and location of markers')
disp('can be extracted.')
disp(' ');
disp('Press ENTER for filename defaults.')
disp(' ')
disp(' ')

disp('_____(1) LOADING 2D DATA SET _____')
disp(' ')
filename2dA=input('Enter the filename of the 2D marker coordinates for camera A (e.g.
acoord.txt)> ', 's');% do not need to use quote mark for s
filename2dB=input('Enter the filename of the 2D marker coordinates for camera B (e.g.
bcoord.txt)> ', 's');
if isempty(filename2dA) filename2dA='acoord.txt'; end                    %default file
names
if isempty(filename2dB) filename2dB='bcoord.txt'; end

disp(' ')
disp('Loading marker data...')
disp(' ')
d1=load(filename2dA);  d2=load(filename2dB); % input the datafile to d1. Matrix is the
same as datafile

%storing the frame numbers (entered in the first row of the data sets)
%and removing the row from the matrix
%three after frmlim has the beginning of frame and end of frame
frmlim=[d1(1,:); d2(1,:)];                                                %row1
contains frame limits for camera1, row2 for camera2

                                    % : indicate all the elements in the first line
d1=d1(2:size(d1,1),:); d2=d2(2:size(d2,1),:);
```

```
mkrnum=size(d2,1)/(frmlim(2,2)-frmlim(2,1)+1);    %mrknum is the number of markers per frame (i.e. 9, 16)

        % return the number of rows, remove first rows from matrix
%cropping the larger matrix; matrices will not be the same size if a camera cannot see all markers
delta=(frmlim(1,:)-frmlim(2,:))*mkrnum;                    %delta is the difference between rows

if delta(1) < 0
        %the next 2 if statements match frame numbers and matrix size
   d1=d1(1-delta(1):size(d1,1),:);                    % Move down to the same rows as d2 and read the data, crop d1
else
   d2=d2(1+delta(1):size(d2,1),:);      %align the beginning
end

if delta(2) > 0
        %this probably won't ever be used (crops off back end)
  d1=d1(1:size(d1,1)-delta(2),:);
else
        % align the end
  d2=d2(1:size(d2,1)+delta(2),:);
end

frmlim=[max(frmlim(:,1)) min(frmlim(:,2))];                %redefine new frame limits
frmnum=frmlim(2)-frmlim(1)+1;
        %frmnum is the number of frames

                                % only for calculating the frame numbers
D=[d1 d2];
disp('done')
disp(' ')
disp(' ')

disp('_____(2) NORMALIZING CAMERA COORDINATES _____')
disp(' ')
filenameAcube=input('Enter the filename of the first calibration set (e.g. acal.txt)> ', 's');
filenameBcube=input('Enter the filename of the second calibration set (e.g. bcal.txt)> ', 's');
filenameref=input('Enter the filename of the reference coordinates (e.g. reference.txt)> ', 's');
if isempty(filenameAcube) filenameAcube='acal.txt'; end
if isempty(filenameBcube) filenameBcube='bcal.txt'; end
if isempty(filenameref) filenameref='reference.txt'; end
```

```
disp(' ')
disp('Loading calibration data and computing DLT coefficients...')
acube=load (filenameAcube); bcube=load (filenameBcube); reference=load(filenameref);
a1=dltfu(reference,acube);
a2=dltfu(reference,bcube);
A=[a1,a2];
disp(' ')
disp('done')
disp(' ')
disp(' ')

disp('_____(3) 3D RECONSTRUCTION  _____')
disp(' ')
disp('3D reconstruction of marker coordinates using DLT coefficients...')
disp(' ')
H=[];

H=reconfu(A,D);

disp('done')
%disp(' ')
disp('Press any key to continue.')
pause
disp(' ')
disp(' ')

disp('_____(4) WRITING OUTPUT FILE _____');
disp(' ')
%OUTPUT filename
filename3d=input('Enter the filename for the OUTPUT (e.g. m3d.txt)> ','s');
if isempty(filename3d) filename3d='m3d.txt'; end

%Reading LV and TM pressure data
filenamePV=input('Enter the filename of the ventricular pressure data (e.g. VP.txt)> ','s');
if isempty(filenamePV) filenamePV='VP.txt'; end                    %default filename
PV=load(filenamePV);                                    %input the ventricular pressure PV

filenameTM=input('Enter the filename of the transmitral pressure data (e.g. TM.txt)>
','s');
if isempty(filenameTM) filenameTM='TM.txt'; end                    %default filename
TM=load(filenameTM);                                    %input the transmitral
pressure TM
disp(' ');

%SYNCHRONIZE pressure
 for h=frmlim(1):frmlim(2)
```

```
   %P=[frame# time LVpressure TMpressure];
        P(h-frmlim(1)+1,:)=[h PV(h+1,:) TM(h+1,2)];
end;

%WRITE the first row: [# of frames, # of markers];
[tempfile] = fopen(filename3d, 'wt');
count = fprintf(tempfile, '%d %d\n', frmnum, mkrnum);

%WRITE sets of data for each frame
[tempfile] = fopen(filename3d, 'at');
for f=1:frmnum
  count = fprintf(tempfile, '\n%d %f %f %f\n', P(f,:));
  Htemp=H((1+(f-1)*mkrnum):(f*mkrnum),1:3);
  count = fprintf(tempfile, '%f %f %f\n', Htemp');
end;

fclose(tempfile);

disp(sprintf('Output is in %s.', filename3d))
disp('Please see help file for formatting.');
disp(' ')

disp('_____END OF PROGRAM _____')
disp(' ')
```

C.2.3 DLTFU.m

```
%_____________________________PROGRAM DLTFU.M_____________________________
%This program is called by SW3D6.m
% Description:          Program to calculate DLT coefficient for one camera
%             Note that at least 6 (valid) calibration points are needed
%             function [A,avgres] = dltfu(F,L,Cut)
% Input:        - F     matrix containing the global coordinates (X,Y,Z)
%                 of the calibration frame
%                       e.g.: [0 0 20;0 0 50;0 0 100;0 60 20 ...]
%               - L     matrix containing 2d coordinates of calibration
%                 points seen in camera (same sequence as in F)
%                 e.g.: [1200 1040; 1200 1360; ...]
%             - Cut   points that are not visible in camera;
%                 not being used to calculate DLT coefficient
%                 e.g.: [1 7] -> calibration point 1 and 7
%                       will be discarded.
%                       This input is optional (default Cut=[])
% Output:       - A     11 DLT coefficients
%             - avgres average residuals (measure for fit of dlt)
%                       given in units of camera coordinates
```

```
%
% Author:       Christoph Reinschmidt, HPL, The University of Calgary
% Date:                 January, 1994
% Last changes: November 29, 1996
% Version:      1.0
% References: Woltring and Huiskes (1990) Stereophotogrammetry. In
%             Biomechanics of Human Movement (Edited by Berme and
%             Cappozzo). pp. 108-127.

function [A,avgres] = dltfu(F,L,Cut)

if nargin==2; Cut=[]; end;

m=size(F,1); Lt=L'; C=Lt(:);

for i=1:m
  B(2*i-1,1)  = F(i,1);
  B(2*i-1,2)  = F(i,2);
  B(2*i-1,3)  = F(i,3);
  B(2*i-1,4)  = 1;
  B(2*i-1,9)  =-F(i,1)*L(i,1);
  B(2*i-1,10) =-F(i,2)*L(i,1);
  B(2*i-1,11) =-F(i,3)*L(i,1);
  B(2*i,5)    = F(i,1);
  B(2*i,6)    = F(i,2);
  B(2*i,7)    = F(i,3);
  B(2*i,8)    = 1;
  B(2*i,9)  =-F(i,1)*L(i,2);
  B(2*i,10) =-F(i,2)*L(i,2);
  B(2*i,11) =-F(i,3)*L(i,2);
end

% Cut the lines out of B and C including the control points to be discarded
Cutlines=[Cut.*2-1, Cut.*2];
B([Cutlines],:)=[];
C([Cutlines],:)=[];

% Solution for the coefficients
A=B\C;
D=B*A;
R=C-D;
res=norm(R); avgres=res/size(R,1)^0.5;
```

C.2.4 RECONFU.m

```
%_____________________________PROGRAM RECONFU.M_____________________________
%This program is called by SW3D6.m
%function [H] = reconfu(A,L)
% Description:          Reconstruction of 3D coordinates with the use local (camera
%                 coordinates and the DLT coefficients for the n cameras).
% Input:          - A  file containing DLT coefficients of the n cameras
%                     [a1cam1,a1cam2...;a2cam1...]
%                 - L  camera coordinates of points
%                     [xcam1,ycam1,xcam2,ycam2...;same at time 2]
% Output:         - H  global coordinates, residuals, cameras used
%                     [Xt1,Yt1,Zt1,residt1,cams_used@t1...; same for t2]
% Author:         Christoph Reinschmidt, HPL, The University of Calgary
% Date:                   September, 1994
% Last change:  November 29, 1996
% Version:      1.1

function [H] = reconfu(A,L)

n=size(A,2);
% check whether the numbers of cameras agree for A and L
if 2*n~=size(L,2); disp('the # of cameras given in A and L do not agree')
                disp('hit any key and then "try" again'); pause; break
end


H(size(L,1),5)=[0];         % initialize H

% _________Building L1, L2:       L1 * G (X,Y,Z) = L2_____________________________

for k=1:size(L,1)  %number of time points
   q=[0]; L1=[]; L2=[];  % initialize L1,L2, q(counter of 'valid' cameras)
  for  i=1:n       %number of cameras
   x=L(k,2*i-1); y=L(k,2*i);
   if ~(isnan(x) | isnan(y))  % do not construct l1,l2 if camx,y=NaN
    q=q+1;
    L1([q*2-1:q*2],:)=[A(1,i)-x*A(9,i), A(2,i)-x*A(10,i), A(3,i)-x*A(11,i);...
                    A(5,i)-y*A(9,i), A(6,i)-y*A(10,i), A(7,i)-y*A(11,i)];
    L2([q*2-1:q*2],:)=[x-A(4,i);y-A(8,i)];
   end
  end

  if (size(L2,1)/2)>1  %check whether enough cameras available (at least 2)
   g=L1\L2; h=L1*g; DOF=(size(L2,1)-3);
```

```
  avgres=sqrt(sum([L2-h].^2)/DOF);
 else
  g=[NaN;NaN;NaN]; avgres=[NaN];
 end

 %find out which cameras were used for the 3d reconstruction
 b=fliplr(find(sum(reshape(isnan(L(k,:)),2,size(L(k,:),2)/2))==0));
 if size(b,2)<2; camsused=[NaN];
    else,    for w=1:size(b,2), b(1,w)=b(1,w)*10^(w-1); end
           camsused=sum(b');
 end

 H(k,:)=[g',avgres,camsused];
end
```

C.3 Strain Calculation Algorithm

```
%_____________________________PROGRAM STRAIN1.M_____________________________
%This program calculates the total distance between the first and last marker of a chord.
%This program uses the infinitesimal strain definition (x-x_initial)/x_initial to calculate strain
%where x is the distance between three markers.  The distance formula is used to
%calculate the distance between two markers √((x2-x1)^2+(y2-y1)^2+(z2-z1)^2).
%It takes the output text file from SW3D6 as the input file.
%The output file is in the form of Frame Number, Time, VP, TM, Total Distance.

clear
clc

%Loading the input file from SW3D6
filename1=input('Please enter the filename of the 3D marker coordinates (eg. m3d.txt):
','s');
if isempty(filename1)
   filename1='m3d.txt';
end

%Reading in the number of frames and the number of markers from the input file
data=dlmread(filename1);
numfrm=data(1,1);
nummrks=data(1,2);

time=zeros(numfrm,1);
frmnum=zeros(numfrm,1);
tm=zeros(numfrm,1);
vp=zeros(numfrm,1);
coord=zeros(nummrks,3);
totaldistance(:,1)=0;
```

```
distance=zeros(numfrm,nummrks-1);

%Input the reference frame which will be used to calculate the initial length of the chord
reffrm=input('\nPlease enter the reference frame: ');

%Input the initial length of the chord so strain measurements can be done
%initial=input('\nPlease enter the initial length of the chord in mm: ');

%This gets the x, y, z coordinates of the reference frame and finds the initial length of the
chord
begin=2+reffrm+nummrks*(reffrm-1);
last=begin+(nummrks-1);
j=1;
for i=begin:last
   matrix(j,:)=[data(i,1) data(i,2) data(i,3)];
   j=j+1;
end

initial=0;
temp=0;
for i=1:nummrks-1
   x=(matrix(i,1)-matrix(i+1,1))^2;
   y=(matrix(i,2)-matrix(i+1,2))^2;
   z=(matrix(i,3)-matrix(i+1,3))^2;
   temp=sqrt(x+y+z);
   initial=temp+initial;
end


%This formats the data by creating multiple matrices
temp=2;
temp1=temp;
temp2=0;
for i=1:numfrm
   frmnum(i,1)=data(temp1,1);
   time(i,1)=data(temp1,2);
   vp(i,1)=data(temp1,3);
   tm(i,1)=data(temp1,4);
   %This inputs the x, y, z coordinates for all the markers
   for j=1:nummrks
      coord(j,:)=[data(temp1+j,1) data(temp1+j,2) data(temp1+j,3)];
   end
   %This calculates the distance between each marker and the total distance between the
first and last marker and also the strain.
   for j=1:nummrks-1
```

```
      distance(i,j)=sqrt((coord(j,1)-coord(j+1,1))^2+(coord(j,2)-
coord(j+1,2))^2+(coord(j,3)-coord(j+1,3))^2);
      totaldistance(i,1)=distance(i,j)+temp2;
      infinitestrain(i,1)=(totaldistance(i,1)-initial)/initial;
      temp2=totaldistance(i,1);
   end
   temp1=1+nummrks+temp;
   temp=temp1;
   temp2=0;
end

%Creates the output file in a .txt format
filename2=input('\nPlease enter the filename of the distance coordinates (eg.
distance.txt): ','s');
if isempty(filename2)
   filename2='distance.txt';
end

output=[frmnum time vp tm distance totaldistance infinitestrain];

dlmwrite(filename2,output,'\t');

disp('Finished')
```

C.4 Lowpass Filter Algorithm

```
%_____________________________PROGRAM LOWPASS.M_____________________________
%This program creates a low pass filter for the marker digitization
%This program uses the fast Fourier Transform to calculate the power spectrum.
%The user can then input the upper and lower bounds for the second order Butterworth
%filter.  The program then shows the power spectrum of the Butterworth filter.
%Using the filter command in Matlab, the data is filtered and an output text file is
%generated.  The final power spectrum of the filtered data is also output.
%The output text file is in the form of time, strain.

fhz_lower=zeros(1,1);
fhz_upper=zeros(1,1);
%Input the strain and time as a matrix
%matrix=infinitestrain;
%time=time;
%If the strain1 program has not been run last use the following to input the strain and
time

%Generate the power spectrum of the strain data
sample=input('\nPlease enter the sample frequency (eg. 500): ');
if isempty(sample)
```

```
   sample=500;
end

R=fft(matrix,512);
Pyy=R.*conj(R)/512;
f=sample*(0:256)/512;
figure
plot(f,Pyy(1:257))
title('Power Spectrum Before Filter')

%Determine the upper and lower bound for the filter
N=2;        %a second order butterworth filter
fhz_lower=input('\nPlease enter the lower bound frequency (eg. 0): ');
if isempty(fhz_lower)
   fhz_lower=2.5*10^-10;
end

fhz_upper=input('\nPlease enter the upper bound frequency (eg. 11.67): ');
if isempty(fhz_upper)
   fhz_upper=70/60*5*2;
end

f_lower=2*fhz_lower/sample;
f_upper=2*fhz_upper/sample;

%Create a Butterworth filter
passband=[f_lower f_upper];
[Bb,Ab]=butter(N,passband);
h=[abs(freqz(Bb,Ab,256))];
ff=sample/(2*256)*(0:256-1);
figure
plot(ff,h)
title('Power Spectrum of Butterworth Filter')

%Filter the strain data
sf=filter(Bb,Ab,matrix);

%Create a text file of the filtered data
filename=input('\nPlease input the filename for the filtered strain data (eg. filtered.txt):
','s');
if isempty(filename)
   filename='filtered.txt';
end

output=[time sf];
```

```
dlmwrite(filename,output,'\t');

figure
plot(time,sf)
title('Strain Data After Filter')

%Generate power spectrum for filtered data
R_after=fft(sf,512);
Pyy_after=R_after.*conj(R_after)/512;
figure
plot(f,Pyy_after(1:257))
title('Power Spectrum After Filter')


disp('Finished')
```

APPENDIX D

HISTOLOGY AND BIOCHEMICAL ASSAY PROTOCOLS

D.1 Hematoxylin & Eosin Stain

Protocol:

1. Stain in Hematoxylin for 30 seconds
2. Rinse in deionized water
3. Dip in acid alcohol
4. Rinse in deionized water
5. Place in Scott's solution for 30 seconds
6. Rinse in deionized water
7. Wash in 95% alcohol for 1 minute
8. Stain in alcoholic Eosin for 30 seconds
9. Dehydrate through ascending grades of alcohol and clear to xylene. Mount in a permanent mounting media.

Results:

1. Cell nuclei: black
2. Collagen: dark pink
3. Elastin: light pink

D.2 Verhoeff & van Gieson Stain

Solutions:

Verhoeff's Iodine:

1. Iodine_____2g
2. Potassium Iodide_____4g
3. Distilled Water_____100ml

Place iodine and potassium iodide into a flask with 20ml of water. Stir until iodine dissolves and then add remaining water.

10% Ferric Chloride:

1. Ferric Chloride_____50g
2. Distilled Water_____500ml

Store at 4°C

Verhoeff's Elastic Stain:

1. Hematoxylin (C.I. 75290), 5% in 95% alcohol_____30ml
2. Ferric Chloride, 10% solution_____12ml
3. Verhoeff's Iodine_____12ml

5% Sodium Thiosulfate:

1. Sodium Thiosulfate_____5g
2. Distilled Water_____100ml

Van Gieson's Solutions:

1. Acid Fuchsin (C.I. 42685), 1% aqueous_____20ml
2. Picric Acid, saturated solution (14g/l)_____380ml

Protocol:

1. Deparaffinize and rehydrate to distilled water.
2. Stain for 20 minutes in Verhoeff's elastic stain. Tissue should appear completely black.
3. Wash in two changes of distilled water.
4. Differentiate in 1% Ferric Chloride. Control differentiation under microscope by rinsing slides in water to check. Differentiate until the elastic fibers are black and the background is colorless. If the slides are over differentiated, return slides to Verhoeff's solution and repeat the stain.
5. Rinse in distilled water.
6. Place in 5% Sodium Thiosulfate for 1 minute to remove iodine.
7. Wash in running tap water for 5 minutes.
8. Counterstain in van Gieson's solution for 1 minute.
9. Dehydrate through ascending grades of alcohol and clear to xylene. Mount in a permanent mounting media.

Results:

1. Elastic fibers: blue-black to black
2. Nuclei: blue to black
3. Collagen: red
4. Other tissue elements: yellow

D.3 Verhoeff & Light Green Stain

Solutions:

Verhoeff's Iodine:

1. Iodine_____2g
2. Potassium Iodide_____4g
3. Distilled Water_____100ml

Place iodine and potassium iodide into a flask with 20ml of water. Stir until iodine dissolves and then add remaining water.

10% Ferric Chloride:

1. Ferric Chloride_____50g
2. Distilled Water_____500ml

Store at 4°C

Verhoeff's Elastic Stain:

1. Hematoxylin (C.I. 75290), 5% in 95% alcohol_____30ml
2. Ferric Chloride, 10% solution_____12ml
3. Verhoeff's Iodine_____12ml

5% Sodium Thiosulfate:

1. Sodium Thiosulfate_____5g
2. Distilled Water_____100ml

Light Green Stock Solution:

1. Light Green SF Yellowish_____0.2g
2. Distilled Water_____100ml
3. Glacial Acetic Acid_____0.2ml

Mix well.

Light Green Working Solution:

1. Light Green Stock Solution_____10ml
2. Distilled Water_____50ml

Protocol:

1. Deparaffinize and rehydrate to distilled water.
2. Stain for 20 minutes in Verhoeff's elastic stain. Tissue should appear completely black.
3. Wash in two changes of distilled water.
4. Differentiate in 1% Ferric Chloride. Control differentiation under microscope by rinsing slides in water to check. Differentiate until the elastic fibers are black and the background is colorless. If the slides are over differentiated, return slides to Verhoeff's solution and repeat the stain.
5. Rinse in distilled water.
6. Place in 5% Sodium Thiosulfate for 1 minute to remove iodine.
7. Wash in running tap water for 5 minutes.
8. Counterstain in Light Green solution for 1 minute.
9. Dehydrate through ascending grades of alcohol and clear to xylene. Mount in a permanent mounting media.

Results:

1. Elastic fibers: blue-black to black
2. Nuclei: blue to black
3. Other tissue elements: light green

D.4 Immunohistochemistry

Solutions:

1% Bovine serum albumin (BSA)/Phosphate buffered saline (PBS):

1. V BSA (Sigma #A2153)_____1g fraction
2. 1X PBS_____100ml

Mix until fully dissolved. Aliquot into 5ml volumes and store at -20°C.

Solution A, Citric Acid (109mM):

1. Citric Acid_____4.2g
2. dH_2O_____200ml

Solution B, Sodium Citrate (100mM):

1. Sodium Citrate_____14.7g
2. dH_2O_____500ml

10mM Citrate Buffer, pH 6.0 (500ml):

1. Solution A_____9ml
2. Solution B_____41ml
3. dH_2O_____450ml

Adjust pH to 6.0. Bring up to 500ml. Final concentrations are 1.96mM citric acid and 8.2mM sodium citrate.

Diaminobenzidine Tetrahydrochloride (DAB):

1. Sigma #D-5905; 10mg tables X 50 tablets.

Elite ABC-Peroxidase Kit :

1. Vector #PK-6100

30% Hydrogen Peroxide:

1. Sigma #H1009 or any other brand

10X PBS:

Boehringer Mannheim #1666789

Protease:

1. Dissolve protease (Sigma #P-8038) in PBS for a stock concentration of 100mg/ml. Aliquot and store at -20°C.

Proteinase K:

1. Dissolve proteinase K (Sigma #P-4914) in dH_2O for a stock concentration of 20mg/ml. aliquot and store at -20°C.

TBS:

1. Tris Base_____12.1g
2. Sodium Choloride_____8.77g
3. dH_2O_____1L

pH to 7.6

Primary Antibody:
Anti-human von Willebrand factor, IgG fraction of antiserum, developed in rabbit
Sigma Product Number F 3520

Secondary Antibody and Normal Animal Sera:
IgG fraction of antiserum, goat anti-rabbit
Vector Laboratories, Inc. Product Number BA-1000

1% Acid Alcohol:
1. HCl (Fisher #A144s)_____2ml
2. 70% Ethanol_____198ml

Hematoxylin:
1. Gill's 2 hematoxylin (Harleco #65067 available from VWR #15204-182)

Scott's Solution:
1. $NaHCO_3$_____2g
2. $MgSO_4 \cdot 7H_2O$_____20g
3. dH_2O_____1000ml

Mix until dissolved.

Protocol:
1. Fixed paraffin embedded tissue is deparafinized, and rehydrated in descending grades of alcohol. Sections are washed in 1X PBS for 5 minutes.
2. For antigen retrieval, dilute 150ul of 100mg/ml of stock protease in 150ml of 1X PBS. Incubate the tissue for 10 minutes with the 100ug/ml protease pretreatment in humid chamber.
3. Wash sections in 1X PBS twice for 5 minutes each.
4. Block endogenous peroxidase using 0.3% H_2O_2 in methanol for 15 minutes.
5. Rehydrate sections in 1X PBS twice for 5 minutes each.
6. Block tissue using 1% gelatin/PBS mixture for 20 minutes.
7. Prepare the working dilution of the primary antibody in 1% BSA in 1X PBS. Blot off gelatin/PBS and apply primary antibody. Incubate sections in a humid chamber for 1 hour. For negative control, do not apply primary antibody.
8. Blot off excess antibody and wash slides in 1X PBS twice for 5 minutes each.
9. Prepare working dilution of the biotinylated secondary antibody in 1% BSA in 1X PBS, and add 2% normal serum from the source animal (goat) of the secondary antibody. Prepare secondary antibody at a 1/400 dilution. Apply antibody and incubate for 30 minutes in a humid chamber.
   Prepare the working solution of the ABC-peroxidase complex from the Vectastain Elite ABC Kit (#PK-6100) after application of the secondary antibody. Mix 5ml of 1X PBS, 2 drops of reagent A, and 2 drops of reagent B. Allow to sit for 30 minutes prior to use.
10. Blot off excess antibody and wash slides in 1X PBS twice for 5 minutes each.

11. Apply prepared ABC mixture to each slide. Incubate in a humid chamber for 1 hour.
12. Blot off excess solution and wash slides in 1X PBS twice for 5 minutes each, followed by one wash in sterile deionized/distilled water for 5 minutes.
13. Make up substrate solution, diaminobenzidine (DAB), immediately before use. DAB is a carcinogen so wear gloves, goggles, work on a diaper, and save liquid waste to be disposed of with chemical waste. In order, add: 15ml of TBS pH 7.6, 1 tables DAB (10mg), and 12ul of 30% H_2O_2. Mix to dissolve table. Filter using Whatman #1. Apply filtered solution to each section. Incubate slides in the dark up to 10 minutes, checking color reaction periodically. Stop reaction by blotting off substrate and rinsing in 1X PBS 3 times for 5 minutes each.
14. Lightly counterstain sections with hematoxylin.
    a. Place in hematoxylin for 10 seconds
    b. Rinse in tap water until clear
    c. Dip once in 1% acid alcohol
    d. Rinse in water
    e. Place in Scott's solution for 20 seconds
    f. Rinse in water
15. Rinse slides well in water until water is clear. Dehydrate through graded alcohols, then xylene and coverslip.

D.5 Biochemical Digestion

D.5.1 Protenaise K

1. Buffer for 100mL
    a. 95mL dH_2O
    b. 5mL 50mM Tris-HCL
    c. 3.72g 0.1M EDTA
    d. 1.168g 0.2M NaCl
    pH to 7.4
2. Aliquot amount needed (1mL/construct or 1M cells)
3. Add: 0.5mg/mL proteinase K and 0.1mg/mL SDS
4. Dissolve and free excess aliquots
5. Add 1mL of proteinase K solution to each sample
6. Place in bath at 55°C and check every 24 hours until digested

D.5.2 Pepsin

1. Calculate the amount of pepsin needed (2mg of dry tissue weight : 1mg of pepsin)
2. Calculate the amount of pepsin/acetic acid solution needed (5mg pepsin/mL in 0.5M acetic acid)
3. Prepare 5mg pepsin/mL in 0.5M acetic acid to give desired final volume from step 2

4. For every 2mg of dry tissue weight, add 1 mg of pepsin to the eppendorf tube (the amount of pepsin/acetic acid solution added to each eppendorf tube is equal to one-tenth the dry weight of the specimen)
5. Place on mechanical shaker overnight
6. Place in water bath at 80°C until the tissue has been digested completely. Depending on the dry weight of the tissue, this process takes from 4 hours to 24 hours. Check tissue every 2 hours.

D.6 Fastin Elastin Assay

1. Precool elastin precipitation reagent in fridge before use
2. Label 1.5mL tubes (standards, blanks, samples)
3. Prepare blanks - 100µL buffer/salt/water solution
4. Prepare standards – 12.5, 25, 50, 75µL of α-elastin standard. Bring each tube up to 100µL with dH_2O
5. Prepare samples - 100µL of sample. Bring each tube up to 100µL with dH_2O
6. Add 1mL of cold elastin precipitating reagent to each tube
7. Incubate in ice-water overnight
8. Next morning, change ice-water to ice and incubate for 30 minutes to bring samples to 0°C
9. Centrifuge while cold at 12,000g for 10 minutes. Elastin will appear as a gel
10. Drain tubes and gently tap on paper towel to remove excess water
11. Add 1mL of dye reagent
12. Add 200µL of 90% saturated ammonium sulfate
13. Vortex until elastin is back in solution
14. Incubate and gently agitate at room temperature for 1 hour
15. Centrifuge tubes at 12,000g for 10 minutes
16. Drain tubes and gently tap on paper towel to remove excess water
17. Add 1mL dissociation reagent
18. Vortex to dislodge pellet
19. Mix gently for 10 minutes to release all dye
20. Add 100µL aliquots into each well
21. Set fluorescence to 513nm and endpoint measurement

D.7 Collagen Assay

1. Label 1.5mL tubes (standards, blanks, samples)
2. Prepare blanks - 100µL buffer/salt/water solution
3. Prepare standards – 5, 10, 25, 50µg of collagen standard. Bring each tube up to 100µL with dH_2O
4. Prepare samples - 100µL of sample
5. Add 1mL of Sircol Dye reagent to each tube
6. Place tubes in a mechanical shaker for 30 minutes
7. Centrifuge at 12,000g for 10 minutes
8. Drain tubes and gently tap on paper towel to remove excess dye

9. Add 1mL of Alkali reagent
10. Vortex until bound dye has been dissolved back into the solution
11. Mix gently for 10 minutes to release all dye
12. Add 200µL aliquots of samples into each well
13. Measure absorbance in microplate reader. Set wavelength to 540nm and endpoint measurement

D.8 Hoescht Dye DNA Assay

10x TEN:

1. 0.01M Tris
2. 0.001M Na_2EDTA
3. 0.1 M NaCl

pH=7.4

Hoechst Dye Solution:

1. Hoechst Stock dye is 1mg/mL in dH_2O
2. Add as 10,000 X into 0.1µg/mL buffer (100µg /100mL 1xTEN)

Dye Stock:

1. Calculate approximate total volume of dye needed. Use 0.2ml per standard/sample
2. Add 10µL of dye stock (10,000X) per 100mL of working dye needed in an amber bottle (dye is light sensitive)
3. Add final volume desired of 1x TEN

Standards:

1. Set up 7 eppendorfs in a tube rack
2. Thaw one 1mL cryovial of the 10µg/mL DNA stock solutions in the -70°C freezer
3. add 500µL of PBE to each eppendorf
4. serial dilute by taking 500µL of the 10µg/mL DNA stock and placing it in the first eppendorf (final concentration of 5µg/mL)
5. mix by pipet, and repeat, taking 500 µL of the 5µg/mL solution and placing it into the next eppendorf (final concentration of 2.5 µg/ml)

*Final standard concentrations: 10µg/ml, 5µg/ml, 2.5µg/ml, 1.25µg/ml, 0.625µg/ml, 0.3125µg/ml, 0.15625µg/ml, and 0µg/ml).

<u>Assay</u>:

1. Pipet 10µl sample and 200µl Hoechst dye aliquots into each well (use the black 96 well plates). Cover the plate with foil until ready to read.
2. Measure fluorescence using microplate reader. Set excitation to 365nm and emission to 458nm

APPENDIX E

BIOCHEMICAL ASSAY RESULTS

E.1 DNA Assay Results

The DNA assay results for each chordae are displayed in Table E.1. The DNA content has been normalized by the dry weight. Table E.2 below shows the DNA content for each specimen for each chordae. The average and standard deviation are given at the bottom of the table. Table E.3 gives the p-value between each chordae. A p-value below 0.05 was considered significant.

Table E.1: DNA assay results for each chordae tendineae. The chordae measured is listed at the top of each column of data.

	Strut		
Sample	**Fluoresence**	**Dry Weight, mg**	**DNA Content, ug/mg**
1	156.750	3.800	0.652
2	155.831	3.800	0.642
3	159.267	3.800	0.679
4	170.989	4.400	0.694
5	176.787	4.400	0.747
6	154.603	4.400	0.543
7	163.631	3.500	0.787
8	159.749	3.500	0.743
9	183.684	3.500	1.019
10	183.124	3.900	0.945
11	185.678	3.900	0.973
12	180.987	4.900	0.734
13	182.84	4.900	0.750
14	238.489	9.100	0.661
15	234.551	9.100	0.642
16	228.507	13.600	0.411
17	232.298	13.600	0.423
18	192.964	5.600	0.732
19	202.912	5.600	0.807
20	194.002	4.800	0.863
21	197.606	4.800	0.895
22	199.658	10.600	0.457
23	201.609	10.600	0.465
24	210.782	17.200	0.309
25	226.518	17.200	0.349
26	236.367	18.100	0.355
27	226.918	18.100	0.332
28	227.227	11.200	0.538
29	230.178	11.200	0.550
30	202.775	9.800	0.508
31	220.744	9.800	0.587
32	200.849	10.400	0.470

Table E.1 (continued).

33	200.452	10.400	0.469

Anterior Marginal			
Sample	**Fluoresence**	**Dry Weight, mg**	**DNA Content, ug/mg**
1	157.821	1.4	1.801
2	156.309	1.4	1.757
3	154.729	1.4	1.712
4	184.527	1.8	2.080
5	183.862	1.8	2.065
6	173.176	0.8	4.085
7	179.982	0.8	4.442
8	175.755	2	1.688
9	179.186	2	1.760
10	183.358	1.7	2.174
11	210.631	1.7	2.848
12	171.469	1.5	2.131
13	170.122	1.5	2.093
14	183.1	1.5	2.457
15	190.035	1.5	2.651
16	187.066	1	4.299
17	181.714	1	4.068
18	189.043	6.5	0.674
19	199.645	6.5	0.745
20	204.759	9.3	0.544
21	202.408	9.3	0.533
22	183.156	3.6	1.147
23	181.409	3.6	1.126
24	205.269	5.4	0.941
25	204.677	5.4	0.936
26	191.296	3.2	1.400
27	190.635	3.2	1.391
28	200.723	6.1	0.801
29	199.382	6.1	0.792

Commissural			
Sample	**Fluoresence**	**Dry Weight, mg**	**DNA Content, ug/mg**
1	162.887	1.8	1.514
2	168.267	1.8	1.635
3	177.208	1.8	1.835
4	155.493	1.8	1.348
5	153.027	1.8	1.293
6	158.7	1.8	1.420
7	179.061	3.1	1.134
8	182.175	3.1	1.176
9	186.899	2.8	1.373
10	186.831	2.8	1.372
11	175.674	2.9	1.163

Table E.1 (continued).

12	176.265	2.9	1.172
13	111.517	2	0.339
14	104.185	2	0.185
15	177.465	1.2	2.874
16	172.92	1.2	2.714
17	203.876	7.8	0.644
18	191.996	7.8	0.578
19	174.098	2.5	1.496
20	190.2	2.5	1.773
21	262.861	12.5	0.605
22	272.644	12.5	0.639
23	182.727	3.7	1.111
24	183.566	3.7	1.121
25	197.776	4.4	1.082
26	204.468	4.4	1.147

Basal			
Sample	**Fluoresence**	**Dry Weight, mg**	**DNA Content, ug/mg**
1	142.069	1.8	1.047
2	151.859	1.8	1.267
3	141.849	1.8	1.042
4	142.976	2.3	0.836
5	163.782	2.3	1.201
6	177.739	2.3	1.446
7	192.001	2.1	1.857
8	163.909	2.1	1.317
9	151.192	2.1	1.073
10	176.824	2.5	1.369
11	182.764	2.5	1.468
12	182.086	5.6	0.650
13	178.002	5.6	0.620
14	197.296	3.6	1.189
15	214.821	3.6	1.394
16	184.808	2.6	1.445
17	185.218	2.6	1.451
18	187.889	3.9	0.996
19	185.246	3.9	0.968
20	178.708	2.1	1.667
21	182.572	2.1	1.744
22	213.241	9.3	0.583
23	225.16	9.3	0.639
24	191.952	5	0.902
25	187.318	5	0.862
26	222.208	10.9	0.533
27	220.372	10.9	0.526
28	174.704	4.9	0.769
29	184.111	4.9	0.851

Table E.1 (continued).

Posterior Intermediate			
Sample	**Fluoresence**	**Dry Weight, mg**	**DNA Content, ug/mg**
1	137.33	1.1	1.540
2	143.971	1.1	1.784
3	151.334	1.1	2.054
4	156.021	4.2	0.583
5	158.311	4.2	0.605
6	152.069	4.2	0.545
7	210.501	6.2	0.780
8	205.495	6.2	0.746
9	203.031	7.9	0.572
10	204.981	7.9	0.583
11	181.323	4.1	0.881
12	209.881	4.1	1.173
13	177.439	2.1	1.641
14	178.137	2.1	1.655
15	173.855	3.1	1.063
16	169.196	3.1	1.000
17	168.685	4.4	0.700
18	175.693	4.4	0.767
19	190.629	4.3	1.035
20	197.805	4.3	1.107
21	264.948	7	1.093
22	240.016	7	0.940
23	204.512	6.1	0.828
24	211.697	6.100	0.879
25	190.26	5.700	0.778
26	186.545	5.700	0.750
27	188.945	4.100	1.068
28	188.581	4.100	1.064

Posterior Marginal			
Sample	**Fluoresence**	**Dry Weight, mg**	**DNA Content, ug/mg**
1	168.427	1.6	1.843
2	166.286	1.6	1.789
3	172.818	1.6	1.954
4	180.354	1.8	1.983
5	193.337	1.8	2.286
6	160.939	1.7	1.620
7	191.432	1.7	2.373
8	182.626	0.8	4.581
9	175.037	0.8	4.183
10	180.678	1.800	1.991
11	170.675	1.800	1.757
12	181.062	1.200	2.999
13	190.081	1.200	3.315
14	182.294	1	4.093

Table E.1 (continued).

15	182.769	1	4.113
16	188.708	0.9	4.855
17	188.601	0.9	4.850
18	181.736	2.6	1.565
19	186.326	2.6	1.641
20	179.064	2.7	1.464
21	174.956	2.7	1.399

Table E.2: DNA content for each chordae tendineae. The average and standard deviation for each chordae is given at the bottom of the table.

Sample	Strut	Anterior Marginal	Commissural	Basal	Posterior Intermediate	Posterior Marginal
1	0.652	1.801	1.514	1.047	1.540	1.843
2	0.642	1.757	1.635	1.267	1.784	1.789
3	0.679	1.712	1.835	1.042	2.054	1.954
4	0.694	2.080	1.348	0.836	0.583	1.983
5	0.747	2.065	1.293	1.201	0.605	2.286
6	0.543	4.085	1.420	1.446	0.545	1.620
7	0.787	4.442	1.134	1.857	0.780	2.373
8	0.743	1.688	1.176	1.317	0.746	4.581
9	1.019	1.760	1.373	1.073	0.572	4.183
10	0.945	2.174	1.372	1.369	0.583	1.991
11	0.973	2.848	1.163	1.468	0.881	1.757
12	0.734	2.131	1.172	0.650	1.173	2.999
13	0.750	2.093	0.339	0.620	1.641	3.315
14	0.661	2.457	0.185	1.189	1.655	4.093
15	0.642	2.651	2.874	1.394	1.063	4.113
16	0.411	4.299	2.714	1.445	1.000	4.855
17	0.423	4.068	0.644	1.451	0.700	4.850
18	0.732	0.674	0.578	0.996	0.767	1.565
19	0.807	0.745	1.496	0.968	1.035	1.641
20	0.863	0.544	1.773	1.667	1.107	1.464
21	0.895	0.533	0.605	1.744	1.093	1.399
22	0.457	1.147	0.639	0.583	0.940	
23	0.465	1.126	1.111	0.639	0.828	
24	0.309	0.941	1.121	0.902	0.879	
25	0.349	0.936	1.082	0.862	0.778	
26	0.355	1.400	1.147	0.533	0.750	
27	0.332	1.391		0.526	1.068	
28	0.538	0.801		0.769	1.064	
29	0.550	0.792		0.851		
30	0.508					
31	0.587					
32	0.470					
33	0.469					
Average	0.63	1.90	1.26	1.09	1.01	2.70
Std. Dev	0.19	1.14	0.61	0.38	0.40	1.24

Table E.3: p-value between each chordae for the DNA assay results. A p-value less than 0.05 was considered significant.

	Strut	Anterior Marginal	Commissural	Basal	Posterior Intermediate	Posterior Marginal
Strut	-	0	0	0	0	0
Anterior Marginal	0	-	0	0	0.208	0.208
Commissural	0	0	-	0.279	0	0
Basal	0	0	0.279	-	0	0
Posterior Intermediate	0	0	0.126	0.378	-	0
Posterior Marginal	0	0.208	0	0	0	-

E.2 Collagen Assay Results

The collagen assay results for each chordae are displayed in Table E.4. The collagen content has been normalized by the dry weight. Table E.5 below shows the collagen content for each specimen for each chordae. The average and standard deviation are given at the bottom of the table. Table E.6 gives the p-value between each chordae. A p-value below 0.05 was considered significant.

Table E.4: Collagen assay results for each chordae tendineae. The chordae measured is listed at the top of each column of data.

Strut			
Sample	**Absorbance**	**Dry Weight, mg**	**Collagen Content, ug/mg**
1	0.5592	9.700	6.068
2	0.5973	9.700	6.482
3	1.2258	13.500	9.558
4	1.2928	13.500	10.080
5	2.1483	15.500	14.589
6	2.2978	15.500	15.605
7	0.184	4.600	4.211
8	0.1818	4.600	4.160
9	0.657	10.400	6.650
10	0.3173	10.400	3.212
11	0.3071	15.000	2.155
12	0.2413	15.000	1.693
13	0.2357	16.000	1.551
14	0.304	16.000	2.000
15	0.3031	7.500	4.254
16	0.1243	7.500	1.745

Table E.4 (continued).

17	0.2767	7.400	3.936
18	0.2954	7.400	4.202
19	0.3744	10.500	3.753
20	0.3891	10.500	3.901

Anterior Marginal			
Sample	**Absorbance**	**Dry Weight, mg**	**Collagen Content, ug/mg**
1	0.2006	3.7	5.707
2	0.2054	3.7	5.844
3	0.1981	2.2	9.478
4	0.1938	2.2	9.273
5	0.3173	2	16.700
6	0.3071	2	16.163
7	0.2413	2.2	11.545
8	0.2357	2.2	11.278
9	0.304	4.7	6.809
10	0.3031	4.7	6.788
11	0.1243	1.4	9.346
12	0.1237	1.4	9.301
13	0.1789	1.6	11.770
14	0.1777	1.600	11.691
15	0.1538	2.500	6.476
16	0.153	2.500	6.442
17	0.0973	1.900	5.391
18	0.1001	1.900	5.546
19	0.3261	5.300	6.477
20	0.3417	5.300	6.786

Commissural			
Sample	**Absorbance**	**Dry Weight, mg**	**Collagen Content, ug/mg**
1	0.1868	4.2	4.682
2	0.1897	4.2	4.754
3	0.1316	1.7	8.149
4	0.1389	1.7	8.601
5	0.0982	2.4	4.307
6	0.0977	2.4	4.285
7	0.1923	1.6	12.651
8	0.1876	1.6	12.342
9	0.2479	3.3	7.907
10	0.2464	3.3	7.860
11	0.1495	3.4	4.628
12	0.1522	3.400	4.712
13	0.0885	2.400	3.882
14	0.0854	2.400	3.746
15	0.0861	2.500	3.625
16	0.0863	2.500	3.634

Table E.4 (continued).

Basal			
Sample	**Absorbance**	**Dry Weight, mg**	**Collagen Content, ug/mg**
1	0.4705	7.9	6.617
2	0.495	7.9	6.962
3	0.2375	4.7	5.615
4	0.2444	4.7	5.778
5	0.1865	1.2	17.269
6	0.1817	1.2	16.824
7	0.2083	2.4	9.644
8	0.2085	2.4	9.653
9	0.2231	6.3	3.935
10	0.237	6.3	4.180
11	0.355	7.1	5.556
12	0.3589	7.1	5.617
13	0.3394	7.8	4.835
14	0.351	7.8	5.000
15	0.0896	3.200	3.111
16	0.0896	3.200	3.111
17	0.0913	2.800	3.623
18	0.0892	2.800	3.540

Posterior Intermediate			
Sample	**Absorbance**	**Dry Weight, mg**	**Collagen Content, ug/mg**
1	0.1898	3.3	6.391
2	0.1859	3.3	6.259
3	0.0947	2.4	4.384
4	0.0954	2.4	4.417
5	0.0773	2.4	3.579
6	0.0755	2.4	3.495
7	0.2547	5.3	5.340
8	0.266	5.3	5.577
9	0.1446	3.5	4.590
10	0.1483	3.5	4.708
11	0.1009	3.1	3.616
12	0.1015	3.100	3.638
13	0.1501	2.800	5.956
14	0.1502	2.800	5.960
15	0.2163	1.500	16.022
16	0.2135	1.500	15.815

Posterior Marginal			
Sample	**Absorbance**	**Dry Weight, mg**	**Collagen Content, ug/mg**
1	0.1124	0.6	20.815
2	0.111	0.6	20.556
3	0.1443	1.9	8.439
4	0.1474	1.9	8.620
5	0.1708	2.5	7.591
6	0.171	2.5	7.600
7	0.2077	1.9	12.146

Table E.4 (continued).

8	0.2041	1.9	11.936
9	0.1137	2.7	4.679
10	0.1128	2.7	4.642
11	0.234	1.8	14.444
12	0.2314	1.8	14.284
13	0.1676	1.1	16.929
14	0.1616	1.1	16.323
15	0.156	1	17.333
16	0.1575	1	17.500
17	0.255	1.500	18.889
18	0.2502	1.500	18.533
19	0.2032	0.800	28.222
20	0.204	0.800	28.333

Table E.5: Collagen content for each chordae tendineae. The average and standard deviation for each chordae is given at the bottom of the table.

Sample	Strut	Anterior Marginal	Commissural	Basal	Posterior Intermediate	Posterior Marginal
1	6.068	5.707	4.682	6.617	6.391	20.815
2	6.482	5.844	4.754	6.962	6.259	20.556
3	9.558	9.478	8.149	5.615	4.384	8.439
4	10.080	9.273	8.601	5.778	4.417	8.620
5	14.589	16.700	4.307	17.269	3.579	7.591
6	15.605	16.163	4.285	16.824	3.495	7.600
7	4.211	11.545	12.651	9.644	5.340	12.146
8	4.160	11.278	12.342	9.653	5.577	11.936
9	6.650	6.809	7.907	3.935	4.590	4.679
10	3.212	6.788	7.860	4.180	4.708	4.642
11	2.155	9.346	4.628	5.556	3.616	14.444
12	1.693	9.301	4.712	5.617	3.638	14.284
13	1.551	11.770	3.882	4.835	5.956	16.929
14	2.000	11.691	3.746	5.000	5.960	16.323
15	4.254	6.476	3.625	3.111	16.022	17.333
16	1.745	6.442	3.634	3.111	15.815	17.500
17	3.936	5.391		3.623		18.889
18	4.202	5.546		3.540		18.533
19	3.753	6.477				28.222
20	3.901	6.786				28.333
Average	5.49	8.94	6.24	6.71	6.23	14.89
Std. Dev	4.05	3.38	3.01	4.21	3.91	6.83

Table E.6: p-value between each chordae for the collagen assay results. A p-value less than 0.05 was considered significant.

	Strut	Anterior Marginal	Commissural	Basal	Posterior Intermediate	Posterior Marginal
Strut	-	0.006	0.545	0.368	0.582	0
Anterior Marginal	0.006	-	0.017	0.08	0.033	0.001
Commissural	0.545	0.017	-	0.708	0.999	0
Basal	0.368	0.08	0.708	-	0.733	0
Posterior Intermediate	0.582	0.033	0.999	0.733	-	0
Posterior Marginal	0	0.001	0	0	0	-

E.3 Elastin Assay Results

The elastin assay results for each chordae are displayed in Table E.7. The elastin content has been normalized by the dry weight. Table E.8 below shows the elastin content for each specimen for each chordae. The average and standard deviation are given at the bottom of the table. Table E.9 gives the p-value between each chordae. A p-value below 0.05 was considered significant.

Table E.7: Elastin assay results for each chordae tendineae. The chordae measured is listed at the top of each column of data.

Strut			
Sample	**Absorbance**	**Dry Weight, mg**	**Elastin Content, ug/mg**
1	0.9364	10.6	30.067
2	1.0137	17.2	20.357
3	0.8972	18.1	16.728
4	0.8313	11.2	24.640
5	0.2173	9.8	2.683
6	0.259	10.4	4.159

Anterior Marginal			
Sample	**Absorbance**	**Dry Weight, mg**	**Elastin Content, ug/mg**
1	0.1271	1	-10.385
2	0.9305	6.5	48.663
3	0.4278	9.3	12.031
4	0.7214	3.6	64.245
5	1.0241	5.4	65.624

Table E.7 (continued).

6	0.5871	3.2	55.209
7	0.2532	6.1	6.704

Commissural			
Sample	**Absorbance**	**Dry Weight, mg**	**Elastin Content, ug/mg**
1	1.011	4.3	81.173
2	0.1829	7	1.758
3	0.2172	6.1	4.304
4	0.1893	5.7	2.616
5	0.206	4.1	5.293

Basal			
Sample	**Absorbance**	**Dry Weight, mg**	**Elastin Content, ug/mg**
1	0.7634	9.3	26.705
2	0.589	5	35.488
3	0.2049	10.9	1.950
4	0.4927	4.9	28.221
Posterior Intermediate			
Sample	**Absorbance**	**Dry Weight, mg**	**Elastin Content, ug/mg**
1	1.011	4.3	81.173
2	0.1829	7	1.758
3	0.2172	6.1	4.304
4	0.1893	5.7	2.616
5	0.206	4.1	5.293

Posterior Marginal			
Sample	**Absorbance**	**Dry Weight, mg**	**Elastin Content, ug/mg**
1	0.1261	1	-10.791
2	0.1327	0.9	-9.008
3	0.9222	2.6	120.360
4	0.2244	2.7	10.808

Table E.8: Elastin content for each chordae tendineae. The average and standard deviation for each chordae is given at the bottom of the table.

Sample	Strut	Anterior Marginal	Commissural	Basal	Posterior Intermediate	Posterior Marginal
1	30.067	-10.385	43.780	26.705	81.173	-10.791
2	20.357	48.663	133.827	35.488	1.758	-9.008
3	16.728	12.031	24.875	1.950	4.304	120.360
4	24.640	64.245	87.347	28.221	2.616	10.808
5	2.683	65.624	8.515		5.293	
6	4.159	55.209	-9.698			
7		6.704				
Average	16.44	34.58	48.11	23.09	19.03	27.84
Std. Dev	11.03	31.02	53.58	14.61	34.77	62.45

Table E.9: p-value between each chordae for the elastin assay results. A p-value less than 0.05 was considered significant.

	Strut	Anterior Marginal	Commissural	Basal	Posterior Intermediate	Posterior Marginal
Strut	-	0.203	0.187	0.433	0.866	0.664
Anterior Marginal	0.203	-	0.581	0.509	0.434	0.813
Commissural	0.187	0.581	-	0.397	0.325	0.597
Basal	0.433	0.509	0.397	-	0.835	0.887
Posterior Intermediate	0.866	0.434	0.325	0.835	-	0.795
Posterior Marginal	0.664	0.813	0.597	0.887	0.795	-

REFERENCES

1. World Health Organization. The world health report 2004. (http://www.who.int)

2. American Heart Association. Heart disease and stroke statistics Update 2004. (http://www.americanheart.org)

3. Gillinov A.M, Wierup P.N., Blackstone E.H., Bishay E.S., Cosgrove D.M., White J., Lytel B.W., and McCarthy P.M. Is repair preferable to replacement for ischemic mitral regurgitation? **The Journal of Thoracic and Cardiovascular Surgery** 2001; 122, 1125-1141

4. Ranganathan N, Lam J.H.C., Wigle E.D., and Silver M.D. Morphology of the human mitral valve: II. The Valve Leaflets. **Circulation** 1970; 31, 459-467

5. Sacks M.S., He Z., Baijens L., Wanant S., Shah P., Sugimoto H., and Yoganathan A.P. Surface Strains in the Anterior Leaflet of the Functioning Mitral Valve. **Annals of Biomedical Engineering** 2002; 30, 1281-1290

6. Millington-Sanders C., Meir A., Lawrence L., and Stolinski C. Structure of chordae tendineae in the left ventricle of the human heart. **Journal of Anatomy** 1998; 192, 573-581

7. Lam J.H.C., Ranganathan N., Wigle E.D., and Silver M.D. Morphology of the human mitral valve: I. Chordae Tendineae: A New Classification. **Circulation** 1970; 31, 449-458

8. Liao J., and Vesely I. A Structural Basis for the Size-related Mechanical Properties of Mitral Valve Chordae Tendineae. **Journal of Biomechanics** 2003; 36, 1125-1133

9. Lim K.O., and Boughner D.R. Mechanical Properties of Human Mitral Valve Chordae Tendineae: Variation with Size and Strain Rate. **Canadian Journal of Physiology and Pharmacology** 1975; 53, 330-339

10. Kunzelman K.S, and Cochran R.P. Mechanical Properties of Basal and Marginal Mitral Valve Chordae Tendineae. **ASAIO Transactions** 1990; 36 (3), M405-408

11. Lim K.O., and Boughner D.R. Morphology and Relationship to Extensibility Curves of Human Mitral Valve Chordae Tendineae. **Circulation Research** 1976; 39, 580-585

12. Sedransk K.L., Grande-Allen K.J., and Vesely I. Failure Mechanics of Mitral Valve Chordae Tendineae. **Journal of Heart Valve Disease** 2002; 11, 644-650

13. Jimenez J.H., He S., Soerensen D.D., He Z., and Yoganathan A.P. Effects of a Saddle Shaped Annulus on Mitral Valve Function and Chordal Force Distribution: An In Vitro Study. **Annals of Biomedical Engineering** 2003; 31(10), 1171-1181

14. Jensen MO. Stentless mitral valve fixation: impact on hemodynamic performance. M.Sc. Thesis, Department of Biomedical Engineering, Georgia Institute of Technology, USA, 2000

15. He S., Lemmon J.D., Weston M.W., Jensen M.O., Levine R.A., Yoganathan A.P. Mitral valve compensation for annular dilation: *In vitro* study into the mechanisms of functional mitral regurgitation with an adjustable annulus model. **Journal of Heart Valve Disease** 1999; 8, 294-302

16. Jensen MO, Fontaine, A., and Yoganathan, A.P. Improved In Vitro Quantification of the Force Exerted by the Papillary Muscle on the Left Ventricular Wall Three Dimensional Force Vector Measurement System **ABME** 2000; 10, 111-124

17. Jimenez J. The Effects of Mitral Annular Dynamics and Papillary Muscle Position on Chordal Force Distribution and Valve Function: An *In Vitro* Study. M.Sc. Thesis, Department of Biomedical Engineering, Georgia Institute of Technology, USA, 2003

18. Y.C. Fung. Biomechanics Mechanical Properties of Living Tissues. Springer-Verlag New York Inc. 1981

19. Nielsen S.L., Nygaard H., Mandrup L., Fontain A.A., Hasenkam J.M., He S., and Yoganathan A.P. Meahcnaism of Incomplete Mitral Leaflet Coaptation-Interaction of Chordal Restraint and Changes in Mitral Leaflet Coaptation Geometry: Insight from In Vitro Validation of the premise of Force Equilibrium. **Journal of Biomechanical Engineering** 2002; 124, 596-608

20. Atkinson T.S., Ewers B.J., and Haut R.C. The Tensile and Stress Relaxation Responses of Human Patellar Tendon Varies with Specimen Cross-sectional Area. **Journal of Biomechanics** 1999; 32, 907-914

21. Goetz W.A., Lim H.S., Pekar F., Saber H.A., Weber P.A., Lansac E., Birnbaum D.E., and C.M.G. Duran. Anterior Mitral Leaflet Mobility is Limited by the Basal Stay Chords. **Circulation** 2003; 107, 2969-2974

22. Messas E., Guerrero J.L., Handschumacher M.D., Conrad C., Chow C., Sullivan S., Yoganathan A.P., and R.A. Levine. Chordal Cutting: A New Therapeutic Approach for Ischemic Mitral Regurgitation. **Circulation** 2001; 104, 1958-1963

23. Maganaris, C.N., and J.P. Paul. Hysteresis Measurements in Intact Human Tendon. **Journal of Biomechanics** 2000; 33, 1723-1727

24. Akhtar S., Meek K.M., and James V. Ultrastructure Abnormalities in Proteoglycans, Collagen Fibrils, and Elastic Fibers in Normal and Myxomatous Mitral Valve Chordae Tendineae. **Cardiovascular Pathology** 1999; 8(4), 191-201

25. Wren T.A.L., Yerby S.A., Beaupré G.S., and Carter D.R. Mechanical Properties of the Human Achilles Tendon. **Clinical Biomechanics** 2001; 16, 245-251

26. W.L. Gore and Associates. GORE-TEX® Suture for Chordae Tendineae Instructions for Use. June 2003

27. Cochran R.P, and Kunzelman K.S. Comparison of Viscoelastic Properties of Suture Versus Porcine Mitral Valve Chordae Tendineae. **Journal of Cardiac Surgery** 1991; 6(4), 508-513

28. Field J.R., and Stanley R.M. Suture Characteristics Following Incubation in Synovial Fluid or Phosphate Buffered Saline. **Injury** 2004; 35, 243-248

29. Fundaro P., Moneta A., Villa E., Pocar M., Triggiani M., Donatelli F., and Grossi A. Chordal Plication and Free Edge Remodeling for MItral Anterior Leaflet Prolapse Repair: 8-year Follow-up. **The Annals of Thoracic Surgery** 2001; 72 (5), 1515-1519

30. Phillips M.R., Daly R.C., Schaff H.V., Dearani J.A., Mullany C.J., and Orszulak T. Repair of Anterior Leaflet Mitral Valve Prolapse: Chordal Replacement Versus Chordal Shortening. **Annals of Thoracic Surgery** 2000; 69, 25-29

31. Duebener L.F., Wendler O., Nikoloudakis N., Georg T., Fries R., and Schäfers H. Mitral-valve Repair Without Annuloplasty Rings: Results After Repair of Anterior Leaflet Versus Posterior-leaflet Defects Using Polytetrafluoroethylene Sutures for Chordal Replacement. **European Journal of Cardio-Thoracic Surgery** 2000; 17, 206-212

32. Totaro P., Tulumello, Fellini P., Rambaldini M., La Canna G., Coletti G., Zogno M., and Lorusso R. Mitral Valve Repair for Isolated Prolapse of the Anterior Leaflet: An 11-Year Follow Up. **European Journal of Cardio-Thoracic Surgery** 1999; 15, 119-126

33. Shi Y, and Vesely I. Fabrication of Mitral Valve Chordae by Directed Collagen Gel Shrinkage. **Tissue Engineering** 2003; 9(6), 1233-1240

34. Yang G., Crawford R.C., and Wang J.H-C. Proliferation and collagen production of human patellar tendon fibroblasts in response to cyclic uniaxial stretching in serum-free conditions. **Journal of Biomechanics**. *In Press.*

35. Tohyama H., and Yasuda K. The effects of stress enhancement on the extracellular matrix and fibroblasts in the patellar tendon. **Journal of Biomechanics** 2000; 33, 559-565

36. Sutker B.D., Lester G.E., Banes A.J., et al. Cyclic strain stimulates DNA and collagen synthesis in fibroblasts cultured from rat medial collateral ligaments. **Transactions of the Orthopedic Research Society** 1990; 15, 130

37. Liao J., Vesely I. Relationship between collagen fibrils, glycosaminoglycans, and stress relaxation in mitral valve chordae tendineae. **Annals of Biomedical Engineering** 2004; 32(7), 977-983

38. Kugel M.A. Anatomical studies on the coronary arteries and their branches: I. Arteria anastomotica auricularis magna. **American Heart Journal** 1928; 3(3), 260-270

39. Timek T.A., Nielsen S.L., Green G.R., Dagum P., Bolger A.F., Daughters G.T., Hasenka J.M., Ingels Jr. N.B., and Miller C.D. Influence of Anterior Mitral Leaflet Second-Order Chordae on Leaflet Dynamics and Valve Competence. **Annals of Thoracic Surgery** 2001; 72, 535-541

40. Akhtar S., Meek K.M., and James V. Immunolocalization of Elastin, Collagen Type I and Type III, Fibronectin, and Vitronectin in Extracellular Matrix Components of Normal and Myxomatous Mitral Heart Valve Chordae Tendineae. **Cardiovascular Pathology** 1999; 8(4), 203-211

41. Derwin K.A., Soslowsky L.J., Green W.D.K., and Elder S.H. A New Optical System for the Determination of Deformations and Strains: Calibration Characteristic and Experimental Results. **Journal of Biomechanics** 1994; 27(10), 1277-1285

42. Miller D.C. Ischemic Mitral Regurgitation Redux-To Repair or to Replace? **The Journal of Thoracic and Cardiovascular Surgery** 2001; 122(6), 1059-1062

43. Gillinov A.M., Wierup P.N., Blackstone E.H., Bishay E.S., Cosgrove D.M., White J., Lytle B.W., and McCarthy P.M. Is Repair Preferable to Replacement for Ischemic Mitral Regurgitation? **The Journal of Thoracic and Cardiovascular Surgery** 2001; 122, 1125-1141

44. Yacoub M.H., and Cohn L.H. Novel Approaches to Cardiac Valve Repair: From Structure to Function: Part I. **Circulation** 2004; 109(8), 942-950

45. Yacoub M.H., and Cohn L.H. Novel Approaches to Cardiac Valve Repair: From Structure to Function: Part II. **Circulation** 2004; 109(9), 1064-1072

46. Garcia Paez J.M., Herrero E.J., Sanmartin C.A., Millan I., Cordon A., Maestro M.M., Rocha A., Arenaz B., and Castillo-Olivares J.L. Comparison of the Mechanical Behaviors of Biological Tissues Subjected to Uniaxial Tensile Testing: Pig, Calf, and Ostrich Pericardium Sutured with Gore-Tex. **Biomaterials** 2003; 24, 1671-1679

47. Louis-Ugbo J., Leeson B., and Hutton W.C. Tensile Properties of Fresh Human Calcaneal (Achilles) Tendon. **Clinical Anatomy** 2004; 17(1), 30-35

48. Frater R.W.M. Editorial: Assumptions and Realities of Mitral Valve Repair. **The Journal of Heart Valve Disease** 2003; 12, 11-13

49. He S., Jimenez J., He Z., and Yoganathan A.P. Mitral Leaflet Geometry Perturbations with Papillary Muscle Displacement and Annular Dilation: An In-Vitro Study of Ischemic Mitral Regurgitation. **The Journal of Heart Valve Disease** 2003; 12, 300-307

50. Chen L., Yin F.C-P., May-Newman K. The Structure and Mechanical Properties of the Mitral Valve Leaflet-Strut Chordae Transition Zone. **Transactions of the ASME** 2004; 126, 244-251

51. Nazari S., Carli F., Salvi S., Banfi C., Aluffi A., Mourad Z., Buniva P., Rescigno G. Patterns of Systolic Stress Distribution on Mitral Valve Anterior Leaflet Chordal Apparatus-A Structural Mechanical Theoretical Analysis. **Journal of Cardiovascular Surgery** 2000; 41(2), 193-202

52. Messas E., Guerrero J.L., Handschumacher M.D., Chow C., Sullivan S., Schwammenthal E., and Levine R.A. Paradoxic Decrease in Ischemic Mitral Regurgitation with Papillary Muscle Dysfunction. **Circulation** 2001; 104, 1952-1957

53. Lillehei C.W. New Ideas and Their Acceptance: As It Has Related to Preservation of Chordae Tendineae and Certain Other Discoveries. **The Journal of Heart Valve Disease** 1995; 4(Suppl. II), S106-S114

54. Gorman III J.H., Gorman R.C., Jackson B.M., Hiramatsu Y., Gikakis M., Kelley S.T., St. John Sutton M.G., Plappert T., and Edmunds Jr. L.H. Distortion of the Mitral Valve in Acute Ischemic Mitral Regurgitation. **Annals of Thoracic Surgery** 1997; 64, 1026-1031

55. Goertzen D.J., Budney D.R., and Cinats J.G. Methodology and Apparatus to Determine Material Properties of the Knee Joint Meniscus. **Med. Eng. Phys.** 1997; 19, 412-419

56. Smutz W.P., Drexler M., Berglund L.J., Growney E., and An K.N. Accuracy of a Video Strain Measurement System. **Journal of Biomechanics** 1996; 29(6), 813-817

57. Downs J., Halperin H.R., Humphrey J., and Yin F. An Improved Video-Based Computer Tracking System for Soft Biomaterials Testing. **IEEE Transactions on Biomedical Engineering** 1990; 37(9), 903-907

58. Gillinov A.M., Cosgrove D.M., Blackstone, Diaz R., Arnold J.H., Lytle B.W., Smedira N.G., Sabik J.F., McCarthy P.M., and Loop F.D. Durability of Mitral Valve Repair for Degenerative Disease. **Journal of Thoracic and Cardiovascular Surgery** 1998; 116, 734-743

59. Salgo I.S., Gorman III J.H., Gorman R.C., Jackson B.M., Bowen F.W., Plappert T., St. John Sutton M.G., and Edmunds Jr. L.H. Effect of Annular Shape on Leaflet Curvature in Reducing Mitral Leaflet Stress. **Circulation** 2002; 106, 711-717

60. Soerensen D., Frakes D., and Ajit Yoganathan. Automated Tracking of Heart Valve Leaflet Markers for Nonrigid Surface Motion Reconstruction. **Biomedical Engineering Society***,* Annual Fall Conference, Nashville, TN, October 2003

61. Iyengar A., Sugimoto H., Smith D.B., and M. Sacks. Dynamic *In Vitro* 3D Reconstruction of Heart Valve Leaflets Using Structured Light Projection. **Annals of Biomedical Engineering** 2001; 29, 963-973

62. Marzan G.T. A Computer Program for Direct Linear Transformation Solution of the Collinearity Condition and Some Applications of it. **Proceedings of the Symposium on Close-range Photogrammetric Systems** 1975, 420-476

63. Timek T.A., Nielsen S.L., Green G.R., Dagum P., Bolger A.F., Daughters G.T., Hasenkam J.M., Ingets Jr. N.B., and Miller D.C. Influence of Anterior Mitral Leaflet Second-Order Chordae on Leaflet Dynamics and Valve Competence. **Annals of Thoracic Surgery** 2001; 72, 535-541

64. Dreyfus G., Aylé N.A., Dubois C., and de Lentdecker P. Long Term Results of Mitral Valve Repair: Posterior Papillary Muscle Repositioning Versus Chordal Shortening. **European Journal of Cardio-Thoracic Surgery** 1999; 16, 81-87

65. di Gioia C.R.T., Brancaccio G., Sinatra R., and Gallo P. Long-term Histologic Features of Synthetic Chordal Replacement for Mitral Valve Repair: A Case Report. **Cardiovascular Pathology** 2001; 10, 87-89

66. Minatoya K., Okabayashi H., Shimada I., Ohno N., Nishina T., Yokota T., Takahashi M., Ishihara T., and Hoover E.G. Pathalogic Aspects of Polytetrafluoroethylene Sutures in Human Heart. **Annals of Thoracic Surgery** 1996; 61, 883-887

67. Lam B., Gillinov A.M., and Cosgrove III D.M. Failed Mitral Valve Repair Caused by Polypropylene Suture. **Annals of Thoracic Surgery** 2003; 76, 1716-1717

68. Reddy V.M., McElhinney D.B., Brook M.M., Silverman N.H., Stanger P., and Hanley F.L. Repair of Congenital Tricuspid Valve Abnormalities with Artificial Chordae Tendineae. **Annals of Thoracic Surgery** 1998; 66, 172-176

69. Adams D.H., Kadner A., and Chen R.H. Artificial Mitral Valve Chordae Replacement Made Simple. **Annals of Thoracic Surgery** 2001; 71, 1377-1379